Phase Transitions of Aqueous Atmospheric Particles

Scot T. Martin*

Division of Engineering and Applied Sciences, Harvard University, 29 Oxford Street, Pierce Hall, Room 122, Cambridge, Massachusetts 02138

Received February 8, 2000

Contents

I. Introduction 3403
A. Background 3403
B. Subject Material 3405
C. Organization 3406
II. Thermodynamics 3406
III. Phase Diagrams 3409
A. Chemical Composition Coordinate 3409
B. Experimental Determination 3411
C. Alternative Representations 3411
D. Equilibrium Phase Changes 3414
E. Ternary and Higher Order Systems 3415
F. Surface Region 3417
IV. Kinetics 3418
A. Classifications 3418
B. Premonitory Behavior 3419
C. Critical Germ Formation 3420
D. Homogeneous Nucleation 3420
i. History 3420
ii. Recent Work and Trends 3420
iii. Experimental Results Demonstrating Important Concepts 3424
E. Heterogeneous Nucleation 3431
i. Nuclei Contained Inside Atmospheric Particles 3431
ii. Observations and Concepts 3432
V. Implementation in Microphysical Models 3433
A. Semiempirical Correlations 3434
B. Classical Nucleation Theory 3434
C. Nonclassical Nucleation Theories 3435
D. Microphysical Models 3436
VI. Comparison between Models and Field Measurements 3437
A. Boundary Layer Particles 3438
i. Contravening Hypotheses: All Aqueous versus All Crystalline 3438
ii. Temporal Variations in Relative Humidity 3438
iii. Campaigns and Observations of Ambient Aerosol Phase Changes 3439
B. Cirrus Clouds 3441
C. Polar Stratospheric Clouds 3442
VII. Outlook 3444
VIII. Acknowledgments 3445
IX. Appendix A: Free Energy Calculations 3446
X. Appendix B: Saturation Ratio 3447
XI. References 3448

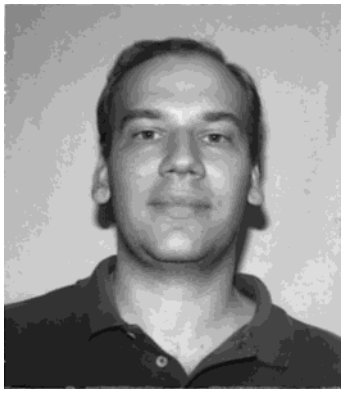

Scot T. Martin, Associate Professor of Environmental Chemistry in the Division of Engineering and Applied Sciences at Harvard University, received a B.S. in Chemistry from Georgetown University in 1991 and a Ph.D. in Physical Chemistry "Photocatalyzed Destruction of Chlorinated Hydrocarbons", from Caltech in 1995. He studied abroad one year (1990) at Oxford University in Chemistry. He completed postdoctoral work, "Phase Transformations of Polar Stratospheric Cloud Particles," in 1995−1996 at MIT in Atmospheric Chemistry. He was an Assistant Professor in Aquatic and Atmospheric Chemistry in the Department of Environmental Sciences and Engineering at the University of North Carolina at Chapel Hill from 1997 until June 2000. He is grateful for support received for his Ph.D. studies (National Defense Science and Engineering Graduate Fellowship), for his postdoctoral work (NOAA Postdoctoral Fellowship in Climate and Global Change), and during his early years as an independent investigator (NSF Presidential Early Career Award for Scientists and Engineers in the Atmospheric Chemistry Program). His laboratory research group is currently active in two areas, including (1) understanding and quantifying the formation by heterogeneous nucleation of salts and ice from aqueous particles containing insoluble oxides and (2) the kinetics and mechanisms of organic ligand-promoted dissolution of hematite and other minerals.

I. Introduction

A. Background

The physical state of a material is described as its phase. Common phases of the molecule H_2O include vapor, liquid water, and ice. Examples of these phases in the atmosphere are humidity, warm clouds, and cirrus clouds, respectively. Water vapor also affects the phase of other atmospheric particles, which are commonly referred to as aerosols. Prominent examples of the hygroscopic chemical species contained in tropospheric particles include NaCl arising from ocean spray over breaking waves and $(NH_4)_2SO_4$ due to anthropogenic activities. The phase of these salts is solid crystalline at low relative humidity (RH), whereas vapor and crystal combine

* To whom correspondence should be addressed. Telephone: (617) 495-7620. Fax: (617) 495-9837. E-mail: scot_martin@harvard.edu. http://www.deas.harvard.edu/~smartin.

10.1021/cr990034t CCC: $35.00
Published on Web 08/30/2000

to form aqueous electrolyte solutions at high relative humidity. Furthermore, ice crystallizes when the aqueous composition becomes dilute under cold and humid conditions. In contrast to the troposphere, the stratosphere is much drier, and particle composition is more homogeneous. Background stratospheric particles are composed of concentrated (60−80 w/w) sulfuric acid with high ionic strengths and negative pH values, except at the lowest temperatures of the polar winter. Below 190 K, a number of acid hydrates may crystallize from the acidic, brine particles. An important process in annual polar ozone depletion is the freezing of concentrated HNO_3 and H_2SO_4 aqueous particles to form ice as well as crystalline acid hydrates such as $H_2SO_4 \cdot 4H_2O$ (sulfuric acid tetrahydrate, SAT) or $HNO_3 \cdot 3H_2O$ (nitric acid trihydrate, NAT).

Atmospheric particles, especially those near the Earth's surface, are traditionally divided into categories based upon their sources,[1] including anthropogenic sulfates and nitrates, sea salts, secondary organics, soot, biogenic organics, those derived from biomass burning, and mineral dusts. Recent measurements of the chemical composition of single particles with mass spectrometric techniques strongly support the view that individual particles often contain several chemical classes due to atmospheric physical mixing and chemical processing. Some particles are likely to undergo phase changes with cycles of relative humidity (e.g., sea salts and partially neutralized nitrates and sulfates), some likely show a hygroscopic response without deliquescence (e.g., sulfates and oxygenated organics), and some likely exhibit only surfaces changes (i.e., reversible water adsorption) with altered relative humidity (e.g., freshly entrained soot and mineral dust particles).

The phase of atmospheric particles affects their physical, chemical, and optical properties. For example, when the dry salt constituents of a particle uptake water to form an aqueous particle, the diameter increases severalfold (see cover art). These larger particles scatter visible wavelength light much more efficiently. The hygroscopic response of atmospheric particles is responsible for reduced visibility associated with smog. Organic particles may also be hygroscopic. For example, biogenic hazes are often observed in the Blue Ridge Mountains. In addition to the effects of relative humidity, particles also change phase with temperature. In cold updrafts present in cloud formation, ice particles form in vapor-supersaturated environments (i.e., $RH_{ice} > 100\%$). As a consequence, they usually grow to be large ($>100\ \mu$m), and this physical property leads to rapid sedimentation. The phenomenon is easily observed by the naked eye as the wisps falling from cirrus clouds. Satellite images and balloon sondes also demonstrate dehydration in the polar stratospheric regions arising from the sedimentation of ice polar stratospheric clouds (PSCs).

Beyond their physical and optical effects, atmospheric aerosols also provide the milieu for many important chemical transformations. For example, multiphase sulfate chemistry in aqueous particles proceeds by the partitioning of SO_2(g) to the aqueous phase followed by oxidation to SO_4^{2-}(aq). Aqueous phase oxidation is believed responsible for the acidification of rain in most regions of the world. However, a phase transition to a crystalline particle removes this oxidation pathway. Another example is N_2O_5 hydrolysis, which proceeds rapidly on aqueous $(NH_4)_2SO_4$ particles but only slowly on $(NH_4)_2SO_4$(s). The various hydrates of polar stratospheric clouds also promote key transformation reactions for chlorine activation such as $ClONO_2$ hydrolysis. The efficiencies of the hydrates and their supercooled aqueous precursors strongly differ.

Before 1985, most work on the phase of atmospheric aerosol was in connection to ice formation in mixed phase clouds and air visibility in the boundary layer. At high relative humidity, those boundary layer particles composed of electrolytes are aqueous and relatively large due to their water content. As a result, they scatter light efficiently. At decreasing relative humidity, they effloresce to form smaller, solid particles that do not scatter light as effectively. Understanding the cycling between these phases is a key to air visibility. In the lower troposphere, clouds between 0 and −40 °C are typically mixed phase with a fraction of supercooled aqueous particles and a fraction of ice particles, which initially form by primary production involving heterogeneous nuclei and then sometimes multiply by secondary ice production mechanisms such as fragmentation. There are important consequences for cloud development and lightning.

After 1985, earnest work began on understanding the low-temperature (<200 K) phase transitions of sulfuric and nitric acid particles in connection to polar stratospheric cloud formation. The focus has been primarily on predicting aerosol phase because important heterogeneous reactions involved in ozone depletion are believed to depend critically on aerosol phase. In addition to liquid versus solid particles, a host of crystalline solids are possible including ice, sulfuric acid tetrahydrate, nitric acid trihydrate, and nitric acid dihydrate among others. Post-1997, work began on aerosols characteristic of the upper troposphere, especially as related to cirrus cloud formation. Upper tropospheric processes are set apart from mid-tropospheric cloud formation due to the cooler temperatures (below −40 °C) and associated diminished absolute water contents. In the upper troposphere, ice formation begins with haze particles (i.e., concentrated aqueous droplets) below −40 °C, whereas warmer mid-tropospheric mixed-phase clouds are characterized by the formation of ice by heterogeneous nucleation (i.e., ice nuclei) contained in a few highly dilute aqueous droplets.

Cirrus clouds are important both for global radiative transfer calculations and possibly for upper atmospheric heterogeneous chemistry. A surprising amount of ammonia and nitric acid is present in the upper troposphere. Understanding cirrus cloud formation then requires investigations of the phase transitions of partially neutralized sulfuric/nitric acid particles. In contrast, the bulk of laboratory research to date has focused primarily on the homogeneous

nucleation of ice in sulfate particles. Most recently, the likely role of various heterogeneous nuclei in promoting phase transitions has been recognized from field measurements, and laboratory work has been initiated.

To set the context for understanding phase transitions in the atmosphere, it is helpful to review briefly the range of temperatures and chemical activities (i.e., partial pressures) of water and other gases in the compartments of the atmosphere. In the lower stratosphere, temperatures range from 210 to 240 K, H_2O partial pressure is relatively constant around 5 ppmv at 50 mbar total pressure, and HNO_3 partial pressure varies from 5 to 20 ppbv. The aerosol is composed of 50 nm concentrated sulfuric acid particles with a total condensed phase sulfate mass loading equivalent to 0.5 ppbv vapor. In the polar winter, temperatures as low as 185 K are common. As a consequence, gas-phase H_2O and HNO_3 condense by Henry's law partitioning into the background aqueous H_2SO_4 particles. Due to extensive dilution, the particle diameters increase 10-fold, and the resulting composition is principally HNO_3/H_2O with trace H_2SO_4.

In the upper troposphere (ca. 200 mbar total pressure), temperatures of 205−230 K are common. Water relative humidity lies between 10% and the approximate limit imposed by the vapor pressure of ice. In some regions of the highest altitudes of the upper troposphere however, relative humidity with respect to ice appears regularly to reach values as high as 150%.[424] In comparison, the lower stratosphere is desiccated. HNO_3 in the upper troposphere (1−300 pptv) partitions into the aerosol at the lower end of the temperature range in enough mass to perturb appreciably the aqueous aerosol composition. The background tropospheric aerosol consists of sulfate-bearing particles in the size range of 10−1000 nm. The particles are partially to fully neutralized by NH_3 and often contain nitrates. These accumulation mode aerosols sometimes also contain small molecular weight oxygenated organic molecules and other larger carbonaceous molecules. The occasional particle (say 1 in 1000) contains a mineral dust component, which could be critical to ice nucleation and cirrus cloud formation. Overall, there is a much greater heterogeneity among aerosol types in the upper troposphere as compared to the stratosphere.

Even more variability occurs in the atmospheric boundary layer. Common conditions include temperatures from 275 to 305 K and water relative humidities from 10 to 100%. Many gases partition into particles, including NH_3 and HNO_3 among others, and the range of concentrations varies greatly from marine to urban to remote continental environments. The interested reader is referred to ref 1. The size distribution of boundary layer aerosol is trimodal containing a nucleation mode (diameter under 10 nm), an accumulation mode (ca. 100−500 nm mode size), and a coarse mode (supermicron). Total mass loadings vary between 1 and 10 $\mu g\ m^{-3}$ in remote regions and between 10 and 100 $\mu g\ m^{-3}$ in polluted areas. Within each size mode, there is significant chemical variability from particle to particle. The interested reader is again referred to ref 1 for details on the physicochemical heterogeneities of particles in the atmospheric boundary layer.

B. Subject Material

This review is a comprehensive account with respect to laboratory work in the atmospheric sciences on the phase transitions of (1) deliquescence and efflorescence of salts with changes in relative humidity, (2) ice formation under conditions of the upper troposphere, and (3) ice and other solid hydrate formation under conditions of the polar stratosphere. The bulk of this body of work has been accomplished in the last 20 years. This review is informative but not comprehensive on the laboratory work concerning ice formation mechanisms characteristic of mixed-phase clouds in the mid-troposphere, which has an extensive history of more than 100 years. In these clouds, primary ice production is believed to occur by heterogeneous nucleation in dilute aqueous droplets. References to more comprehensive accounts of that literature are provided in several places in this review.[2−8]

There is rapid development in the science of the phase transitions of atmospheric chemistry as well as a growing recognition of the importance of the condensed phase for diverse atmospheric problems. Laboratory work on cirrus and PSC cloud formation at low temperatures and salt crystallization at low relative humidities include 8 publications in 1999,[9−16] 19 in 1997−1998,[17−35] 14 in 1995−1996,[36−49] 18 in 1993−1994,[50−66] and 18 between 1977 and 1993.[67−84] Earlier work on salt crystallization is found in refs 85−88. In addition, there have been numerous papers describing field and modeling studies. The emphasis in this review is to cover principles, which will remain applicable even with new research, and to apply those principles in the context of contemporary relevant systems. Both the thermodynamics of phase equilibria and the kinetics of phase nucleation (homogeneous and heterogeneous) are discussed. The emphasis, however, is on kinetics.

This review is necessarily limited in scope. Gas-to-solid new organic particle formation will not be studied.[1] Other gas-to-solid transitions are not usually important in atmospheric chemistry: water condenses on preexisting cloud condensation nuclei in a gas-plus-solid to liquid transformation.[2] Above 100% RH, cloud droplets form followed by precipitation and/or evaporation. Transport and dynamics are believed to be more important than chemistry in cloud development. These processes are discussed in ref 2. For the most part, processes discussed in this review occur below 100% RH with respect to liquid water. New particle production in the troposphere from gas-to-liquid conversion is an active area of research but is not covered in this review.[89−92] Mass transfer aspects are not discussed in detail. These processes can be particularly important and even dominant in cloud formation.[93] The occurrence and possibly important effects of organic molecules on the hygroscopic response of atmospheric particles is not discussed.[94−97] The purpose of this review is to emphasize the chemistry of phase transitions in

concentrated aqueous salt particles pertinent to the atmosphere.

Although no textbook exists with examples of phase transitions chosen from atmospheric chemistry, excellent texts on the principles of phase transitions are found in the disciplines of materials science,[98] chemical engineering,[99,100] chemistry,[101] ceramics,[102] and geology.[103] Recently, electronic resources have also become available.[104,105] A history of short summaries on developing theories of polar stratospheric clouds exists in refs 61 and 106−110. In a recent review, techniques are described for the thermodynamic modeling of aqueous solutions and associated equilibrium solid phases at temperatures and with electrolyte systems relevant to the atmosphere.[111] An excellent introduction to the properties of supercooled aqueous solutions is provided in a chapter by Franks (ca. 1982).[5] Recent chapters discussing atmospheric phase transitions appear in refs 4, 6, and 112−117 while earlier documents can be found in refs 81, 85−88, and 118−120. General references for atmospheric chemistry include refs 1, 2, 121, and 122; general references for aerosol physics include refs 123−125.

C. Organization

This review is organized into sections on thermodynamics, phase diagrams, kinetics, microphysical models, field measurements, outlook, and two appendices. In the section on thermodynamics, the chemical potential (μ) is introduced as the master variable determining which of several possible spatial and chemical arrangements (i.e., phases) is most favored by nature under specific temperature and relative humidity conditions. Appendices A and B describe how to employ Pitzer models of concentrated electrolytes accessible through the worldwide web to complete energy calculations of common atmospheric chemical systems. The definitions of phase transitions processes (including freezing, melting, dissolution, precipitation, crystallization, sublimation, deliquescence, or efflorescence) are provided.

The section on phase diagrams covers the interpretation of two-component and higher phase diagrams, including the concepts of liquidus and solidus regions, tie lines, the lever rule, invariant points (viz., eutectic, peritectic, eutonic, and peritonic points), incongruent and congruent melting, and the Gibbs phase rule. Relevant phase diagrams of many atmospheric systems are chosen as examples to elucidate concepts. The most commonly employed axes coordinates are temperature and mole fraction, but several other important representations are shown (e.g., molality, relative humidity, weight percent, water partial pressure, and ice or water saturation ratio). Process changes along test tube trajectories as compared to idealized atmospheric trajectories are discussed. The distinction is made between interior and surface phases of particles, and the special role of water is discussed for the restructuring of surface regions of hygroscopic salts at relative humidities well below deliquescence.

The section on kinetics discusses the rates at which a metastable phase converts to a lower energy phase. Rates of phase changes often depend on the structural and chemical changes accompanying the phase transition. The useful classifications of phase transitions (including first-order, second-order, reconstructive, displacive, and order−disorder) are introduced. Premonitory behavior, spinodal decomposition, and critical germ formation are discussed. Examples of hysteresis and supercooling in atmospheric chemical systems are provided, and the laboratory work on homogeneous and heterogeneous nucleation in this area is comprehensively reviewed. End points in laboratory work are often expressed as freezing temperatures, minimum RH before efflorescence, critical saturation ratio, or critical supercooling. However, the most versatile expression of homogeneous nucleation results is data reduction into terms of the volume homogeneous nucleation rate, J. With regard to heterogeneous nucleation, the differences between stochastic and singular hypotheses and their implications are discussed. Finally, in this section critical differences are pointed out between an idealized trajectory of aqueous composition and an atmospheric trajectory, which often are not the same due to mass transfer effects.

The section on microphysical models discusses approaches to including nucleation kinetics in integrated models of atmospheric processes (e.g., cloud development). The principal approach is to reduce laboratory data to J values and then fit the parameters of classical nucleation theory to those values. In this way, J values at conditions relevant to atmospheric processes (e.g., appropriate cooling rates and particle sizes) are incorporated into microphysical models. One very difficult bridge to cross in these applications is that the bulk of laboratory studies are on homogeneous nucleation of one-component aqueous salts whereas field measurements of single particles in the atmosphere show that these particles consist of electrolytes as well as insoluble organic and inorganic. The inorganic material is probably especially important as a surface for heterogeneous nucleation.

In the section concerning field measurements, several representative campaigns and their results are reviewed in the context of observing and quantifying phase transitions in four atmospheric regimes, including the boundary layer, mixed-phase clouds, upper tropospheric cirrus clouds, and polar stratospheric clouds. At the end of the review, an outlook section is provided on important research needs.

II. Thermodynamics

A collection of atoms can alternatively arrange as several types of molecules in several phases (e.g., liquid or gas). According to the first and second law of thermodynamics, we know that nature has a tendency to choose an arrangement that maximizes entropy under the constraint of energy conservation. At constant temperatures and pressures, this tendency is quantified by the Gibbs free energy, G. Each arrangement of atoms as molecules and phases has an associated value G, and the favorable direction of change is to minimize G. These are the relationships represented on phase diagrams. It is important to realize that the time scale for movement in the

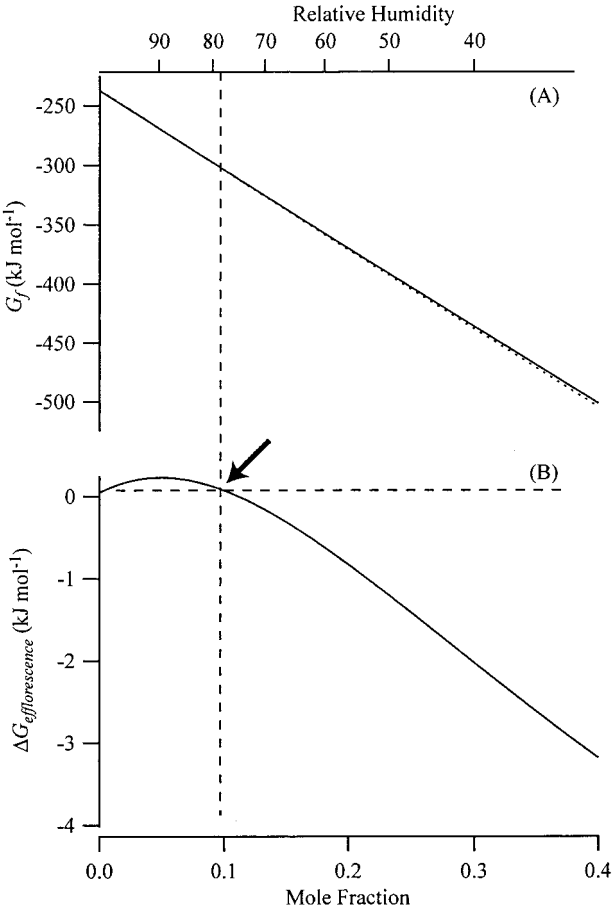

Figure 1. (A) Free energy of formation, G_f, of an aqueous ammonium sulfate solution (solid line) or water vapor and an ammonium sulfate crystal (dotted line) at 298 K. (B) Change in free energy for efflorescence (i.e., an aqueous solution changing to a water vapor and salt crystal). The arrow indicates the mole fraction at which the phase transition becomes exoergic. Relative humidities (upper axis) corresponding to the mole fractions (lower axis) are indicated. The free energies are calculated employing the methods described in Appendices A and B. (Thermodynamic values are adjusted slightly to match the known deliquescence RH of 79.5%.)

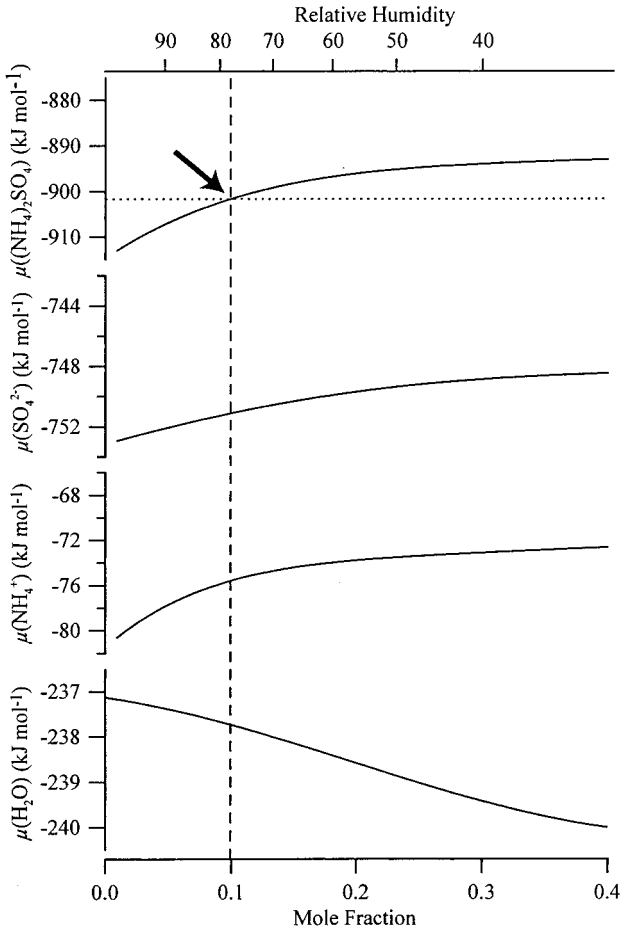

Figure 2. Chemical potentials, μ (lower three panels), of aqueous sulfate, aqueous ammonium, and water as a function of mole fraction composition in the binary aqueous $(NH_4)_2SO_4/H_2O$ system at 298 K. The upper panel shows the chemical potential of the solid salt (dotted line) and a virtual salt in equilibrium with the aqueous solution (solid line). The arrow indicates the mole fraction at which the phase transition becomes exoergic. Relative humidities (upper axis) corresponding to the mole fractions (lower axis) are indicated. The free energies are calculated employing the methods described in Appendices A and B. (Thermodynamic values are adjusted slightly to match the known deliquescence RH of 79.5%.)

direction of favorable change may often be much longer than an observer is interested in watching, in which case the change from a state of higher G to lower G is dubbed kinetically hindered. In phase transitions, this phenomenon commonly occurs for systems attempting to go from disordered phases (e.g., aqueous solution) to ordered phases (e.g., crystals), so that supersaturation and supercooling commonly occur. The kinetics of phase changes is the subject area of nucleation. Contrarily, for all atmospheric systems studied to date, ordered to disordered processes are not inhibited, and melting and dissolution readily occur. In these cases, phase diagrams (i.e., diagrams encapsulating results of free energy considerations) are useful guides to physical processes. In kinetically inhibited transitions, phase diagrams are still useful tools in that they at least provide constraints and driving forces on transitions.

Examples of the results of quantitative free energy calculations are shown in Figures 1 and 2. The details of how to employ tools available on the web servers to accomplish these quantitative calculations are provided in Appendices A and B. [Free energy calculations for atmospheric systems have one important simplification as compared to materials science or geology because the total pressure on the system rarely exceeds 1 atm, except for particles under 1 μm when the curvature induces pressure (i.e., the Kelvin effect). The effects of total pressure on nucleation rates of germ formation are also believed to be small over the domain of atmospheric systems, e.g., a 100-nm particle experiences 14 atm of pressure, as calculated by the Laplace equation. The effect is to reduce the freezing temperature of water droplets by a fraction of a degree. See Figure 6 of ref 126.] In Figures 1 and 2, ammonium sulfate and water are considered as arranged either (a) as a crystal and gaseous water or (b) as an aqueous solution. State *a* is denoted as the dashed line in Figure 1A, and state *b* is denoted as the solid line. Two facts are readily seen. First, state *a* is favored at low relative humidities. Second, the free energy

difference between *a* and *b* is small as compared to the absolute magnitude of the free energies, and thus it is difficult to discern whether *a* or *b* is favorable at high relative humidities. For this reason, the result of subtracting the free energies is shown in Figure 1B. The solid line in Figure 1B shows the driving force for an aqueous solution to form gaseous water and a crystal. Above 79.5% RH, the proposed reaction is endoergic, so an aqueous state is favorable whereas below 79.5% RH, the proposed process is exoergic and the crystalline state surrounding by gaseous water is favorable. There is thus a driving force for efflorescence for an aqueous solution below 79.5% RH.

An alternative approach to the thermodynamics of a system is provided by the chemical potential, as shown in Figure 2. A chemical potential of species *i*, μ_i, is $(\partial G/\partial n_i)_{T,P}$. As discussed in Appendix B, if a crystal of $(NH_4)_2SO_4$(s) is in equilibrium with an aqueous solution, then the chemical potential of the crystal is the sum of chemical potentials of the constituent aqueous ions. In this context, one can imagine a crystal in equilibrium with any aqueous system, and the chemical potential of this virtual crystal is prescribed by the aqueous constituents. In reality, the chemical potential of a pure crystal is fixed, so it is favorable for the crystal to uptake water and dissolve if the chemical potential of the virtual crystal is smaller than that of the pure crystal. As shown in Figure 2 (top), this condition is satisfied at 79.5% RH at 298 K. Useful thermodynamic quantities for free energy calculations of other electrolytes common in atmospheric particles and at other temperatures are provided in Table 1.

Table 1. Thermodynamic Properties of Species Common to Atmospheric Particles at 298.15 K[63,127−129] [a]

species	$\Delta G_f°$ (kJ mol^{-1})	$\Delta H_f°$ (kJ mol^{-1})	$C_P°$ (J mol^{-1} K^{-1})
NaCl(s)	−384.138	−411.153	50.50
$NaNO_3$(s)	−367.00	−467.85	92.88
$NaHSO_4$(s)	−992.8	−1125.5	85[b]
Na_2SO_4(s)	−1270.06	−1387.08	128.20
NH_4Cl(s)	−202.87	−314.43	84.1
NH_4NO_3(s)	−183.87	−365.57	139.3
NH_4HSO_4(s)	−823[b]	−1026.96	127.5[b]
$(NH_4)_2SO_4$(s)	−901.67	−1180.85	187.49
$(NH_4)_3H(SO_4)_2$(s)	−2207[b]	−1730[b]	315[b]
H^+(aq)	0	0	0
Na^+(aq)	−261.905	−240.12	46.4
NH_4^+(aq)	−79.31	−132.51	79.9
NO_3^-(aq)	−108.74	−205.0	−86.6
Cl^-(aq)	−131.228	−167.159	−136.4
SO_4^{2-}(aq)	−744.53	−909.27	−293.0
HSO_4^-(aq)	−755.91	−887.34	−84.0
HCl(g)	−95.299	−92.307	29.12
HNO_3(g)	−74.72	−135.06	53.35
NH_3(g)	−16.45	−46.11	35.06
H_2O(l)	−237.13	−285.83	75.29
H_2O(g)	−228.57	−241.82	33.58
H_2O(s) at 273.15 K	−241.29	−293.72	37.66
$H_2SO_4 \cdot H_2O$(s) at 220 K	8.39		
$H_2SO_4 \cdot 2H_2O$(s) at 220 K	−2.48		
$H_2SO_4 \cdot 3H_2O$(s) at 220 K	−8.81		
$H_2SO_4 \cdot 4H_2O$(s) at 220 K	−14.83		
$H_2SO_4 \cdot 6.5H_2O$(s) at 220 K	−23.28		
$HNO_3 \cdot H_2O$(s) at 230 K	21.99		
$HNO_3 \cdot 2H_2O$(s) at 230 K	−64.04		
$HNO_3 \cdot 3H_2O$(s) at 230 K	−8.69		
$HCl \cdot 3H_2O$(s) at 220 K	1.36		

[a] The described state for the aqueous ions is 1 *m*. The free energy of formation for all species is with respect to the elements at 298.15 K, except for the low-temperature acid hydates. The free energy of formation for these hydrates is with respect to the low-temperature 1 *m* aqueous ions, except NAD for which 1 atm gases at low temperatures is the initial state. An extensive table of values relevant to aqueous species is found in Stumm and Morgan.[130] [b] These values are estimated as explained in ref 128.

Common processes describing a change from one or more physical state to another have been given special names such as freezing, melting, dissolution, precipitation, crystallization, sublimation, deliquescence, or efflorescence. The concepts overlap to some extent, and authors have specific, particular usages. However, the following definitions and usage context are often applicable. Deliquescence and efflorescence specifically involve water vapor. When a crystalline material uptakes gas-phase water to form an aqueous solution, deliquescence occurs. This understanding is evidently part of a broader concept of dissolution. Deliquescence should not be confused with hygroscopic growth, which is the condensation of water vapor into an aqueous solution as relative humidity increases. The distinction is seen clearly for NaCl(s). At 75% RH (298 K), NaCl(s) changes entirely to NaCl(aq), which is deliquescence. Further increases in relative humidity dilute the concentration of NaCl(aq) by water condensation, which is hygroscopic growth. For an atmospheric particle of fixed salt content, the diameter of the particle responds to changes in water content. The precise distinction between deliquescence and hygroscopic growth is given in the discontinuity and continuity, respectively, of d*D*/d(RH) for the NaCl example. This distinction also holds for multicomponent systems (e.g., NaCl/KCl/H_2O).

Efflorescence is the reverse of deliquescence. As relative humidity decreases over an aqueous solution, water evaporates continuously until the highly concentrated electrolyte spontaneously crystallizes with the accompanying release of all remaining water to the gas-phase. Efflorescence is a specific process in the more encompassing concept of crystallization. Efflorescence and deliquescence are usually employed in the context of the cycling of relative humidity at a fixed temperature.

For cycles in temperature, the terms freezing, melting, precipitation, and dissolution are usually employed for changes in state between liquid and solid phases. Any alterations in the gas phase are often not considered. The term freezing is generally reserved for ice or hydrate formation (e.g., SAT) from an aqueous solution, while the term precipitation is often employed for crystallization from aqueous salt solutions as temperature falls, e.g., NaCl or $(NH_4)_2SO_4$. The terms melting and dissolution are employed as conjugates to the terms freezing and precipitation, respectively, for processes occurring during warming.

Processes specifically referring to the gas-phase exchange include sublimation, reverse sublimation, condensation, and evaporation. The last two terms are preferably reserved for gas/liquid exchange, whereas sublimation refers to gas/solid exchange. The terms are applied equally for both cycles in vapor pressure and in temperature. Beyond these several

terms referring to specific processes, many phase transition processes are not classified by specific terms. For these cases, general terms such as crystallization or solid−solid transition are often employed.

III. Phase Diagrams

A diagram depicting the thermodynamically favorable phases under variable conditions is called a phase diagram. Variable conditions often include component compositions, temperature, or vapor pressures. The coordinates of the phase diagram map the space of possible or relevant conditions. Each point in the diagram thus corresponds to one set of conditions. At each point, the arrangement of atoms in several configurations (e.g., phases) can be considered, and one arrangement yields a minimum in free energy. This phase is noted on the diagram at the one specific coordinate. This process is then generalized to create regions in the phase diagram possessing the property of a common phase. Depending on the complexity of a problem, representations of phase diagrams of 1−4 coordinates formally exist, although two- and three-coordinate systems are most common in atmospheric chemistry.

Examples of phase diagrams relevant to atmospheric chemistry and associated concepts are shown in Figures 3−18. Many representations (i.e., choice of axes) are possible, and one common form is shown in Figure 3 for binary systems. The ordinate is temperature, and the abscissa is composition. Gray regions indicate where crystal forms are thermodynamically favorable. For example, if a test tube containing 0.1 mol fraction of HNO_3 at 300 K is cooled, ice saturation is obtained near 244 K. A cooled test tube containing 0.2 mol fraction of HNO_3 obtains unity saturation with respect to NAT at 251.5 K. A white region showing where aqueous solutions are favorable compared to solids is termed the liquidus.

Figure 3 reveals a number of interesting features in atmospheric systems. The acids HNO_3, H_2SO_4, and HCl form an array of hydrates, as does NaCl. NH_4NO_3 exhibits several solid−solid-phase transitions when warmed, labeled I−IV. Each solid has the stoichiometry NH_4NO_3, but the atoms are arranged in different crystal structures. These related solids are termed polymorphs or modifications. $(NH_4)_2SO_4$ exhibits an interesting set of polymorphs as a high-temperature paraelectric crystal (labeled α-) and a low-temperature ferroelectric crystal (labeled β-). Polymorphism is also seen for $(NH_4)_3H(SO_4)_2$ (letovicite). Another interesting feature is shown in NH_4HSO_4/H_2O at 298 K. As expected in this chemical system, an aqueous solution with a low mole fraction composition equilibrates with a high water relative humidity (i.e., Raoult's law). However, reducing relative humidity leads to the evaporation of water, and the associated enrichment of the electrolyte until saturation is obtained with respect to a crystalline phase. Interestingly, at 298 K, the aqueous solution first reaches saturation with letovicite rather than ammonium bisulfate. However, at warmer temperatures (>301 K), the system first saturates with respect to the bisulfate.

A. Chemical Composition Coordinate

There are several common choices for the unit of the composition axis, including mole fraction, total ion mole fraction, weight percent composition, and molality. Examples are shown in Figures 3−7. Each choice has its benefits and limitations, and as discussed below, the most informative choice is often mole fraction. The scientifically most judicious choice is probably total ion mole fraction because these are natural units for application of Raoult's law. An example is shown in Figure 4. The disadvantage is that the determination of the total ion mole fraction is not easy when incomplete dissociation of electrolytes occurs, e.g., the presence of H^+, SO_4^{2-}, and HSO_4^-. Direct measurements of speciation or estimation by reference to a physical model of aqueous solutions is then necessary. Figure 4 was constructed by employing the model of Clegg et al.[134] From Figure 4, it is apparent that on an ion per ion basis, solutions of sulfuric acid yield greater freezing point depressions than ammonium bisulfate or sulfate in the order: $H_2SO_4(aq) \gg NH_4HSO_4(aq) > (NH_4)_2SO_4(aq)$. Unlike total ion mole fraction, solute mole fraction, weight percent, and molality are easily calculated.

The main benefit of the mole fraction unit is the comparison of chemically related solutes, as revealed in Figure 5. In the atmosphere, $H_2SO_4(aq)$ particles can be wholly or partially neutralized by exposure to $NH_3(g)$. The net effect is a change in the chemical identity of the solute without a change in its mole fraction composition (omitting differences in hygroscopicity and thus composition at a fixed atmospheric relative humidity). Figure 5 shows the change in the liquidus region as neutralization proceeds from $z = 0$ to $z = 2$ in $(NH_4)_zH_{2-z}SO_4$. Neutralized solutions achieve saturation at warmer temperatures and smaller mole fractions. In addition, the favorable crystal at higher mole fractions changes in sequence from SAT to THD to AS.

In literature, the most common unit employed by laboratory atmospheric chemists is weight percent. An example is shown in Figure 6. Weight percent is easy to calculate because mass fractions of solute and solvent are easily assayed on a balance. Beyond this utility, weight percent offers no benefits. Molality is a favored unit because it is the natural unit for freezing point depression. Electrolytes often exhibit ice freezing point depressions that are proportional to molality:[140]

$$\delta T = K_f\, m_{solute} \tag{1}$$

where δT is the ice freezing point depression, K_f is the cryoscopic constant, and m_{solute} is the solute molality. Similar to mole fraction, molality also exhibits the useful property that its value is constant when chemical composition changes as by $NH_3(g)$ uptake to neutralize $H_2SO_4(aq)$. Alas, molality suffers the property of having no termination value and a limiting value of infinity as the electrolyte concentrates. For this reason, the abscissa in Figure 7 does not terminate but is extended by an arrow. Comparison of Figures 3 and 7 shows that molality skews the appearance of phase diagrams to favor concentrated

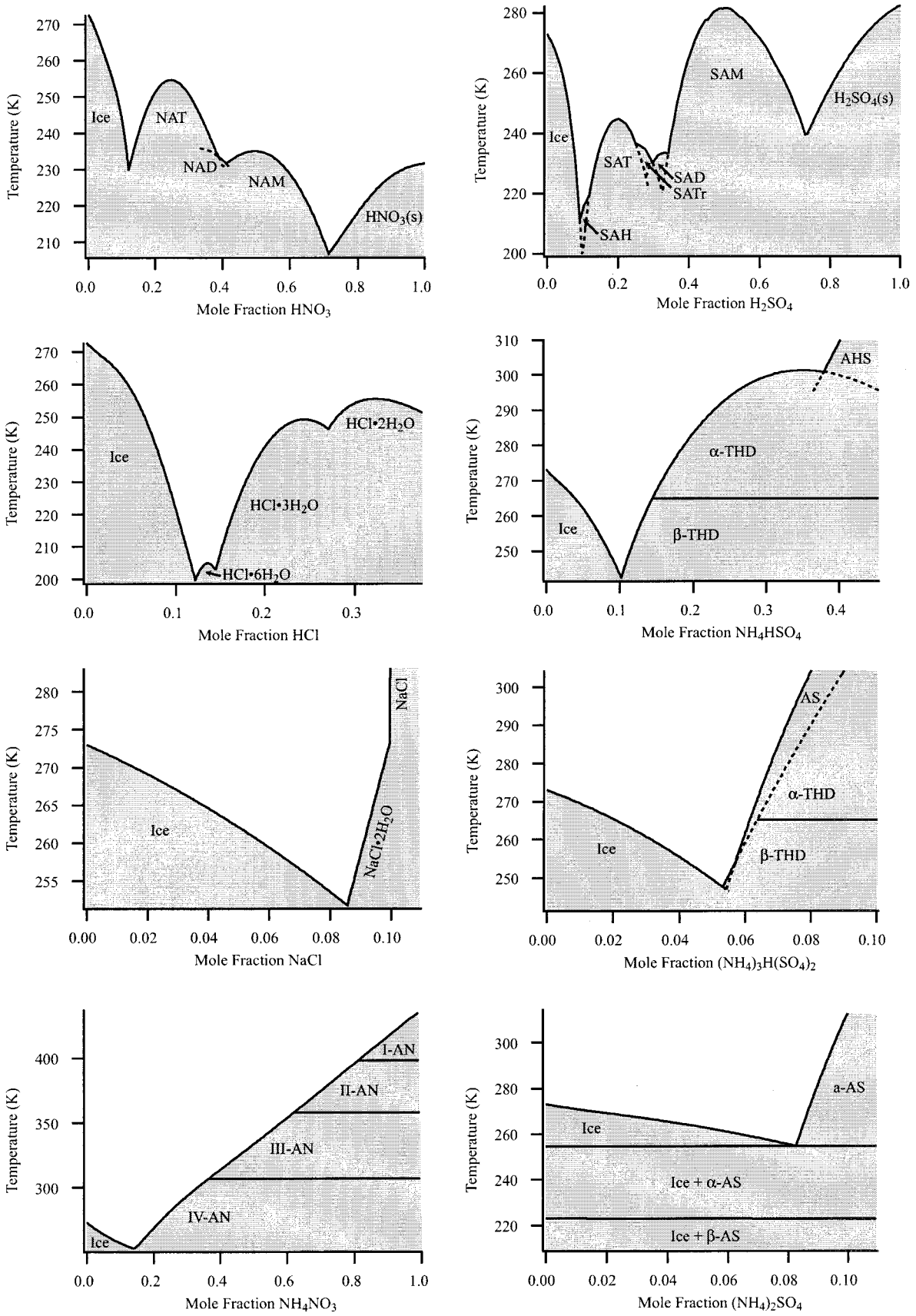

Figure 3. Liquidus phase diagrams of common atmospheric electrolytes in the coordinates of temperature and mole fraction. Solid lines show equilibrium between aqueous solutions and crystalline phases. Gray areas indicate regions where aqueous solutions are supersaturated with respect to a solid phase. Dashed lines show aqueous compositions metastable to one solid but in equilibrium with another. Abbreviations are as follows: AHS, NH_4HSO_4; AN, NH_4NO_3; AS, $(NH_4)_2SO_4$; NAD, $HNO_3·2H_2O$; NAM, $HNO_3·H_2O$; NAT, $HNO_3·3H_2O$; SAD, $H_2SO_4·2H_2O$; SAH, $H_2SO_4·6.5H_2O$; SAM, $H_2SO_4·H_2O$; SAT, $H_2SO_4·4H_2O$; SATr, $H_2SO_4·3H_2O$; and THD, $(NH_4)_3H(SO_4)_2$. Data sources are as follows: HNO_3/H_2O,[66,131] H_2SO_4/H_2O,[132] HCl/H_2O,[133] NH_4HSO_4/H_2O,[14,34,135] $NaCl/H_2O$,[136] $(NH_4)_3H(SO_4)_2/H_2O$,[134,135] NH_4NO_3/H_2O,[137] and $(NH_4)_2SO_4/H_2O$.[138,139] The solute mole fraction (x) relates to molality (m) and weight percent (w) as follows: $m = 1000x/(18(1 - x))$ and $w = 100M_w x/(18 + (M_w - 18)x)$ where M_w is the molecular weight of the solute.

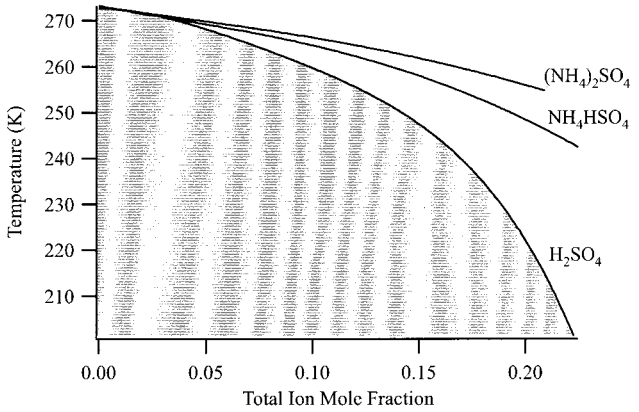

Figure 4. Ice liquidus curves in the ternary $(NH_4)_2SO_4/H_2SO_4/H_2O$ system for the compositions H_2SO_4(aq), NH_4HSO_4(aq), and $(NH_4)_2SO_4$(aq). The abscissa is the total ion mole fraction (i.e., $1 - x_{H_2O}$) as calculated from the model of Clegg et al.[134] Except for Figure 4, mole fraction always refers to the undissociated solute mole fraction (as defined in Figure 3) throughout this paper.

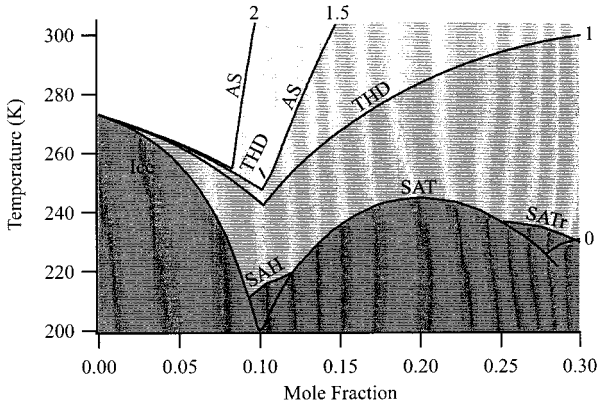

Figure 5. Dependence of the liquidus curve in the system $(NH_4)_2SO_4/H_2SO_4/H_2O$ on the ammonia content, $(NH_4)_zH_{2-z}SO_4$, where z varies from 0 to 2 and is denoted on several curves in the figure. The liquidus curve occurs at lower temperatures with increasing acid content. The equilibrium solid phases are denoted, viz. ice, AS, THD, SAH, SAT, and SATr. An aqueous solution having $z = 0$, 1, 1.5, or 2 is metastable to at least one solid if its temperature−mole fraction coordinate lies in a shaded region.

electrolytes. For these reasons, one purpose of this review is to argue that laboratory and modeling scientists working in the field of phase transitions should adopt solute mole fraction as their unit of choice.

B. Experimental Determination

The accurate determination of a phase diagram requires careful experimental work. Good compilations for classical work on many systems are provided in refs 141−143. However, systems of atmospheric interest are often at temperatures colder than reported in compiled work. For this reason, recent experimental work on the NH_4HSO_4/H_2O system was completed.[10,14,16] Other work on HNO_3/H_2O,[144,145] H_2SO_4/H_2O,[60] and $H_2SO_4/HNO_3/H_2O$[146] was carried out in the past decade to supplement existing information. Despite careful work, important discrepancies remain in the phase diagrams. For example,

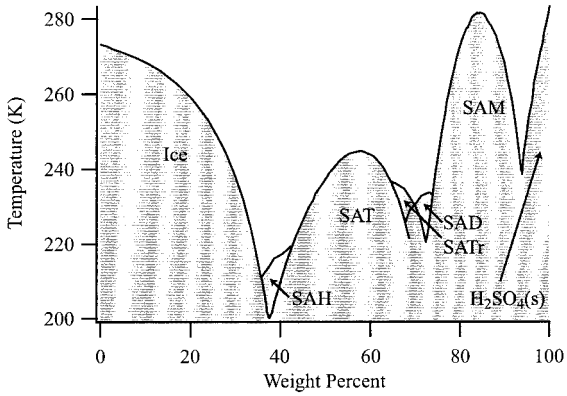

Figure 6. Aqueous sulfuric acid phase diagram represented in the coordinates of temperature and weight percent composition. The gray regions indicate that an aqueous solution is supersaturated with respect to a solid phase.

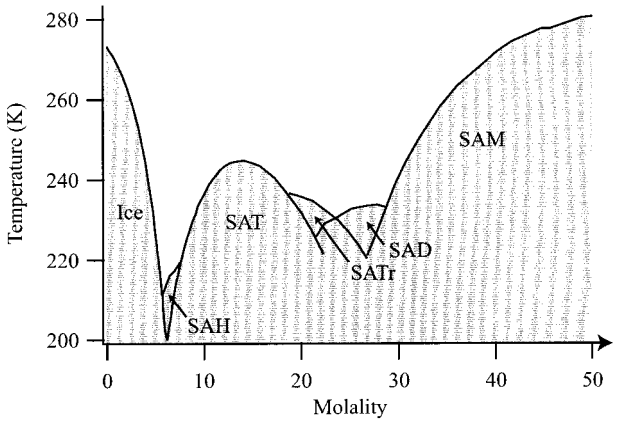

Figure 7. Aqueous sulfuric acid phase diagram represented in the coordinates of temperature and molality. The gray regions indicate that an aqueous solution is supersaturated with respect to a solid phase. The concentration axis is truncuated at 50 *m* because pure H_2SO_4 is infinite molal.

although the binary system H_2SO_4/H_2O has been intensively studied, Figure 8 shows several unresolved basic discrepancies between two seminal works by Hulsmann and Biltz[147] and Gable et al.[132] The black regions show that Hulsmann and Biltz report the formation of sulfuric acid octahydrate and do not observe sulfuric acid trihydrate, while Gable et al. report the formation of sulfuric acid hemihexahydrate instead of the octahydrate. To some extent, Hornung et al.[425] reconcile these differences through careful experiments that focus on this discrepancy and report the occurrence of both the hemihexahydrate and the octahydrate in the equilibrium phase diagram. The crystal structures of these two hydrates are provided by Mootz and Merschenz-Quack.[426] Accurate phase diagrams are difficult to determine both because careful temperature and composition measurements are necessary and because nucleation of the most thermodynamically stable phases often fails to occur readily.

C. Alternative Representations

Besides temperature−composition, there are other useful representations of phase diagrams, especially

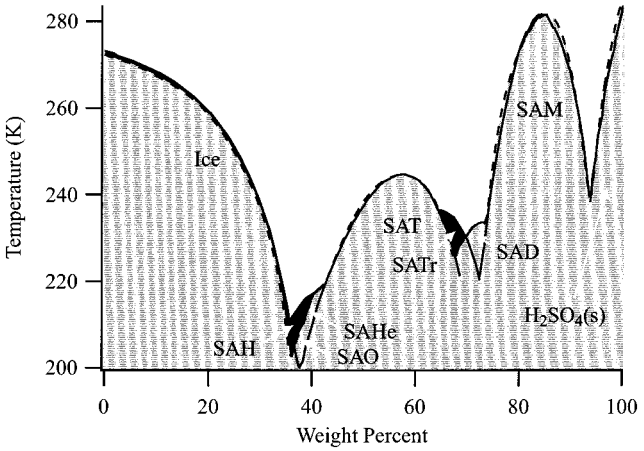

Figure 8. Aqueous sulfuric acid phase diagram from Gable et al.[132] (solid lines) as compared to Hulsmann. and Biltz (dashed lines).[147] The differences between the two liquidus curves are shown in black. Gable et al. report crystallization of $H_2SO_4 \cdot 6.5H_2O$ (SAH) and $H_2SO_4 \cdot 3H_2O$ (SATr) whereas Hulsman and Blitz do not obtain SATr and obtain $H_2SO_4 \cdot 8H_2O$ (SAO) and $H_2SO_4 \cdot 6H_2O$ (SAHe) in the vicinity of SAH. Accurate phase diagrams require extensive laboratory work and even then discrepancies among workers often remain.

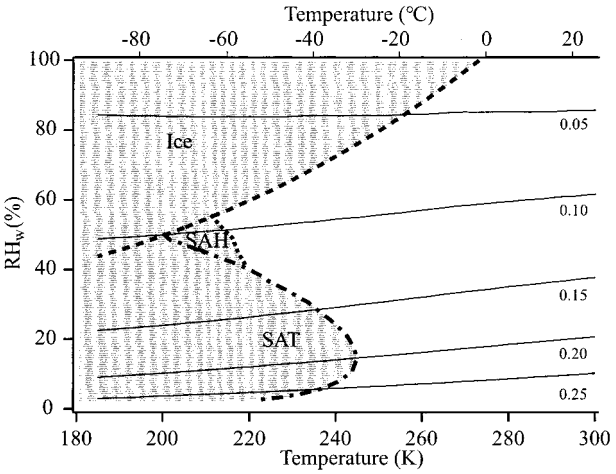

Figure 9. Aqueous sulfuric acid phase diagram represented in the coordinates of relative humidity with respect to water and temperature. The gray regions indicate that an aqueous droplet is supersaturated with respect to a solid phase, including ice (— —), SAH (- - -), and SAT (— - —). The thin solid lines show the mole fraction composition of an aqueous droplet equilibrated with water vapor and temperature. Measurements of the coordinate quantities are obtained within air parcels by aircraft and balloons at high temporal and spatial resolution. Remote sensing of RH_w and temperature are also sometimes possible from satellite-based images, though usually at lower temporal and spatial resolutions. In the atmosphere, changes in RH_w and temperature are sometimes rapid enough (e.g., updrafts in cirrus or polar stratospheric cloud formation) that aqueous droplet composition does not maintain equilibrium with the gases.

in the atmospheric sciences. Examples are shown in Figures 9 and 10. In Figure 9, relative humidity with respect to water is the ordinate, and temperature is the abscissa. The liquidus region of aqueous sulfuric acid is again shown as the white area, and regions supersaturated with respect to one or more solids are gray. An air parcel at 260 K and 20% RH may experience increasing relative humidity, corresponding to a vertical move at 260 K to higher relative humidities. At 88% RH, aqueous particles reach unity saturation with respect to ice. The representation in Figure 9 is particularly favored by atmospheric scientists conducting field measurements because airborne platforms are usually equipped to measure RH and temperature.[148−150] With this information and the diagram in Figure 9 as well as knowledge that the particle composition is H_2SO_4/H_2O, one knows if aqueous particles are thermodynamically favored.

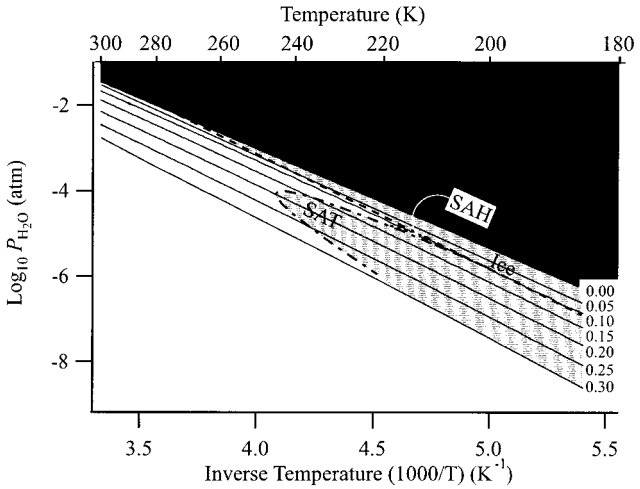

Figure 10. Aqueous sulfuric acid phase diagram represented in coordinates of log pressure and inverse temperature (Clausius−Clapeyron plot). The solid lines show the water vapor pressure of aqueous sulfuric acid solutions for concentrations ranging from 0 to 0.30 mol fraction. The gray regions indicate supersaturation with respect to several solids, including ice (— —), SAH (- - -), and SAT (— - —). The near edge of the black region is liquid water.

Another useful representation of the phase diagram is the Clausius−Clapeyron plot, log P_{H_2O} plotted against inverse temperature. For a system at constant composition (e.g., a beaker of sulfuric acid in the lab), the Clausius−Clapeyron equation[140] holds when

$$\log_{10}\frac{P(T)}{P_{\mathrm{ref}}} = -\frac{\Delta H}{2.303R}\left(\frac{1}{T} - \frac{1}{T_{\mathrm{ref}}}\right) \qquad (2)$$

where $P(T)$ is the water vapor pressure at temperature T, P_{ref} is the water vapor pressure at the reference temperature T_{ref}, and ΔH is the enthalpy of condensation for gaseous water and sulfuric acid to form an aqueous solution. Equation 2 can be written as follows:

$$\log_{10} P(T) = -\frac{\Delta H}{2.303R}\frac{1}{T} + \left(\frac{\Delta H}{2.303R}\frac{1}{T_{\mathrm{ref}}} + \log_{10} P_{\mathrm{ref}}\right) \qquad (3)$$

A log P_{H_2O} plotted against inverse temperature is then linear, and the slope yields ΔH for a particular concentration of an aqueous solution. This result is shown in Figure 10 for H_2SO_4/H_2O mole fractions from 0 to 0.30.

Also shown in Figure 10 are the regions in gray where aqueous solutions are supersaturated with

respect to ice, SAH, and SAT. Of particular interest, as an atmospheric aqueous particle cools at constant log P_{H_2O}, its composition adjusts (i.e., dilutes) to maintain the same vapor pressure at colder temperatures. In Figure 10, this is a horizontal movement from low to high inverse temperature. For log $P_{H_2O} = -4.3$, an aqueous particle reaches saturation with respect to SAT at 4.11 inverse temperature and 0.22 mol fraction composition. SAT also is in equilibrium at the same vapor pressure with 0.14 mol fraction aqueous composition at 4.32 inverse temperature. Thus, according to the thermodynamic description, an aqueous particle cooling would first form SAT at 4.11 inverse temperature and then melt to again form an aqueous solution at 4.32 inverse temperature. The implication is that SAT is "water-poor" and "water-rich" at these temperature extrema,[60] meaning that the composition is slightly altered from a stoichiometric solid to $H_2SO_4 \cdot (4 + x)H_2O$, where x is positive for water-rich and negative for water-poor. The value $|x|$ is undoubtedly small and may be difficult to measure by conventional means.[151] Even so, the concept of impure phases is important in phase transitions, and chemical potentials of the constituents (viz. $\mu(SO_4^{2-})$, $\mu(H^+)$, and $\mu(H_2O)$) in the water-poor hydrate are not equal to those in the water-rich hydrate. In the two cases, the chemical potentials are respectively equal to those in the concentrated and dilute aqueous solutions on the two branches of the liquidus curve. Similarly, water-rich and water-poor hydrates also exist for HNO_3 and HCl.[112,152] Ice in equilibrium with aqueous acid solutions is slightly impure, and measurements have been carried out for HCl showing up to 6.2×10^{-5} mol fraction contamination at the eutectic (vide infra) between ice and the hexahydrate and for HNO_3 of up to 7.4×10^{-7} mol fraction at the eutectic of ice and the trihydrate (Figure 3).[153,154] The possible incorporation of acids into and on ice PSCs is discussed in ref 429.

Quite commonly, the utility of a phase diagram is enhanced by plotting additional information, as shown in Figures 11−13. For example, at constant temperature each composition of H_2SO_4/H_2O has a unique water vapor pressure. In $\log_{10}$ units (atm), these vapor pressures are shown as contours in Figure 11. A decrease of 6−8% P_{H_2O} per degree K is common. As a result, over the atmospheric temperature range, water vapor pressure decreases by up to 6 orders of magnitude at a fixed composition. In contrast, at a fixed temperature, water vapor pressure varies only with relative humidity, i.e., at most by 2 orders of magnitude.

Figure 11 also introduces the important idea of trajectories. In the laboratory, the water vapor pressure over a test tube of solution can be studied. When the temperature decreases, the vapor pressure also decreases so water molecules condense into the solution. However, for all practical purposes, the composition of the aqueous solution can be regarded as unchanged because the number of moles of water in solution vastly exceeds the number of moles in the gas phase. In this case, a test tube trajectory for cooling in Figure 11 can be regarded as a vertical line of constant composition. In the atmosphere, the opposite condition prevails. Most of the water is in the gas phase (excluding fogs and clouds), so the water pressure remains constant while the particle composition adjusts to obtain a vapor pressure equal to the partial pressure. For this reason, one of the contours in Figure 11 represents an idealized atmospheric trajectory. To a good approximation, a rising air parcel cools adiabatically due to expansion.[155] The numerical effect of decreased total pressure on the water partial pressure is only secondary.[138] Then, the composition of aqueous particles in a rising air parcel dilutes. Given the information of an initial temperature and composition, one can place a point in Figure 11, and one can estimate the aqueous composition at any cooler temperature by following the contour (absent particle curvature, thermal transfer, and mass accommodation effects).[60,138]

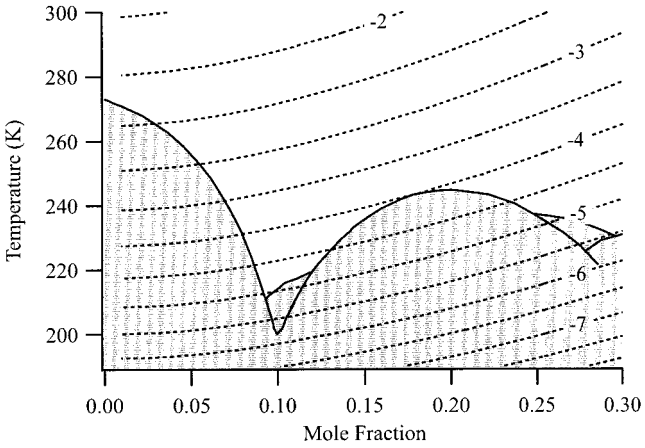

Figure 11. Contours of constant water vapor pressure ($\log_{10}$ atm) are shown for aqueous sulfuric acid solutions in temperature−mole fraction coordinates. The gray regions indicate that the aqueous solution is supersaturated with respect to at least one solid.

The ice saturation ratio of an aqueous solution is obtained by dividing the water vapor pressure over the solution by the vapor pressure of ice, as shown in Figure 12 for H_2SO_4/H_2O over a range of temperatures and compositions. A unity ice saturation ratio exists along the ice freezing point depression line. One idealized atmospheric trajectory is shown for log $P_{H_2O} = -5$. The intersection of this trajectory with unity ice saturation is the ice frost point and occurs at 213 K. Even though ice becomes thermodynamically stable at that point, the nucleation of ice near the phase line occurs more slowly than the rate of changes in the chemical system (i.e., dT/dt and da_{H_2O}/dt) during atmospheric processes, which occur on the scale of seconds[156,157] to weeks. For this reason, a warm particle in the liquidus region for log $P_{H_2O} = -5$ is initially concentrated sulfuric acid. When the air parcel cools, the aqueous particles become saturated with respect to several solids, yet no solid nucleation occurs. As discussed later (see section IV, Kinetics), the ice nucleation rate does not become comparable to the rate of changes in the chemical system (i.e., dT/dt and da_{H_2O}/dt) in typical atmospheric trajectories until the ice saturation ratio approaches 1.5. The result is that ice nucleation is described to occur for $S = 1.5$. The background lower stratosphere conditions (215−240 K) are typically

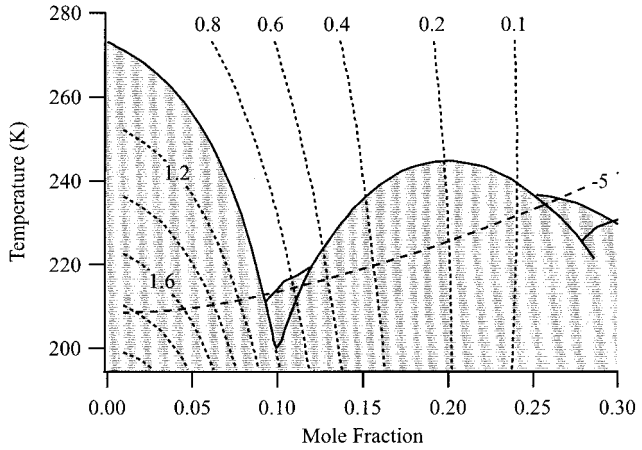

Figure 12. Contours of constant saturation ratio with respect to ice are shown for aqueous sulfuric acid solutions in temperature−mole fraction coordinates. Note that relative humidity with respect to ice is 100 times the saturation. The temperature−composition trajectory of an aqueous droplet maintaining vapor equilibrium within an air parcel having a 213 K ice frost point ($P_{H_2O} = 10^{-5}$ atm) is shown. The gray regions indicate that the aqueous solution is supersaturated with respect to at least one solid.

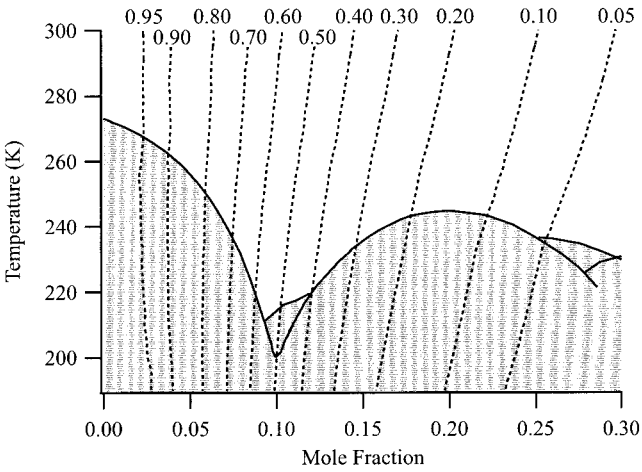

Figure 13. Contours of constant water activity over a flat surface are shown for aqueous sulfuric acid solutions in temperature−mole fraction coordinates. The gray regions indicate that the aqueous solution is supersaturated with respect to at least one solid.

even drier (log $P_{H_2O} = -6.6$), and a concentrated sulfuric acid aerosol called the Junge layer exists alongside the global ozone layer. At all times, these aqueous aerosols are saturated with respect to one or more sulfuric acid hydrates, yet nucleation of solids does not occur.

Similar to the ice saturation ratio, the water saturation ratio (i.e., water activity) is obtained by dividing the solution's water vapor pressure by the liquid water's vapor pressure, as shown in Figure 13. Water activity is equivalent to relative humidity when the aqueous composition of particles is fully equilibrated with the vapor phase (i.e., rapid mass transfer) and the Kelvin effect is negligible (i.e., 1 μm diameter). For an ideal solution obeying Raoult's law, the water activity lines in Figure 13 would depend solely on mole fraction composition and would thus be vertical with respect to temperature. In fact, sulfuric acid undergoes temperature-dependent dissociation, favoring SO_4^{2-} at lower temperatures.[26] [Note that the calculations shown in Figure 4B of the ref 26 are wrong, although the experimental data and the qualitative trends of Figure 4B are correct. Download a corrected version at author's website.] Thus, the total ion mole fraction is greater at lower temperatures for the same H_2SO_4 solute mole fraction. Partially for this reason, the slope in Figure 13 is from right-to-left with decreasing temperature. In addition, sulfuric acid exhibits nonideal behavior. In the atmosphere, changes in relative humidity in the atmospheric boundary layer often occur with only modest changes in temperature. Then, at constant temperature, a decrease in relative humidity leads to the evaporation of water from an aqueous sulfuric acid particle. There are accompanying changes in particle physicochemical properties, such as size and light scattering or aqueous concentration and heterogeneous chemistry.

D. Equilibrium Phase Changes

Phase diagrams can be powerful tools to quantify changes in a system accompanying a process, such as cooling. Several important concepts are illustrated in Figure 14. The most common representation of a phase diagram is shown in Figure 14A with each region labeled. Beginning with a test tube trajectory with decreasing temperature at point A (i.e., a vertical drop in temperature at constant mole fraction composition), a 0.05 mol fraction of aqueous solution is in the liquidus region (white) until intersecting with the ice line at point B. Further cooling to point C indicates that the original liquid system at point A has now rearranged into ice and aqueous liquid, with the overall composition remaining constant. By point D, the system is rearranged into ice and NAT, again the overall composition remaining constant. In this analysis, thermodynamic equilibrium is assumed to be maintained at points A−D.

An immediate question is the fractionation into ice and liquid or into ice and NAT such that the overall composition does not change. Figure 14B shows tie lines in regard to relative amounts of materials. An aqueous system cools along the 0.22 mol fraction line into the NAT and aqueous liquid region. The tie lines shown provide segment lengths A′ and B′ at 240 K. At this temperature, the relative amounts of NAT to aqueous liquid is the ratio of A′ to B′. The aqueous phase composition is given by the intersection of segment A′ and the liquidus line. Note that the composition of NAT is water-rich as indicated by the bowed dashed line (solidus) although exaggerated in mole fraction extent for clarity. [Figure 5 of ref 19 provides a visual example of H_2SO_4/H_2O particles supported on a microscope slide as they change from crystalline to crystalline/aqueous to aqueous during melting on the ice liquidus line.]

Figure 14B shows several other important concepts. Cooling along the dashed line (0.22 mol fraction) yields a dilute liquid-phase composition at 229.5 K that is saturated with respect to ice. Ice and NAT both precipitate until no aqueous liquid remains. This invariant temperature/composition point is called the eutectic. When a 0.30 mol fraction solution is cooled, NAT crystallizes and the aqueous solution concen-

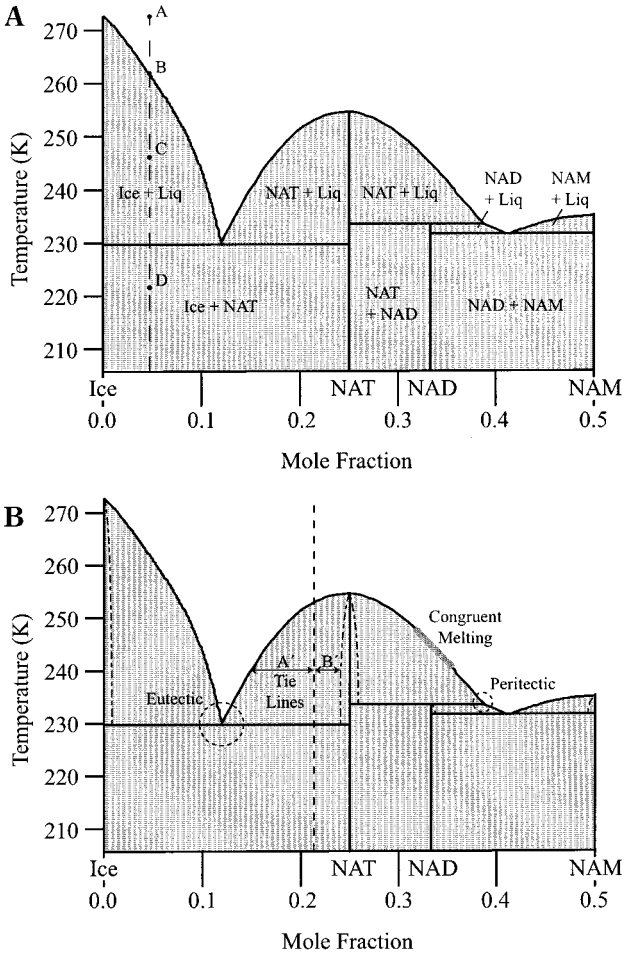

Figure 14. Concepts and labels in phase diagrams of binary systems shown for aqueous nitric acid. (A) Labeling emphasizes equilibrium solids. The temperature and overall chemical composition of a system specify an $\{x,y\}$ point in the diagram. This point falls within one of the labeled areas indicating the equilibrium solids and liquids present in the system. For example, a system at 220 K of overall composition of 0.3 mol fraction contains NAT and NAD crystals and no liquid. (B) Labeling emphasizes processes accompanying phase changes. Eutectic and peritectic points, tie lines, congruent melting, and solidus composition are discussed in the text.

trates until the peritectic point is reached. At this point, the aqueous-phase and NAT combine to form NAD: one liquid and one solid combine to form a second solid and the same composition liquid, albeit the liquid phase is at an adjusted total mass fraction of the entire system as necessary to form the second solid. In this example, the aqueous liquid is eventually exhausted, and NAT and NAD crystals remain. However, if the original solution were 0.35 instead of 0.30, then the NAT crystals would be exhausted before the aqueous solution. In this case, the NAD and aqueous solution would continue to exist until the eutectic point between NAD and NAM was obtained. These features and their dependence on 0.30 versus 0.35 overall composition are reflected in Figure 14A. The formation of a liquid and solid from a solid is termed incongruent melting and is associated with a peritectic. Congruent melting refers to a solid forming a liquid. Other classic processes important in materials science, geology, and other disciplines do not have any known examples in atmospheric phase transitions, including spinodal decomposition (demixing), eutectoid, and peritectoid. [Free energy calculations akin to Figures 1 and 2 show that suggestions in refs 74 and 75 that spinodal decomposition could occur in $(NH_4)_2SO_4/H_2O$ and other electrolyte systems are surely wrong at 298 K. At lower temperatures, Rasmussen suggests that spinodal decomposition occurs in ice formation from aqueous solutions.[126,158,159]]

E. Ternary and Higher Order Systems

Atmospheric systems often contain several electrolytes. For example, the dominant species in polar stratospheric clouds are $H_2SO_4/HNO_3/H_2O$. Seawater salts are roughly 48.7 mol % Cl^-, 41.7% Na^+, 4.7% Mg^{2+}, 2.5% SO_4^{2-}, 0.1% Ca^{2+}, and 0.1% K^+. Gibbs' Phase Rule provides the number degrees of freedom, F, in a system containing C components and P phases as[160]

$$F = C - P + 2 \tag{4}$$

Then, for the binary systems (i.e., $C = 2$) so far considered, $F = 4 - P$. When aqueous solution and gas are present (i.e., $P = 2$), two degrees of freedom remain, and a two-dimensional plane sheet of paper is a convenient medium of expression. Typically, the degrees of freedom are assigned to temperature and composition, which become the axes. Immediately moving to three components, however, three degrees of freedom are present. Several unique approaches have been developed over the years to express valuable information about multidimensional systems on two-dimensional sheets of paper, as shown in Figures 15−17. In Figure 15, temperature is fixed, and the remaining degrees of freedom are expressed as two composition axes. In Figure 16, a triangle is employed to express composition.[18] Although there are three axes, only 2 degrees of freedom are employed because at all times $1 = x_{H_2O} + x_{H_2SO_4} + x_{HNO_3}$. The third axis is merely informational. The trick to Figure 16 is that an additional axis is temperature and comes out of the page. In three dimensions, Figure 16 appears as hills and valleys.[18,162] Figure 17 contains five components and has 5 degrees of freedom when gas−liquid are present.[161] Water activity (i.e., relative humidity) comes out of the page. The remaining 4 degrees of freedom are the vertexes of the square, and this artifice is possible for this particular system because of shared ions in the components.

The phase diagram of the ternary system NaCl/Na_2SO_4/H_2O at 298 K is shown in Figure 15. The liquidus region is shown in white, and contours of constant relative humidity for different aqueous solution concentrations are shown. For aqueous solutions enriched in Na_2SO_4, the solid decahydrate $Na_2SO_4 \cdot 10H_2O$(s) is thermodynamically preferred to Na_2SO_4(s). In the atmosphere, changes in relative humidity are accompanied by water evaporation or condensation. However, the ratio of NaCl:Na_2SO_4 remains constant. In this case, an atmospheric trajectory is a line of constant slope passing through the origin, as shown in the figure for the 1:1 composition. Once the decahydrate begins to form, the

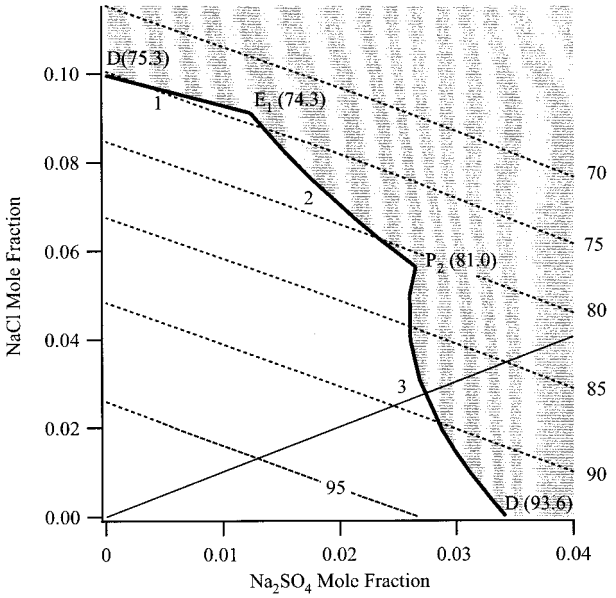

Figure 15. Representation of a ternary chemical system shown for the isothermal phase diagram of $NaCl/Na_2SO_4/H_2O$ (298 K). Solubility limits of NaCl (1), Na_2SO_4 (2), and $Na_2SO_4 \cdot 10H_2O$ (3) are shown. Contours of constant relative humidity for aqueous solutions are shown as dashed lines: The deliquescence points (*D*) are shown for NaCl(s) and $Na_2SO_4 \cdot 10H_2O$(s) as well as the eutonic point (*E*) (sometimes called mutual deliquescence point) of NaCl(s)/Na_2SO_4(s) and the peritonic point (*P*) of Na_2SO_4(s)/$Na_2SO_4 \cdot 10H_2O$(s). The thin line shows the aqueous composition trajectory of a 1:1 chemical system as relative humidity changes. The figure is calculated from the model of Clegg et al.[134]

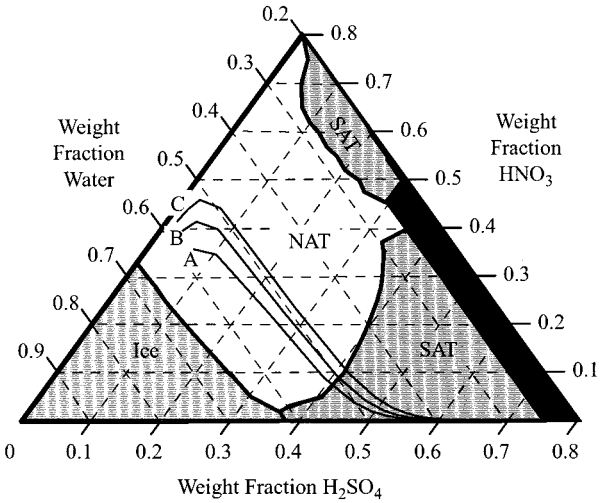

Figure 16. Representation of a ternary chemical system including the dependency on temperature shown in a triangle representation of $H_2SO_4/HNO_3/H_2O$. The intersection of the three dashed lines provides the composition of an aqueous solution. The diagram is a two-dimensional projection of a three-dimensional figure. The temperature axis (*z*-axis) comes directly out of the page toward the reader in the direction of increasing temperature. The shaded regions indicate the first solid to obtain unity saturation upon cooling the aqueous solution; specific temperatures are omitted from the diagram. The solids considered in this example are ice (light gray), sulfuric acid tetrahydrate (SAT, dark gray), and nitric acid trihydrate (NAT, white). The lines A−C are the trajectories of the equilibrium aqueous compositions upon cooling under typical polar stratospheric conditions: A, 50 mb, 5 ppm H_2O, 0.5 ppb H_2SO_4, and 5 ppb HNO_3; B,10 ppb HNO_3; and C, 20 ppb HNO_3. The aqueous particles are supercooled with respect to one or more solids throughout most of the trajectory (not specifically shown in diagram). (Adapted with permission from ref 18. Copyright 1998 American Geophysical Union.)

relative aqueous solution content of Na_2SO_4(aq) decreases while enriching in NaCl(aq). Then, the aqueous composition follows the liquidus line until 81.0% RH. At that point, there is a peritonic transition. The decahydrate evaporates to form Na_2SO_4(s) in equilibrium with the aqueous liquid. Further decreases in RH are accompanied by additional crystallization of Na_2SO_4 until 74.3% RH. At that point, NaCl(s) also crystallizes, and the aqueous liquid partitions entirely into NaCl(s) and Na_2SO_4(s). This point is called the eutonic, at which point the aqueous composition is in equilibrium with two solids. It is also the minimum RH required for the presence of an aqueous phase. Tie lines can also be drawn in this representation.[163]

A partial (the included phases are aqueous, ice, SAT, and NAT) phase diagram for the ternary system $H_2SO_4/HNO_3/H_2O$ is shown in Figure 16. Temperature comes out of the page, and the diagram shows the first solid to crystallize, if thermodynamic equilibrium is maintained, when an aqueous solution of a composition indicated by the axes is cooled. Ice, NAT, and SAT are favored toward the respective H_2O, HNO_3, and H_2SO_4 vertexes. The diagram does not explicitly show the temperatures at which the solids form, although the representation can do so by the addition of temperature contour lines.[144] The lines A−C indicate idealized composition trajectories of aqueous particles under typical polar stratosphere conditions during cooling. Explicit temperatures are again omitted. For most portions of the aqueous trajectories shown, the aqueous particles are metastable with respect to several solids, including NAT and SAT. This fact is again not shown explicitly in this two-dimensional representation, but a three-dimensional rendering reveals that the aqueous trajectories pass inside the envelope of unity saturation with respect to the solids.[18] Figure 16 thus provides valuable information, but understanding it requires the explanation provided in this paragraph of omitted temperatures and implicit metastability. The proper understanding of the projection of multidimensional phase diagrams into two-dimensional representations quite often requires specific education on the system and the representation.

Continental boundary layer aerosols are often found to be composed predominantly of sulfates in the eastern half of the United States and of nitrates in the western half, although on many occasions mixed sulfates and nitrates are present. In addition, these acids can be partially to wholly neutralized by ammonia coming from fertilizers and animal husbandry. The result is a five-component system, $(NH_4)_2SO_4/H_2SO_4/NH_4NO_3/HNO_3/H_2O$. Potukuchi and Wexler have successfully represented this system in a useful way in two dimensions, as shown in Figure 17.[161] Any aqueous composition at 298 K is reduced to coordinates *X* and *Y*. The diagram then shows the first solid to form upon reducing relative humidity, according to a thermodynamic description. The au-

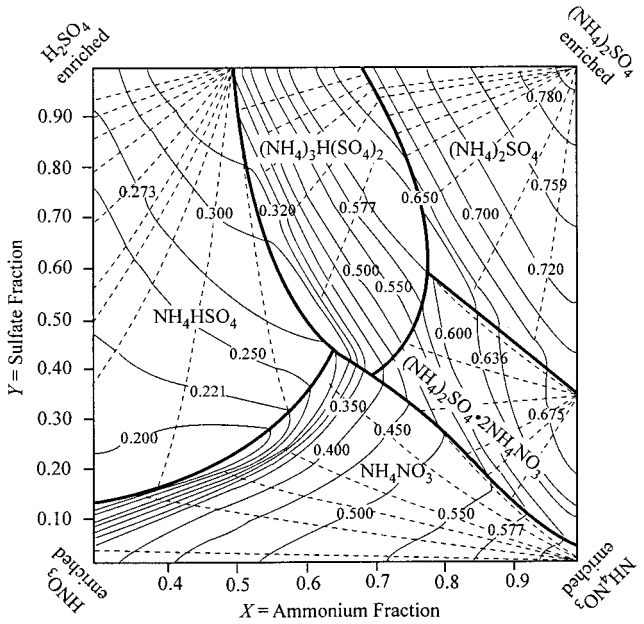

Figure 17. Phase diagram of an isothermal five-component chemical system shown for $(NH_4)_2SO_4/H_2SO_4/NH_4NO_3/HNO_3/H_2O$ (298 K). The system is successfully reduced to a two-dimensional representation by employing an artifice for the axes that recognizes the ion commonalities of the components. An aqueous solution composed of $a-d$ moles of $(NH_4)_2SO_4$, H_2SO_4, NH_4NO_3, and HNO_3, respectively, contains $(2a + c)NH_4^+$, $(2b + d - x)H^+$, $xHSO_4^-$, $(a + b - x)SO_4^{2-}$, and $(c + d)NO_3^-$ moles where x is set by the equilibrium constant for bisulfate formation. The total number of cations is $(2a + 2b + c + d)$, and the fraction arising from ammonium is $(2a + c)/(2a + 2b + c + d)$, which is the X-axis coordinate in the figure. As this coordinate increases, more $(NH_4)_2SO_4$ and NH_4NO_3 are in solution. Similarly for the Y-axis, the total fraction of the anions arising from sulfate is $(a + b)/(a + b + c + d)$. As this coordinate increases to unity, more H_2SO_4 and $(NH_4)_2SO_4$ are in solution. The solid lines indicate the water activities of aqueous solutions of the indicated $\{X,Y\}$ compositions in equilibrium with the solid phases noted in the figure. Water activity is visualized as coming out of the page toward the viewer. The dashed lines show changes in aqueous phase composition accompanying material removal by crystallization as relative humidity decreases. (Adapted with permisson from ref 161. Copyright 1995 Elsevier Science.)

thors added dashed lines to indicate the subsequent liquid phase composition with reducing relative humidity as more solid crystallizes (i.e., the liquidus lines). When the dashed lines intersect the heavy lines, a second solid precipitates. For continued reductions in RH, the aqueous composition follows the heavy lines until an invariant point is reached with the intersection of a second heavy line. These invariant points are analogous to eutonic and peritonic in three-component systems: the aqueous solution may cease to exist by fully crystallizing into two or more solids, or alternatively, one crystal may disappear entirely through the absorption or release of aqueous phase material with an associated crystallization into one or more new solids. In the latter case, further reductions in relative humidity continue to change the aqueous composition. The two cases are respectively distinguished by a local minimum or a local saddle point in the RH values. The three central invariant points in Figure 17 are local saddle points analogous to peritonic points in three-dimensional systems. The result is that, for any composition containing HNO_3, the aqueous phase never ceases to exist at 298 K. Pure sulfate systems also fail to crystallize completely for $X < 0.5$ at 298 K. Including water, the system has five components and thus possesses 4 degrees of freedom (eq 4) under isothermal conditions when two phases (viz., aqueous and vapor) are present. At all times, 1 degree of freedom is also used in Figure 17 to specific water activity. Then, the maximum number of solids that can be present in equilibrium with the aqueous phase is three, which are the indicated invariant points in the system.

An interesting example to consider is an aqueous system initially at 85% RH with $X = 0.80$ and $Y = 0.90$. These coordinates specify a nonunique composition for $(NH_4)_2SO_4/H_2SO_4/NH_4NO_3/HNO_3 = a:b:c:d$. When we let $a = 10$ and $c = 1$, we obtain $b = 2.43$ and $d = 0.38$. Upon decreasing relative humidity, according to Figure 17, the first solid to form under equilibrium conditions is $(NH_4)_2SO_4$(s) at 71% RH, and the system consists of $(NH_4)_2SO_4$(s) and aqueous solution between 67 and 71% RH. At 67% RH, a second solid precipitates. The overall sequence of equilibrium phases from 85 to 20% RH is as follows: {aqueous solution from 85 to 71%}, {$(NH_4)_2SO_4$(s) and aqueous solution from 71 to 67%)}, {$(NH_4)_2SO_4$(s), $(NH_4)_3H(SO_4)_2$(s), and aqueous solution from 67 to 59%}, {$(NH_4)_3H(SO_4)_2$(s), $(NH_4)_2SO_4$(s)·$2NH_4NO_3$(s), and aqueous solution from 59 to 37%}, {$(NH_4)_2SO_4$(s)·$2NH_4NO_3$(s), NH_4NO_3(s), and aqueous solution from 37 to 27%}, and {NH_4NO_3(s), NH_4HSO_4(s), and aqueous solution from 27 to 20%}. Another complex example is seawater, roughly consisting of 7 chemical components, which passes through a complex array of equilibrium crystals (including hydrates) and aqueous phases on decreasing relative humidity or temperature.[421]

F. Surface Region

Aqueous atmospheric particles solidify when dried or cooled sufficiently. Although the interior of the particle is crystalline, the surface region has an aqueous character (sometimes labeled quasi-liquid layer) of adsorbed water and high mobility ions.[164,165] The liquid character of the surface region (also called a surface phase) is especially prevalent as the melting temperature or deliquescence relative humidity is approached. All nominally dry ionic solids are coated by fractional monolayer coverage of water ($0.05 < \theta < 2$) at atmospheric relative humidities.[166] For example, the adsorption isotherm of H_2O on polycrystalline NaCl is shown in Figure 18.[167] The adsorption isotherm constitutes one representation of a phase diagram for the surface region. Ice is also believed to have a surface region with properties better classified as liquid than solid, especially above -12 °C.[8,168−170] As such, nucleation of the liquid phase during the melting of ice appears to occur in the disordered surface region, and further melting then proceeds inward.[171−173]

The conceptual framework for understanding the surface region is the electrochemical potential, μ, which is constant for a species in equilibrium from

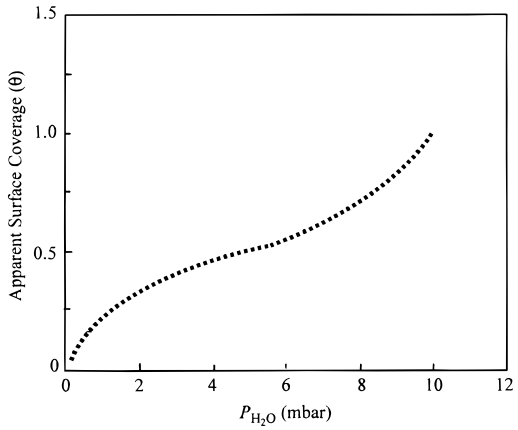

Figure 18. Adsorption isotherm of H_2O on polycrystalline NaCl. (Adapted with permission from ref 167. Copyright 1974 Elsevier Science.)

one phase through the interface into the next phase.[8,174] This requirement initiates surface reconstruction at most interfaces. For example, the surface atoms at a NaCl interface formed by abrupt termination of the crystal with its vapor experience an unbalanced force field. A strong force originates from the interior crystal atoms, and a weak force exists on the vapor side. The net result is an increased electrochemical potential of the surface atoms. The potentials of the surface atoms relax to bulk crystalline values by atomic relocation in the initially unbalanced force field (i.e., surface reconstruction). Furthermore, if the vapor phase contains water (i.e., humidity), then at the unreconstructed abrupt termination there is initially a discontinuity in μ_{H_2O}. Gas-phase water thus has a driving force to enjoin the surface and equalize its electrochemical potential, while Na^+ and Cl^- synergistically reconstruct to reduce μ_{Na^+} and μ_{Cl^-} of the surface region to those values of the bulk crystal. A surface region of accommodated H_2O and disrupted Na^+ and Cl^- results. A disordered surface region containing water and high mobility Na^+ and Cl^- ions is reasonably labeled a liquid region, albeit of properties still very much distinct (and likely more viscous) than an aqueous solution.

Although probably unimportant for quantifying the direct effect optical properties of atmospheric aerosols, surface regions are crucial for understanding atmospheric heterogeneous chemistry. A critical reaction in polar ozone depletion, for example, is catalyzed on ice particles: $ClONO_2 + HCl \rightarrow HNO_3 + HOCl$. The high reactivity is attributed to the solvating liquidlike surface region induced by the dissociative uptake of HCl to form aquated H^+ and Cl^-.[152] Another example is the HNO_3 reaction on sea salt (nominally NaCl). This reaction results in a measurable increase in $NaNO_3$ in marine aerosol.[164] Under dry UHV conditions, HNO_3 rapidly passivates the (100) surface of NaCl. In H_2O vapor of even modest relative humidity, ionic mobility increases in the surface region and the NaCl reactive surface regenerates.[175] Thus, a complete description of the solid phase of atmospheric particles includes both the phase of the interior region (largely responsible for optical properties) and the phase of the interfacial region between the crystal and a water-bearing O_2/N_2 gas (viz. the atmosphere). The interphase is largely responsible for chemical properties. [Exact reconstruction depends on the extent of favorable interaction, e.g., Fe_2O_3 interacts much less than NaCl. H_2O dissociates to form >FeOH surface groups, and ionic mobility is much less than a salt.]

IV. Kinetics

The previous two sections on thermodynamics and phase diagrams provide useful descriptions of processes maintaining thermodynamic equilibrium. This condition is often met for long time scales (e.g., geology) or large-volume systems. However, in the atmospheric sciences, time scales are often relatively short, ranging from seconds to days, and the volume of a system is often $10^{-3}-10^3$ cubic micrometers. In these systems, the nucleation kinetics of new phases is a dominant issue. Will a disordered aqueous medium rearrange into an ordered crystal during the time scale of interest? If not, then the crystalline phase can be removed from the phase diagram (i.e., simply erased). The extended liquidus regions is termed metastable, as was described for Figure 12. For systems of atmospheric interest, it appears true that order-to-disorder transitions are rapid [see one exception in ref 18 and a contrasting report in ref 17], and system behavior is accurately described by the phase diagrams during melting or deliquescence. However, for freezing or efflorescence, a kinetic barrier must usually be overcome. It is possible to modify the appearance of the phase diagram to describe nucleation processes of a system. If so, this diagram is usually dubbed the kinetic phase diagram to be distinguished from the thermodynamic phase diagram.

A. Classifications

Phase transitions are often classified as first-order or second-order or, alternatively, as reconstructive, displacive, or order−disorder. For most atmospheric chemical systems, the phase transitions are first-order and reconstructive. A kinetic barrier is faced because a critical germ must form; classical nucleation theory is a common conceptual framework to classify the rate of germ formation. The order of a transition refers to the continuity of the derivatives of thermodynamic functions. When changing from one phase to another (e.g., ice to liquid), the free energies of the two phases at the equilibrium temperature are equal ($\Delta G = 0$). The function G_{system} is G_{liq} for T above 0 °C and G_{ice} for T below 0 °C. All G are equal at 0 °C. However, at 0 °C, $dG/dT = -S$ is discontinuous because $S_{ice} \neq S_{liq}$. Incidentally, $H_{ice} \neq H_{liq}$, so the first-order transition is detectable by scanning calorimetry. This transition is also known as reconstructive because bonds must be broken and reformed into highly different geometries. Because phase transitions in atmospheric chemistry usually involve the formation of a crystal from an aqueous medium, they are first-order and kinetically inhibited.

Some phase transitions are a gentler rearrangement of atoms. Bonds may shift without breaking, a

process called a displacive transformation. These phase transitions usually occur readily at the temperature expected for thermodynamic equilibrium and are not kinetically inhibited. The transitions from high quartz at 573 °C to low quartz is an often-cited example. The transition is still first-order because the two crystallographic states have distinct free energy−temperature dependencies, but the phase transition does not require the formation of critical germ. The phase transition occurs instead as a collective atomic rearrangement of bond angles. Solid−solid-phase transitions such as hydrate formation (e.g., $CaSO_4$ and $CaSO_4 \cdot 2H_2O$) often also face no nucleation barrier because water molecules intercalate into the structure on a molecule-by-molecule basis in a diffusional process akin to the hydration or drying of clays; however, the phase transition can still be slow because diffusion coefficients in solid-state materials are near 10^{-9} cm^2 s^{-1} at 298 K.

In contrast to a first-order transition, second-order changes are better described as gradual transformations. Ice melting to liquid is a first-order transition; a ferromagnetic substance gradually losing its magnetization with increasing temperature until it is paramagnetic at the Curie point is a gradual second-order transformation with a transition temperature at the Curie point. These phase transitions are not common in atmospheric chemical systems, except in the academic sense of variations due to shifting equilibrium constants as temperature and pressure are altered.

B. Premonitory Behavior

A question occurs to what extent one phase might anticipate the formation of a second.[172] In the most general description of a first-order phase transition, $G_A(T)$ and $G_B(T)$ for a two-phase system vary independently. Phase *A* is metastable to phase *B* when $G_A(T) > G_B(T)$. No structural similarities between *A* and *B* are suggested or required, and phase *A* need not resemble phase *B* in any way. Furthermore, knowledge about phase *B* provides no information about phase *A*. However, in many specific cases we can expect much more. For example, as ice approaches its melting temperature, its surface region takes on a liquidlike character. Knowledge of liquid water can then be employed to know something about ice surface properties. [A loose analogy can be made to the adage of "Knowledge of thermodynamics of a reaction tells you nothing of the rates of the reaction"—yet linear free energy relationships (LFERs) abound. Quite often, knowledge of phase *A* tells you something about phase *B*, especially near the transition point.] The structural similarities are rationalized by stating that, whether in state *A* or *B*, molecules have an overall tendency to converge to the same minimum free energy (as discussed in the section on Thermodynamics). In the limit of complete convergence, a phase transition is second-order. Structural similarities between phases *A* and *B* are especially common in interfacial regions where molecular movement and reconstruction are somewhat fluid. These rearrangements were initially dubbed premonitory rearrangements.[176] However, this phrase is misleading because it suggests that phase *A* rearranges in anticipation (or through knowledge) of phase *B*. Phases *A* and *B* are better described as converging on a common free energy arrangement in the interfacial region.

Premonitory phenomena thus described are associated with an ordered phase approaching a transition to disorder. In transitions in the other direction, the kinetic theory of nucleation prescribes the formation and dissipation of clusters, both prior to and after an initial point of bulk metastability. According to classical nucleation theory, these clusters should have structural similarities to the new phase. The rationalization is that a germ of a new phase should resemble the new phase. The steady-state description inherent in nucleation theory provides that a population distribution of ordered clusters exists in the disordered phase at any one instant. Prior to the point of metastability, thermodynamics guides that all of these kinetically formed clusters will disperse. After metastability is achieved, one such cluster must become critical to propagate that phase. [The germ size at which the energy gain for relieving supersaturation equals the energy cost of surface formation is termed a critical germ.] Prior to that event, however, the cluster population steadily increases with deepening metastability. In some chemical systems, the steady-state population of clusters reaches such a concentration that the disordered phase begins to take on a semblance to the ordered phase. Whether this population influences the structure or properties of the disordered medium enough to call it quasi-ordered depends on the properties of each chemical system in question as well as the sensitivity of an experimental apparatus to observe those changes.

Another interesting connection between phases *A* and *B* can sometimes be found in the thermodynamics and rates of a phase transition. For example, many properties of liquid water appear to extend toward highly energetically unfavorable singularities at −45 °C while, at the same time, conventional laboratory measurements have not succeeded in supercooling water below −40 °C.[2] These coupled observations are rationalized by stating that the tremendous thermodynamic driving force favors the rapid nucleation of another atomic arrangement (e.g., ice). According to this view, liquid water as a possible phase simply ceases to exist. Other workers, however, suggest that the numerical extrapolations leading to the "end of liquid water" at −45 °C are not accurate and instead present experimental evidence consistent with liquid water to 136 K or cooler.[428] A second example of the connection between thermodynamic extremes and nucleation kinetics occurs in binary systems having a miscibility gap in their phase diagram. When a sufficiently metastable composition is obtained, the spinodal line is crossed, and decomposition occurs to phase separation proscribed by the tie lines in the miscibility gap.[100] The spinodal composition is entirely determined by the free energy function and a local maximum. Rather like a thin book that can fall left or right when placed upright—and fall it certainly shall—a spinodal composition can

reduce its free energy by phase separating, and a chance fluctuation (i.e., a very small activation energy) enriching one component in a local region is self-reinforcing.

C. Critical Germ Formation

Rates of phase transitions in atmospheric chemical systems are most commonly rationalized by classical theories of homogeneous and heterogeneous nucleation.[151,177−179] In a disordered aqueous medium, the dynamic nature of the solution consists of ions associating into clusters for brief moments and then dissociating again into aqueous species. In general, small clusters are not favored because the surface energy associated with forming the cluster exceeds the energy released from forming a crystal in a supersaturated solution. However, if by random collisions, a sufficiently large cluster (viz. a critical cluster) forms, then the energy released from its three-dimensional association exceeds the energy cost of creating the two-dimensional interface with the surrounding aqueous medium. In this case, this germ continues to grow into an ever-larger crystal until the solution saturation ratio achieves unity. Thus, both crystal nucleation (viz. a germ) and crystal growth must occur to convert a supersaturated aqueous phase into crystalline components.[180,181] In atmospheric systems, particles with lifetimes longer than several hours generally range from 0.05 to 10 μm diameter. [Particles larger than 10 μm sediment rapidly while particles smaller than 50 nm are rapidly scavenging by coagulation. See ref 1.] For this size range, crystal growth is rapid and considered instantaneous relative to the nucleation time. [At temperatures below 180 K, crystal growth times become long relative to crystal nucleation times even for small aqueous droplets.[182] See accounts of HNO_3/H_2O[37] and H_2SO_4/H_2O.[183]]

Nucleation occurs by two mechanisms. In homogeneous nucleation, an aqueous three-dimensional medium spontaneously and stochastically nucleates a crystalline germ after a sufficient time period due to random molecular associations. The nucleation statistics are Poisson type.[28] In heterogeneous nucleation, a foreign surface is in contact with the aqueous medium. A nascent crystalline germ abutted to this surface often has a lower total surface energy due to lower surface tension between the germ and the surface as compared to the germ and aqueous solution. In this case, critical clusters form more often at the foreign surface than in the aqueous medium. The result is an increased occurrence of nucleation events, i.e., faster crystallization.

D. Homogeneous Nucleation

i. History

Salt crystallization by homogeneous nucleation in small particles composed of supersaturated aqueous electrolytes was the subject of early seminal work first by Orr[85] and then by Winkler and Junge[86,87] for processes of decreasing relative humidity. In 1958, Orr showed that whereas small NaCl(s) particles absorb water near 70% RH, NaCl(aq) particles retain water until 40% RH at 298 K. Similarly, small $(NH_4)_2SO_4$ particles deliquesced at 75% RH but did not effloresce until 40% RH. In 1972, Winkler and Junge reported that NaCl particles deliquesce at 75% RH and retain water until under 50% RH. Since that early work, Tang began a 20-year program in 1977 on phase transitions relevant to atmospheric chemistry. Other workers became interested in the early 1980s because aerosol phase transitions were recognized as important to air visibility. In 1990, the first publications appeared on mechanisms for polar stratospheric cloud formation.

The history of ice formation by homogeneous nucleation in supercooled pure water extends past 50 years.[2,184] Research accounts are available in refs 7, 185, and 186. In the atmosphere, mixed-phase clouds usually form by heterogeneous nucleation (vida infra) above −40 °C. Glaciation of all particles in a cloud by homogeneous nucleation occurs for some wet, cold clouds in the mid-troposphere. The upper troposphere and lower stratosphere are too dry for dilute particles of nearly pure water composition to form. Homogeneous nucleation of ice in these systems must occur from 1 to 10 *m* salt solutions.

ii. Recent Work and Trends

The laboratory work on the homogeneous nucleation kinetics of cirrus and PSC cloud formation at low temperatures and salt crystallization at low relative humidities from 1977 to early 2000 is summarized in Table 2. This review excludes the extensive body of experimental work done on ice formation mechanisms above −40 °C that are relevant to the properties of mixed-phase cloud systems in the lower troposphere. Recent examples of such work are found in refs 187−190. A trend in Table 2 is apparent in studying $(NH_4)_2SO_4$/H_2SO_4/NH_4NO_3/H_2O systems at 298 K for two decades. These systems are the dominant chemical constituents in the polluted boundary layer. Similarly, NaCl/KCl/H_2O systems are studied because they are believed to be representative of marine sea salt. However, inspection of Table 2 shows that these aerosols, important both on a mass and number density basis as global and regional aerosol, receive comparatively little study especially at conditions other than 298 K. The HNO_3/H_2SO_4/H_2O chemical systems are studied in detail at low temperatures in connection to their role as the constituents from which polar stratospheric clouds form. In the last two years, $(NH_4)_2SO_4$/H_2SO_4/H_2O systems at low temperatures are also receiving attention because they may be the mother liquor for ice nucleation during cirrus cloud formation.

Table 2 reveals that many temperature ranges, observation times, system size parameters, techniques, and chemical compositions have been studied. Intercomparison of laboratory results requires careful consideration of each of these parameters. Homogeneous nucleation rates, for example, are believed to depend linearly on the volume of the chemical system (eq 5), so an investigator observing a phase transition for 20-μm particles in 60 s would require another investigator working with 0.2-μm particles to wait 700 days to observe the same transition when all

Table 2. Summary of Laboratory Work on Phase Transitions of Aqueous Electrolytes Relevant to Atmospheric Sciences[a]

chemical system	sample descript	temp range (K)	transition observed	observation time	size	composition	solids observed	technique	year	ref
HNO_3/H_2O	A	160−188	a	0.42 min	0.2 μm	$0.24 < x_{HNO_3} < 0.46$	NAD NAT	IR-AFT	2000	191
HNO_3/H_2O	D	183−194	a	2−12 K min^{-1}	7−33 μm	$x_{HNO_3} = 0.33$	NAD	OM	2000	192
NaCl/H_2O $MgCl_2/H_2O$ NH_4HSO_4/H_2O NH_4NO_3/H_2O	A	238−298	e, d	0.17 min	0.4 μm	$0.02 < a_{H_2O} < 0.90$ $0.02 < a_{H_2O} < 0.90$ $0.02 < a_{H_2O} < 0.90$ $0.02 < a_{H_2O} < 0.90$	NaCl hydrate none none	IR-AFT	2000	193
$(NH_4)_2SO_4/H_2O$	D, E	195−235	i, m	10 K min^{-1}	10−55 μm	$0.80 < a_{H_2O} < 1.00$	ice	OM, DSC	2000	194
$(NH_4)_2SO_4/H_2SO_4/H_2O$	A	213−233	i	0.20 min	0.05, 0.2 μm(aq)	$(NH_4)_zH_{2-z}SO_4/H_2O$ $z = 0, 1, 2$	ice	CFD-OPC	2000	195
NaCl/H_2O	A	298	e	0.17 min	0.4 μm	$0.15 < a_{H_2O} < 0.90$	NaCl	IR-AFT	1999	9
NH_4HSO_4/H_2O	E	179−234	i, m	5 K min^{-1}	1−10 μm 3 μL	$0.55 < a_{H_2O} < 1.00$	ice THD	DSC	1999	10
$(NH_4)_2SO_4/H_2O$	A	234−295	e, d	0.13−0.90 min	0.80 μm (aq)	$0.35 < a_{H_2O} < 0.90$	α-AS	IR-AFT	1999	11
$(NH_4)_2SO_4/H_2O$	A	224−273 238−283	i, m e, d	1 and 30 min	0.35 μm (aq)	$0.35 < a_{H_2O} < 1.0$	ice α-AS β-AS	IR-AFT	1999	12
$(NH_4)_2SO_4/H_2O$	A	298	e, d	1 min	1 μm (s)	$0.35 < a_{H_2O} < 0.90$	α-AS	IR-AFT	1999	13
NH_4HSO_4/H_2O	L	243−298	a, m	60 min	100 mL (aq)	$0.45 < a_{H_2O} < 0.95$	ice THD	V, TT	1999	14
$H_2SO_4/HNO_3/H_2O$	E	150−270	i, a, m	1−3 K min^{-1}	few mg	$0.0 < x_{HNO_3} < 0.35$ $0.0 < x_{H_2SO_4} < 0.01$	ice	DSC	1999	15
NH_4HSO_4/H_2O	L	240−298	m	120 min	40 mL	$0.06 < x_{HNO_3} < 0.13$	ice THD	V	1999	16
$H_2SO_4/HNO_3/H_2O$	F, L	185−230	m, c, a	10 min	films, 1 mL	$6 < S_{NAT} < 690$ $x_{H_2SO_4} = 0.20$	SAT NAT	IR−F, TT	1998	17
$H_2SO_4/HNO_3/H_2O$	L	233	i	1.3×10^4 min	30 mg (s)	{0.20,0}, {0.23,0.066}, {0.11,0} {H_2SO_4,HNO_3} (x)	SAT	TT	1998	18
H_2SO_4/H_2O	D	170−240	i, m	10 K min^{-1}	5−20 μm	$0.60 < a_{H_2O} < 1.00$	ice	OM	1998	19
HNO_3/H_2O	A	155−175	a	0.17 min	0.2 μm	$x_{HNO_3} = 0.25$	NAT	IR-AFT	1998	20
$(NH_4)_2SO_4/H_2O$	A	298	d, e	1 min	0.4 μm	$0.3 < a_{H_2O} < 0.95$	α-AS	IN	1998	21
NH_4NO_3/H_2O						$0.15 < a_{H_2O} < 0.95$				
$(NH_4)_2SO_4/H_2O$	S	233−303	d, e, a, m	120 min	5−10 μm (s)	$0.2 < a_{H_2O} < 0.95$	ice α-AS AST	SPL	1998	22
HNO_3/H_2O	A	188−240	a	10−150 min	1 μm (aq)	$x_{HNO_3} = 0.25, 0.29, 0.33$	NAD	IR−SC	1998	23
HNO_3/H_2O	A	176−179	a	0.25 min	0.8 μm (aq)	$x_{HNO_3} = 0.33$	NAD	IR-AFT	1998	24
seawater	S	298	e,d	na	20 μm	$0.00 < a_{H_2O} < 0.95$	NaCl	SPL	1997	427
$(NH_4)_2SO_4/H_2O$ $NH_4HSO_4/H_2O(D_2O)$ NaCl/H_2O seawater (H_2O/D_2O)	A	298	e, d	1 or 30 min	0.45 μm (aq)	$0.02 < a_{H_2O} < 1.0$	α-AS NaCl uni	IR-AFT	1997	25
H_2SO_4/H_2O	D	135−298	i, m	10 min	5−10 μm (aq)	$0.02 < x_{H_2SO_4} < 0.22$	ice SAT	IR−P	1997	26
$H_2SO_4/HNO_3/H_2O$	A	188−204	i, a, m	180 min	0.7 μm (aq)	stratospheric trajectory	none	IR−SC	1997	27
$H_2SO_4/HNO_3/H_2O$	L	140−280	i, a, m	1.7−600 min	0.5−4 mL	$0.02 < x_{H_2SO_4} < 0.51$; stratospheric trajectory, $x_{HNO_3} = 0.21$with $0 < x_{H_2SO_4} < 0.004$	ice SAT SAH NAT	TT	1997	28
H_2SO_4/H_2O	S	191−298	i, a	60 min	20−30 μm	$0.07 < x_{H_2SO_4} < 0.38$	ice	SPL	1997	29
H_2SO_4/H_2O	S	165−255	a, m	1.0×10^4 min	5−10 μm (s)	$0.06 < x_{H_2SO_4} < 0.22$	SAO	SPL	1997	30
NH_4HSO_4/H_2O	S	233−303	d, e, a, m	1.3×10^3 min	5−10 μm (s)	$0.05 < x_{NH_4HSO_4} < 0.58$	AHSO	SPL	1997	31[b]
HNO_3/H_2O	A	194	a	60 min	1.2 μm (aq)	$x_{HNO_3} = 0.29$	NAD	IR−SC	1997	32
$Ba(NO_3)_2/H_2O$	S	298	e, d	na	14−16 μm (aq)	$0.60 < a_{H_2O} < 1.00$	$Ba(NO_3)_2$	SPL	1997	33
$Sr(NO_3)_2/H_2O$						$0.20 < a_{H_2O} < 1.00$	$Sr(NO_3)_2$			
$Ca(NO_3)_2/H_2O$						$0.01 < a_{H_2O} < 0.70$	$Ca(NO_3)_2$			
H_2SO_4/H_2O	A	160−240	a, m, i	1 min	na	$0.07 < x_{H_2SO_4} < 0.51$	ice SAO	IR-AFT	1997	34
HNO_3/H_2O	F	160−180	a	1−60 min	1.5−1.7 μm (aq)	$x_{HNO_3} = 0.25, 0.33$	NAD NAT	IR−F	1997	35
HNO_3/H_2O	F	160−190	v	0.3 K min^{-1}	1−2 μm film	$0.0 < x_{HNO_3} < 0.06$	ice NAT	IR−F	1996	36
HNO_3/H_2O	A	77, 190−204	a	0.5−30 min	0.12−0.96 μm (aq)	$x_{HNO_3} = 0.33$	NAD	IR−SC	1996	37
$H_2SO_4/HNO_3/H_2O$	F	196.0−197.2	c	5 min	100 μm coating	$x_{H_2SO_4} = 0.20$, $7 < S_{NAT} < 70$	SAT NAT	V	1996	38
H_2SO_4/H_2O	A	190−240	i	2 min	0.06−0.5 μm	$0.0 < x_{H_2SO_4} < 0.09$	ice	IR-AFT	1996	39

Table 2. (Continued)

chemical system	sample descript	temp range (K)	transition observed	observation time	size	composition	solids observed	technique	year	ref
$NaNO_3/H_2O$	S	298	e, d	na	20 μm (s)	$0.0 < a_{H_2O} < 0.85$	$NaNO_3$	SPL	1996	40
$(NH_4)_2SO_4/H_2O$	A	298	d, e	0.5−40 min	0.35 μm (aq)	$a_{H_2O} < 0.01$; $a_{H_2O} = 0.30$	α-AS	IR-AFT	1996	41
HNO_3/H_2O	L	163−223	a, m	0.08−12 K min^{-1}	1 μL	$x_{HNO_3} = 0.25, 0.35, 0.50$	NAT NAD NAM	TP-XRD	1996	42
H_2SO_4/H_2O	A	189−240	i, a	300 min	0.26 μm (aq)	$0.09 < x_{H_2SO_4} < 0.78$	none	IR−SC	1995	43
$H_2SO_4/HNO_3/H_2O$	L	192−268	i;a;m	2.8×10^3 min	5 μL (aq)	$7.5 > -\log_{10} P_{HNO_3}$ (Torr) > 4.5 $5.0 > -\log_{10} P_{H_2O}$ (Torr) > 1.0	mixed acid hydrates NAD NAM	V	1995	44
$H_2SO_4/HNO_3/H_2O$	F	189−194	c, a	60−120 min	2 μm film	$6 < S_{NAT} < 114$	NAT SAT	IR−F	1995	45
H_2SO_4/H_2O	F	200−240	a, m	na	100 μm coating	$0.36 < x_{H_2SO_4} < 0.51$	SAM	VIS	1995	46
$H_2SO_4/HNO_3/H_2O$	L	184.9−194.5	i, a	20−180 min	1 mL	stratospheric trajectory	ice NAT SAT	TT	1995	47
$NaBr/H_2O$ KCl/H_2O KBr/H_2O NH_4Cl/H_2O $(NH_4)_2SO_4/H_2O$	S	298	e	na	na	na	na	SPL	1995	48, 49
$NaCl/H_2O$	S	298	e, d	60 min	10 μm (aq)	$0.45 < a_{H_2O} < 0.95$	NaCl	SPL	1994	50
$NaCl/KCl/H_2O$						$0.61 < a_{H_2O} < 0.95$	NaCl KCl			
$CsCl/H_2O$						$0.32 < a_{H_2O} < 0.95$	CsCl			
$CsCl/KCl/H_2O$						$0.43 < a_{H_2O} < 0.95$	CsCl KCl			
KF/H_2O						$0.09 < a_{H_2O} < 0.95$	KF			
$KF/KCl/H_2O$						$0.09 < a_{H_2O} < 0.95$	KF KCl			
$NaNO_3/H_2O$						$0 < a_{H_2O} < 0.95$	none			
$NaNO_3/Na_2SO_4/H_2O$						$0.16 < a_{H_2O} < 0.95$	$NaNO_3$ Na_2SO_4			
$(NH_4)_2SO_4/H_2O$	S	298	d, e	$1-1.3 \times 10^3$ min	6−8 μm (s)	$0.10 < a_{H_2O} < 1.00$	α-AS	SPL	1994	51
NH_4HSO_4/H_2O						$0.05 < a_{H_2O} < 1.00$	uni			
$(NH_4)_3H(SO_4)_2/H_2O$						$0.40 < a_{H_2O} < 1.00$	THD			
Na_2SO_4/H_2O						$0.55 < a_{H_2O} < 1.00$	Na_2SO_4			
$NaHSO_4/H_2O$						$0.10 < a_{H_2O} < 1.00$	none			
$NaNO_3/H_2O$						$0.05 < a_{H_2O} < 1.00$	$NaNO_3$			
$(NH_4)_2SO_4/Na_2SO_4/H_2O$	S	278−308	d	na	6−8 μm (s)	$0.40 < a_{H_2O} < 0.90$	$(NH_4)_2SO_4$ Na_2SO_4	SPL	1994	52
$NaCl/NaNO_3/H_2O$							NaCl $NaNO_3$			
$NaCl/Na_2SO_4/H_2O$							NaCl Na_2SO_4			
$H_2SO_4/HNO_3/H_2O$	A	192−212	c, a	60−120 min	1−2 μm film	$6 > -\log_{10} P_{HNO_3}$ (Torr) > 5.6	NAT	IR−F	1994	53[c]
						$4 > -\log_{10} P_{H_2O}$ (Torr) > 3.5	SAT			
$H_2SO_4/HNO_3/H_2O$	L	188−213	i, a	2 K min^{-1} 1.3×10^3 min	3−5 μL 0.03−3 mL	stratospheric trajectory	uni	TT	1994	54[d]
HNO_3/H_2O	L	193-210	c	30−120 min	0.2 μmol	exposure (nonequilibrium) conditions $\log_{10} P_{H_2O}$ (Torr) $= -3.5$ $5 < P_{H_2O}:P_{HNO_3} < 300$	NAP	V	1994	55
$KCl/H_2O(D_2O)$	S	298	e, d	100 min	10^{-9} cm^2	$0.55 < a_{H_2O} < 0.90$	KCl	SPL	1993	56
KCl/H_2O/methanol						$0.27 < a_{H_2O} < 0.550.10 < a_{MeOH} < 0.14$	KCl			
$NaBr/H_2O(D_2O)$						$0.27 < a_{H_2O} < 0.61$	NaBr			
NaBr/methanol						$0.72 < a_{MeOH} < 0.94$	NaBr			
$NaBr/H_2O$/methanol						$0.22 < a_{H_2O} < 0.500.05 < a_{MeOH} < 0.09$	NaBr			
$NaBr/H_2O$/acetone						$0.22 < a_{H_2O} < 0.550.15 < a_{acetone} < 0.29$	NaBr			
$NaCl/KCl/H_2O$	S	278−308	d	10 min	6−8 μm (s)	$0.0 < a_{H_2O} < 0.95$	NaCl KCl	SPL	1993	57
$Na_2SO_4/NaNO_3/H_2O$						$0.0 < a_{H_2O} < 0.95$	Na_2SO_4 $NaNO_3$			
$(NH_4)_2SO_4/H_2O$						$0.0 < a_{H_2O} < 0.95$	α-AS			
$NaNO_3/H_2O$						$0.0 < a_{H_2O} < 0.95$	$NaNO_3$			
KCl/H_2O						$0.0 < a_{H_2O} < 0.95$	KCl			
$HNO_3/HCl/H_2O$	F	150−190	c	20−120 min	0.9 μm film	$7 > -\log_{10} P_{HCl}$ (Torr) > 5	ice NAT HAH	IR−F	1993	58

Table 2. (Continued)

chemical system	sample descript	temp range (K)	transition observed	observation time	size	composition	solids observedd	technique	year	ref
H_2SO_4/H_2O	F	180−230	i, a, m	0.1−20 K min^{-1}	1 μm film	stratospheric trajectory	SAT	IR−F	1993	59
H_2SO_4/H_2O	F, E	140−300	a, m	na	several μm film	$0.04 < x_{H_2SO_4} < 0.3$	$H_2SO_4 \cdot nH_2O n =$ 1,2,3,4,6.5,8	IR−F, DSC	1993	60
$H_2SO_4/HNO_3/H_2O$	F, E	150−254	i, a	na	15 μm film	various	ice SAT SAH NAT	IR−F, DSC	1993	61
H_2SO_4/H_2O	L	163−273	i, a	1 K min^{-1}	10 mL	$0.0 < x_{H_2SO_4} < 0.62$	ice	TT	1993	62
HNO_3/H_2O	L	190−230	a	several days	5 to 50 μm button	$7 > -\text{Log}_{10}P_{HNO_3}$ (Torr) > 2.5	NAM	V	1993	63[e]
						$4.5 > -\log_{10} P_{H_2O}$ (Torr) > 1	NAD NAT			
HNO_3/H_2O	A	160−185	a, i	22 min	0.1−1 μm (aq)	$1 < P_{H_2O}:P_{HNO_3} < 10$	NAD NAT	IR−SC	1993	64
HNO_3/H_2O	L	191−210	c	5−250 min	0.2 μmol	$3 < P_{H_2O}:P_{HNO_3} < 300$ $\log_{10} P_{H_2O} = -3.5$	NAM NAD NAT NAM	V	1993	65
HNO_3/H_2O	E	183−298	m	3 K min^{-1}	10 μL	$0.05 < x_{HNO_3} < 0.50$	NAD NAT NAM	DSC	1993	66
HNO_3/H_2O	F	173−243	v	45 K min^{-1}	3 μm	$0.58 < P_{H_2O}:P_{HNO_3} < 4.6$	NAD α-,β- NAT	IR−F	1992	67
HNO_3/H_2O	F	173−203	v	45 K min^{-1}	film	$1 < P_{H_2O}:P_{HNO_3} < 3$	ice NAM NAD α-,β-NAT	IR−F	1992	68
HNO_3/H_2O	F	188−213	c	0.25 K min^{-1}	film	$6.5 > -\log_{10} P_{HNO_3}$ (Torr) > 5.5	NAD	IR−F	1992	69
				60 min		$3.8 > -\log_{10} P_{H_2O}$ (Torr) > 3.5	NAT			
HNO_3/H_2O	F	188−213	c	1−2 K min^{-1} 30 min	1−2 μm film	$1 < P_{H_2O}:P_{HNO_3} < \infty$	ice NAM NAD NAT	IR−F	1990	70
$NaCl/H_2O$	S	293	d	60 min	20 μm	$0.44 < a_{H_2O} < 0.85$	NaCl	SPL	1987	71
$NaBr/H_2O$						$0.22 < a_{H_2O} < 0.80$	NaBr			
KCl/H_2O						$0.59 < a_{H_2O} < 0.85$	KCl			
KBr/H_2O						$0.52 < a_{H_2O} < 0.85$	KBr			
NH_4Cl/H_2O						$0.45 < a_{H_2O} < 0.90$	NH_4Cl			
Na_2SO_4/H_2O						$0.55 < a_{H_2O} < 0.90$	Na_2SO_4			
$(NH_4)_2SO_4/H_2O$						$0.48 < a_{H_2O} < 0.90$	α-AS			
$CaCl_2/H_2O$						$0.10 < a_{H_2O} < 0.85$	$CaCl_2 \cdot 4H_2O$			
$MnCl_2/H_2O$						$0.30 < a_{H_2O} < 0.70$	$MnCl_2 \cdot 2.3H_2O$			
$MnSO_4/H_2O$						$0.40 < a_{H_2O} < 0.90$	$MnSO_4 \cdot 2.8H_2O$			
$FeCl_3/H_2O$						$0.48 < a_{H_2O} < 0.95$	$FeCl_3 \cdot 6H_2O$			
NH_4NO_3/H_2O	S	298	v, e	180 min	2 μm (s)	$x_{NH4NO_3} \rightarrow 1.0$	NH_4NO_3	SPL	1987	72
$NaCl/KCl/H_2O$	S	293	e, d	60 min	11.0−21.2 μm (aq)	$0.45 < a_{H_2O} < 0.95$	NaCl KCl	SPL	1987	73
$NaCl/KBr/H_2O$						$0.35 < a_{H_2O} < 0.90$	NaCl KBr			
$NaCl/(NH_4)_2SO_4/H_2O$						$0.40 < a_{H_2O} < 0.80$	NaCl α-AS			
$NaCl/H_2O$	S	293	e	10 min	20 μm (aq)	$0.44 < a_{H_2O} < 0.85$	NaCl	SPL	1987	74
$NaBr/H_2O$						$0.22 < a_{H_2O} < 0.80$	NaBr			
KCl/H_2O						$0.59 < a_{H_2O} < 0.85$	KCl			
KBr/H_2O						$0.52 < a_{H_2O} < 0.85$	KBr			
NH_4Cl/H_2O						$0.45 < a_{H_2O} < 0.90$	NH_4Cl			
Na_2SO_4/H_2O						$0.55 < a_{H_2O} < 0.90$	Na_2SO_4			
$(NH_4)_2SO_4/H_2O$						$0.48 < a_{H_2O} < 0.90$	α-AS			
$MnCl_2/H_2O$						$0.30 < a_{H_2O} < 0.70$	$MnCl_2 \cdot 2H_2O$			
$FeCl_3/H_2O$						$0.48 < a_{H_2O} < 0.95$	$FeCl_3 \cdot 6H_2O$			
$NaCl/KCl/H_2O$	S	298	d, e	na	3−4 μm (s)	$0.60 < a_{H_2O} < 0.96$, $0 < x < 1$ $NaCl_xKCl_{1-x}$	NaCl KCl	SPL	1986	75
$(NH_4)_2SO_4/H_2SO_4/H_2O$	S	298	e, d	20 min	1 ng	$(NH_4)_zH_{2-z}SO_4/H_2O$, $1 < z < 2$	α-AS THD AHS	SPL	1985	76
$(NH_4)_2SO_4/H_2SO_4/H_2O$	A	298	d, e	0.2 a_{H_2O} min^{-1}	2 μm	$(NH_4)_zH_{2-z}SO_4/H_2O$, $1 < z < 2$	uni	IN	1985	77
$(NH_4)_2SO_4/Na_2SO_4/H_2O$		298				$(NH_4)_zNa_{2-z}SO_4/H_2O$, $0 < z < 2$	uni			
$NaCl/H_2O$	S	298	e	10 min	2−3 μm (s)	na	NaCl	SPL	1984	78
$(NH_4)_2SO_4/H_2O$	S	298	e, d	5 min	0.5 ng (s)	$0.30 < a_{H_2O} < 0.95$	α-AS	SPL	1984	79
NH_4Cl/H_2O	E	190−278	i, e	na	na	$0.65 < a_{H_2O} < 1.00$	ice	DSC	1984	80

Table 2. (Continued)

chemical system	sample descript	temp range (K)	transition observed	observation time	size	composition	solids observed	technique	year	ref
$NaCl/H_2O$	A	298	d, e	0.002−0.17 min	0.67 μm (s)	na	NaCl	OPC	1980	81
KCl/H_2O						na	KCl			
$NaCl/KCl/H_2O$						na	NaCl KCl			
NH_4NO_3/H_2O						$0.3 < a_{H_2O} < 0.90$	none			
$(NH_4)_2SO_4/H_2SO_4/H_2O$						$0.50 < a_{H_2O} < 1.00$, {100:0}, {88.3:11.7}, {83.3:16.7}, {0:100} {$(NH_4)_2SO_4$:H_2SO_4)} (w/w)	α-AS THD			
$(NH_4)_2SO_4/H_2SO_4/H_2O$	A	298	d	na	na	$0.2 < a_{H_2O} < 0.90$	α-AS AHS	IN	1978	82
$NaSO_4/H_2O$						$0.2 < a_{H_2O} < 0.90$	uni			
$MgSO_4/H_2O$						$0.2 < a_{H_2O} < 0.90$	none			
$ZnSO_4/H_2O$						$0.2 < a_{H_2O} < 0.90$	none			
$NaCl/KCl/H_2O$	A	298−303	d	1 min	0.5 μm (s)	$0.65 < a_{H_2O} < 0.96$, {80:60}, {64:36}, {20:80} {NaCl:KCl} (w/w)	NaCl KCl	OPC	1978	83
$(NH_4)_2SO_4/H_2SO_4/H_2O$						$0.50 < a_{H_2O} < 1.00$, {100:0}, {88.3:11.7}, {83.3:16.7}, {0:100} {$(NH_4)_2SO_4$:H_2SO_4)} (w/w)	α-AS THD			
NH_4HSO_4/H_2O	A	278−298	d	na	0.5 μm (aq)	$0.39 < a_{H_2O} < 1.00$	AHS	OPC	1977	84

[a] Reverse sorted by year to provide perspective on development of techniques and evolution of interest in terms of which compositions, temperature ranges, and phase transitions studied. Studies on ice and acid hydrate formation, melting, salt crystallization, and deliquescence from aqueous electrolytes are included. Extensive work done on ice formation from water and very dilute electrolytes is omitted. Sample Description: A, aerosol; D, deposited particles; E, emulsion; F, film; L, liquid volume, typically test tubes; S, single particle. Phase transitions: a, acid or salt freezing (crystallization); c, ice or acid hydrate condensation; d, deliquescence; e, efflorescence; i, ice freezing; m, ice or acid melting; v, ice or acid hydrate vaporization. Size parameter: units of μm refer to diameters of particles and units of mass or volume refer to contiguous chunks of material, often in a test tube. Techniques: CFD-OPC, continuous flow thermal diffusion chamber with optical particle counter detection; DSC, differential scanning calorimetry; IN, integrating nephelometer; IR-AFT, infrared-aerosol flow tube; IR−F, transmission mode infrared spectroscopy of a film; IR-P, infrared spectroscopy of particles deposited on the inner walls of a light pipe; IR-SC, infrared spectroscopy in an aerosol settling chamber; OM, optical microscope; OPC, optical particle counter detection of growth in a monodisperse aerosol with increasing relative humidity; SPL, single-particle levitation; TP-XRD, temperature-programmed X-ray diffraction; TT, test tube with visual observation of latent heat release; V, nitric acid and/or water vapor pressure measurements; VIS, visual observation of flow tube coating. Key to solids: AHS, NH_4HSO_4; AHSO, $NH_4HSO_4 \cdot 8H_2O$ (existence is controversial); AS, $(NH_4)_2SO_4$; AST, $(NH_4)_2SO_4 \cdot 4H_2O$ (existence is controversial); HAH, $HCl \cdot 6H_2O$; NAD, $HNO_3 \cdot 2H_2O$; NAM, $HNO_3 \cdot H_2O$; NAP, $HNO_3 \cdot 5H_2O$; NAT, $HNO_3 \cdot 3H_2O$; SAH, $H_2SO_4 \cdot 6.5H_2O$; SAM, $H_2SO_4 \cdot H_2O$; SAO, $H_2SO_4 \cdot 8H_2O$; SAT, $H_2SO_4 \cdot 4H_2O$; THD, $(NH_4)_3H(SO_4)_2$; uni, unidentified solid. na, not available. [b] See refs 14 and 16. [c] See ref 45. [d] See ref 47. [e] See ref 423.

other conditions are equal. Similarly, some techniques such as differential scanning calorimetry vary temperature continuously as an integral part of the measurement whereas most other techniques are isothermal. The charged particle levitation and optical microscope techniques observe single particles whereas aerosol flow tube apparatus often have minimum detection limits of 10^8 particles. Because phase transitions are stochastic, observing an ensemble of particles is a boon for rapidly attaining an average result, but single-particle techniques offer the advantage of a more precise understanding of the phase transition mechanism. In addition, much progress is made by studying thin films of aqueous electrolytes or, perhaps surprisingly, test tubes containing milliliter volumes. In Table 2, the important parameters of each experimental system are provided to aid in the comparison of results stemming from different laboratories.

iii. Experimental Results Demonstrating Important Concepts

1. Hysteresis Effect When Drying. A difference between deliquescence and efflorescence RH values (i.e., the hysteresis effect) is commonly observed for aqueous salt particles. Figure 19 depicts the hysteresis effect for $(NH_4)_2SO_4/H_2O$ at 298 K. A dry crystalline particle at low relative humidity absorbs water at 79.5% RH to form an aqueous salt particle with a concomitant increase in volume. The hygroscopic salt particle swells with further increases in RH. If the RH is subsequently decreased, water partially evaporates from the aqueous particle, which thus shrinks in a reversible process, until the deliquescence RH value is reached. Though thermodynamically favored, crystallization does not occur at that RH value due to the sluggishness of critical germ nucleation. Instead, the aqueous particle continues to shrink until nearly 35%, at which point efflorescence occurs in submicron particles observed for several minutes. The upper axes show associated changes in the mole fraction aqueous composition, the saturation ratio, and the free energy driving force of an aqueous particle dissociating into a crystalline particle and gaseous water.

Figure 20 shows the effect of the addition acid to $(NH_4)_2SO_4/H_2O$ to form a $(NH_4)_2SO_4/H_2SO_4/H_2O$ system at 298 K.[76] Near the neutral composition ($z = 2.0$), the addition of acid raises the efflorescence RH value slightly before a monotonic decrease to zero at bisulfate ($z = 1.0$). For this composition, crystallization by homogeneous nucleation is not observed in aqueous particles observed for hours. The eutonic values observed for the crystallized systems indicate that $NH_4HSO_4(s)$ and $(NH_4)_3H(SO_4)_2(s)$ form for $z < 1.5$ while $(NH_4)_3H(SO_4)_2(s)$ and $(NH_4)_2SO_4(s)$ are favored above $z > 1.5$. It is not certain which of the two crystals in each pair first formed from the

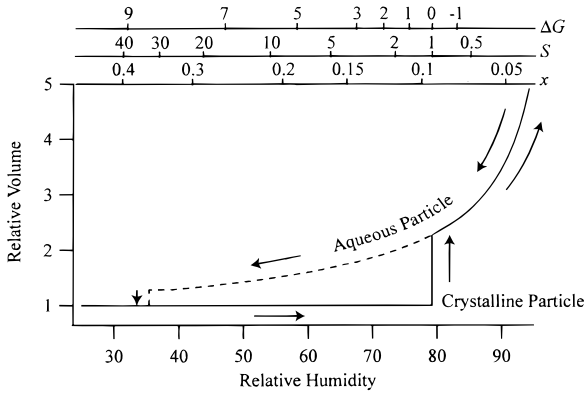

Figure 19. Relative volume of an ammonium sulfate particle with cycles in increasing and decreasing relative humidity at 298 K. Unity volume corresponds to a nonporous, spherical crystalline ammonium sulfate particle. At 79.5% RH, deliquescence occurs and the particle spontaneously forms an aqueous spherical droplet. Upon decreasing RH, the particle remains aqueous (dashed line) until 35% RH when efflorescence occurs in chemically pure particles. Changes in volume occur from the evaporation and condensation of water vapor. A *hysteresis effect* is apparent because the volume on decreasing RH (upper loop) is 125−200% larger than increasing RH (lower loop) in the 35−79% range. In authentic atmospheric particles, crystallization can occur at higher RH values due to the presence of insoluble impurities that induce crystallization at lower supersaturations. The upper axes show the mole fraction, x, of the aqueous particles; saturation ratio, S, with respect to crystalline ammonium sulfate; and the free energy change, ΔG (kJ mol^{-1}), of ammonium sulfate crystal and water vapor combining to form an aqueous solution (i.e., deliquescence). Density, curvature, and mass transfer effects are not considered.

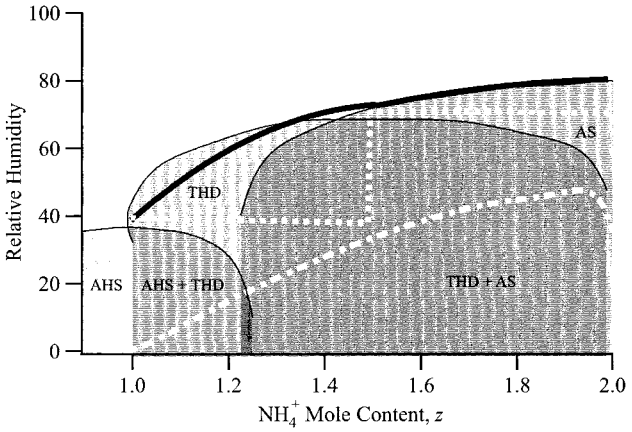

Figure 20. Dependence of efflorescence relative humidity on ammonium content for aqueous $(NH_4)_zH_{2-z}SO_4$ droplets. Efflorescence values of aqueous particles are shown by the dashed−dotted lines.[76] Relative humidity values for initial water uptake by dry particles are shown by the dashed line. RH values of saturated solutions are shown by the solid line. The hysteresis gap is the region between the solid and dashed−dotted lines. The shaded regions indicate saturation with respect to one or more solid. The thin lines are unity saturation with respect to $(NH_4)_2SO_4$, $(NH_4)_3H(SO_4)_2$, and NH_4HSO_4 as derived from the model of Clegg et al.[134] The straight edges on the shaded regions are arbitrarily drawn, and the real system undoubtedly contains curvature, but accurate data are not available.

saturated aqueous solution. However, it is interesting that the efflorescence behavior is a continuous function because a discontinuity might be expected when a different crystal forms favorably, as reported by Tang and Munkelwitz[75] in different mole fractions of NaCl/KCl mixed with H_2O. Below 0.6 mol fraction of KCl, the efflorescence RH is 45% whereas it changes abruptly to 65% above that mole fraction. The results shown in Figure 20 for the $(NH_4)_2SO_4/H_2SO_4/H_2O$ system disagree with Han and Martin,[196] who found only $(NH_4)_2SO_4$(s) crystallizes from particles in this chemical system for RH < 10%. The work shown in Figure 20 was carried out by single-particle levitation and provided for observations times of hours whereas Han and Martin carried out their experiments as a flowing aerosol stream with an observation time shorter than 1 min. These different observation times may rationalize the differences in observed efflorescence behavior.

The efflorescence RH values for selected chemical systems are summarized in Table 3. The general effect of a hysteresis gap between deliquescence and efflorescence RH values is apparent. A comparison of the deliquescence RH values among different laboratories shows good agreement. The results for efflorescence RH values, however, do not show uniform agreement. In cases of differences, rationalizations based upon differing observation times or system volumes are sometimes possible. In other cases, many scientists accept the lowest reported value and assume that significantly higher values indicate impurities acting as good heterogeneous nuclei are contained within the aqueous droplet. The chemical systems $NaNO_3/H_2O$, NH_4HSO_4/H_2O, and NH_4NO_3/H_2O are noteworthy because several workers agree that these systems do not readily crystallize at even the lowest RH values, at least for the particle volumes and observation times considered.

2. Supercooling with Decreasing Temperature. When low solute mole fractions of the $(NH_4)_2SO_4/H_2SO_4/H_2O$ system are cooled, ice forms. Figure 21 shows the difference between melting and freezing temperatures as a function of solute mole fraction for 5−50-μm droplets cooled at 10 K min^{-1}.[10,19,194] A decrease in both the melting and the freezing temperatures is obtained for acidified compositions. The effective role of H_2SO_4 in preventing crystallization is not entirely understood and is not confined entirely to ice. For example, concentrated HNO_3/H_2O solutions ($x = 0.209$) nucleate NAT readily at 215−218 K, but the addition of even small amounts of H_2SO_4 (e.g., $x = 0.001$) significantly depresses the NAT formation temperature.[28] The small concentration of H_2SO_4 and its large effect on nucleation kinetics is not well-understood and suggests an active role by H_2SO_4 in preventing critical cluster formation.

A common feature of experiments on nucleation kinetics is often disagreement among workers employing different apparatus. Refs 12, 39, and 195 disagree with Figure 21, for example. Reasons for some of the differences might be as simple as reporting freezing temperatures instead of J values for apparatus that employ different observation times and particle volumes. More subtle reasons might include mass transfer aspects in the apparatus and different sensitivities to fractions of frozen particles. An analysis of the common apparatus with a view-

Table 3. Deliquescence and Efflorescence Relative Humidities of Selected Chemical Systems at 298 K[a]

system	deliquescence RH	efflorescence RH	comment	ref
$CaCl_2/H_2O$	32.3 ($\cdot 6H_2O$)		293 K	71
$CaCl_2/H_2O$	not observed ($\cdot 4H_2O$)		293 K	71
$CsCl/H_2O$	66.5	32.3 ± 0.003		50
$FeCl_3/H_2O$	77 ($\cdot 6H_2O$)	48	293 K	71,74
KBr/H_2O	81 ± 1	52	293 K	71,74
KCl/D_2O	88	62		56
KCl/H_2O	84.3	53		81
KCl/H_2O	91	59		56
KCl/H_2O	84.3	59	293 K	71,74
KF/H_2O	17.7	9.0 ± 0.1		50
$MnCl_2/H_2O$	57.4 ($\cdot 4H_2O$)	30	293 K	71,74
$MnSO_4/H_2O$	84.1 ($\cdot 5H_2O$)		293 K	71
Na_2SO_4/H_2O	84	57		51
Na_2SO_4/H_2O	85 (anhydrous)	55	293 K	71,74
Na_2SO_4/H_2O	93 ($\cdot 10H_2O$)		293 K	71
$NaBr/H_2O$	45 (anhydrous)	22	293 K	71,74
$NaBr/H_2O$	58 ($\cdot 2H_2O$)		293 K	71
$NaCl/H_2O$	75 ± 1	43 ± 2		25
$NaCl/H_2O$	75.7	43		81
$NaCl/H_2O$	75.3	45.5 ± 0.6		50
$NaCl/H_2O$	75 ± 1	44	293 K	71,74
$NaCl/H_2O$	75 ± 2	40 ± 2		193
$NaCl/H_2O$		50 ± 15		9
$NaCl/KCl/H_2O$	73.8 ± 0.5			83
$NaCl/KCl/H_2O$	73.8	38 for $x_{NaCl} > 0.4$		75,81
$NaCl/KCl/H_2O$		64 for $x_{NaCl} < 0.4$		
$NaNO_3/H_2O$	74.5	not reproducible; eff. $0 < a_{H_2O} < 0.30$		51
$NaNO_3/H_2O$	74.3	not observed		50
$NaNO_3/H_2O$	70	40		40
NH_4Cl/H_2O	77	45	293 K	71,74
NH_4HSO_4/H_2O	39 ± 2	not observed		25
NH_4HSO_4/H_2O	39			81
NH_4HSO_4/H_2O	40	not reproducible; eff. $0 < a_{H_2O} < 0.22$		51
NH_4HSO_4/H_2O	39.0 ± 0.5			84
NH_4HSO_4/H_2O		not observed		193
$(NH_4)_2SO_4/H_2O$	79 ± 1	33 ± 2		25
$(NH_4)_2SO_4/H_2O$	79 ± 2	35 ± 2		13
$(NH_4)_2SO_4/H_2O$	79.5	36		81
$(NH_4)_2SO_4/H_2O$	80	37		51
$(NH_4)_2SO_4/H_2O$	80.0 ± 1.2	34.7 ± 0.4		79
$(NH_4)_2SO_4/H_2O$	81	48	293 K	71,74
$(NH_4)_2SO_4/H_2O$	80	42		21
$(NH_4)_3H(SO_4)_2/H_2O$	69			81
$(NH_4)_3H(SO_4)_2/H_2O$	69	35		51
$(NH_4)_2SO_4/(NH_4)_3H(SO_4)_2/H_2O$	69.0 ± 0.5			83
NH_4NO_3/H_2O	60	not observed		21
NH_4NO_3/H_2O		not observed		72
NH_4NO_3/H_2O		not observed		193
$(NH_4)_3H(SO_4)_2/NH_4HSO_4/H_2O$	39.0 ± 0.5			83
$2NH_4NO_3 \bullet (NH_4)_2SO_4/H_2O$	56.4			81
$(NH_4)_2SO_4/NH_4NO_3/H_2O$	77	18	3:2 molar ratio	77

[a] Not observed often indicates extreme conditions, close to 0% RH. In one case, $P(H_2O)$ was reduced to below 10^{-5} Torr for NH_4NO_3/H_2O.[72] Pure aqueous systems of $NaNO_3/H_2O$, NH_4HSO_4/H_2O, and NH_4NO_3/H_2O do not commonly effloresce. In the reported literature, the *minimum* efflorescence RH is usually accepted, and higher reported values are generally understood to indicate impurities in the chemical systems that can induce heterogeneous nucleation. In systems containing two or more salt components, the efflorescence RH depends on the molar ratio of the constituents (e.g., $NaCl/KCl/H_2O$).

point of intercomparing results is a critical need.

The concept of idealized trajectories was introduced for Figure 11. Supercooling as described by Figure 21 is appropriate for test tube trajectories, but more convenient expressions are possible for atmospheric trajectories. In particular, temperature and relative humidity with respect to ice are often made during field campaigns (cf. Figure 9). Hence, it is convenient to express supercooling in those terms: At constant temperature what ice supersaturation ratio must be obtained for homogeneous ice nucleation to begin? The inset of Figure 22 is a combination of the

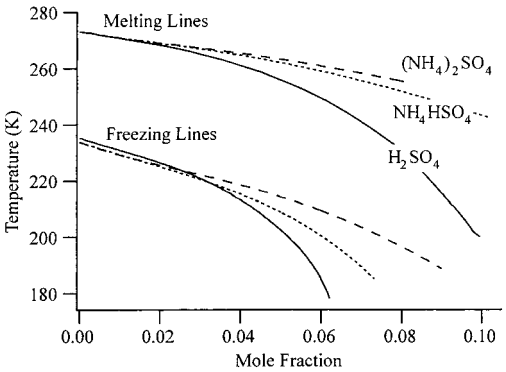

Figure 21. Kinetic phase diagram indicating the temperature and mole fraction at which ice nucleation becomes rapid in aqueous $(NH_4)_2SO_4/H_2SO_4/H_2O$ solutions (i.e., the freezing lines) when homogeneous nucleation is believed to be the freezing mechanism. The data are from refs 10, 19, and 194 for 5−50 μm droplets cooled at 10 K min^{-1}. The gap between freezing and melting lines shows the region of supercooling. Freezing lines depend on observation time and system volumes (eq 5); volume nucleation rates (Figure 31) obviate these extensive properties of freezing lines. As compared to melting lines, freezing lines are more difficult to determine and often are different depending on the experimental method employed. Disagreements with Figure 21 are found in refs 12, 39, and 195, for example.

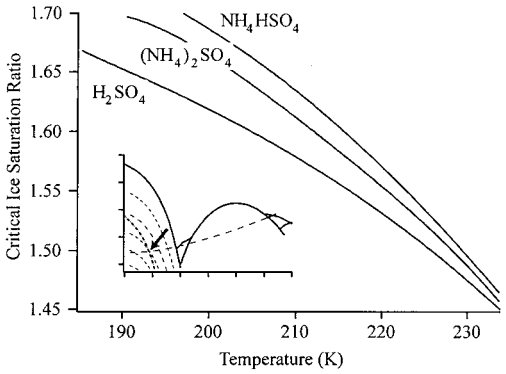

Figure 22. Kinetic phase diagram represented in coordinates of critical ice saturation ratio and temperature. The inset of Figure 22 is described in Figure 12. The composition of an aqueous particle dilutes in a cooling air parcel until the idealized atmospheric trajectory intersects the freezing line where ice forms, as indicated by the inset arrow. Ice saturation at freezing is called the *critical ice saturation ratio.* The critical ice saturation ratio is shown as a function of temperature as inferred from the experiments shown in Figure 21 for 5−50 μm droplets of H_2SO_4/H_2O, NH_4HSO_4/H_2O, and $(NH_4)_2SO_4/H_2O$ cooled at 10 K min^{-1}. Data sources are the same as those in Figure 21.

contours of constant ice saturation ratio from Figure 12 and the supercooling from Figure 21. The intersection of the supercooling line with an idealized atmospheric trajectory occurs at a specific ice saturation ratio and temperature. By considering many trajectories, a set of freezing conditions can be assembled. Figure 22 shows the critical ice saturation ratio that must be attained for freezing to occur as a function of temperature for the systems H_2SO_4/H_2O, NH_4HSO_4/H_2O, and $(NH_4)_2SO_4/H_2O$. It should be noted that the three lines must intersect for pure water at 233 K. Figure 22 shows that homogeneous ice nucleation from $(NH_4)_2SO_4/H_2SO_4/H_2O$ haze to initiate cirrus cloud formation requires saturation ratios exceeding 1.45 for the warmest clouds and 1.55 for typical temperatures in the upper troposphere.

The idealized trajectories shown in the inset of Figure 22 are for aqueous solutions of constant water vapor pressure over a flat surface. In the real atmosphere, the aqueous composition of particles often does not fully equilibrate with the vapor phase during rapid cooling. Even when equilibrium is maintained, the trajectories are size-dependent due to the Kelvin effect. In addition, constant water partial pressure may not be maintained due to scavenging by, for example, ice particles formed by heterogeneous nucleation. The critical ice saturation lines shown in Figure 22 do not incorporate these complexities. In addition, they are derived for 5−50-μm particles cooled at 10 K min^{-1}. For an accurate application to atmospheric results, these kinetic results are better converted to homogeneous volume nucleation rates, J (cm^{-3} s^{-1}), and then applied in a microphysical model.

Figure 22 begs the question of whether the functional forms of critical ice saturation ratio values versus temperature are constrained to occupy a particular region of the saturation ratio−temperature space. We can explore this question by considering an ideal solution. The activity−mole fraction relationship of three hypothetical systems showing linear (Raoult's law), quadratic, and cubic responses are shown in Figure 23A. For the linear form, contours of constant ice saturation ratio are calculated in Figure 23B by employing the known vapor pressure temperature dependencies of liquid water and ice.[127,197] Overlaid in Figure 23B is the supercooling line obtained by setting $\lambda = 2$ where the freezing temperature is given as 233 K + $\lambda\Delta T(x)$ where $\Delta T(x)$ is the equilibrium freezing point depression and x is the total ion mole fraction composition (see eq 11). As with the inset in Figure 22, Figure 23B is sufficient to construct a diagram of critical ice saturation ratio versus temperature (Figure 23C). Within ice saturation ratio−temperature coordinates, the ideal solution behaves remarkably similarly to H_2SO_4/H_2O, NH_4HSO_4/H_2O, and $(NH_4)_2SO_4/H_2O$. The functional form is insensitive to changes in the hygroscopic model to quadratic or cubic form, the number of ions into which the salt dissociates, or the molecular weight of the salt. The sensitivity to increasing changes of ±25% λ is shown by the dashed lines. The conclusion is that, in the ice saturation ratio−temperature representation, the functional form is constrained to a limited region, and so most aqueous particles, all other factors being equal (e.g., particle size), will behave similarly with regard to homogeneous nucleation along idealized atmospheric trajectories.

Figure 24 shows another relationship useful for modeling phase transitions in the atmosphere. One often knows the ice frost point temperature of an air parcel. It would be convenient to know how much supercooling occurs below that temperature before ice formation begins. The inset in Figure 24 shows that the temperature difference is equal to the segment length normal to the horizontal line prescribed by T_{frost} and the intersection point of the

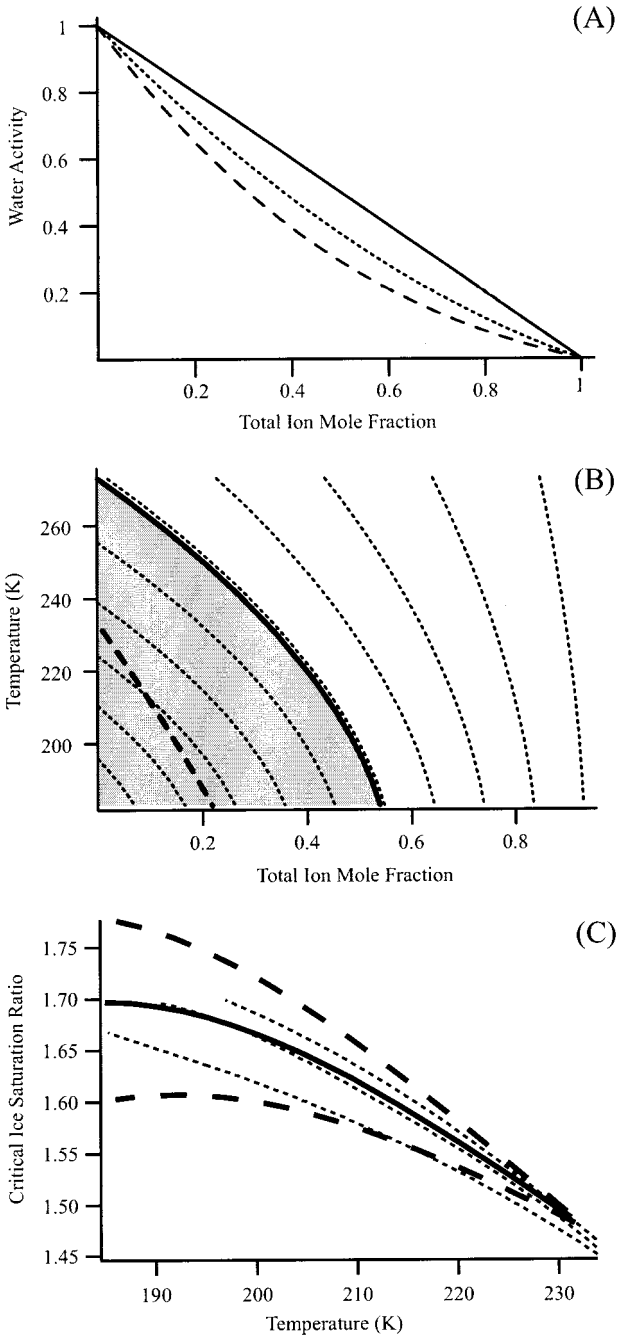

Figure 23. Ideal solution behavior. (A) Water activity for three different solution behaviors, including linear (Raoult's law, $a = 1 - x$) (solid line), quadratic ($a = (1 - x + (1 - x)^2)/2$) (dotted line), and cubic ($a = (1 - x + (1 - x)^2 + (1 - x)^3)/3$) (dashed line) dependencies on total ion mole fraction. (B) Phase diagram showing ice saturation (thick line) of an ideal linear solution. Ice saturation ratio contours (dashed lines) and ice freezing line ($\lambda = 2$) are shown. The diagram can be compared to the inset of Figure 22. The positions of the lines are sensitive to the hygroscopicity of solution (i.e., panel A) and the freezing parameter, λ. (C) Critical ice saturation ratio as a function of temperature for an ideal solution (thick line, $\lambda = 2$). This line is *not* sensitive to the choice of the hygroscopic model, to the number of ions into which the salt dissociates (ν), or to the molecular weight of the salt. The sensitivity to λ is shown for 25% variation (dashed line); an increase in λ yields a higher critical ice saturation. For comparison to Figure 22, the critical ice saturation lines of $(NH_4)_2SO_4$(aq), NH_4HSO_4(aq), and H_2SO_4(aq) are shown (dotted lines).

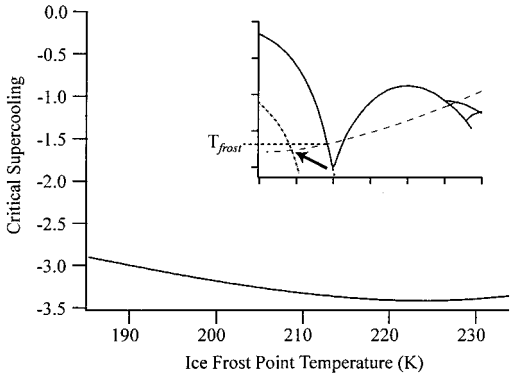

Figure 24. Kinetic phase diagram represented in coordinates of critical supercooling and temperature. The inset is described in Figure 12. The composition of an aqueous particle dilutes in a cooling air parcel until the idealized atmospheric trajectory intersects the freezing line where ice forms, as indicated by the arrow. The temperature difference between the freezing temperature and the ice frost point of the air parcel is called the *critical supercooling*. The critical supercooling in H_2SO_4/H_2O particles as a function of an air parcel's ice frost point temperature is shown. Data sources are the same as those in Figure 21.

idealized atmospheric trajectory and the supercooling line. The supercooling values are compiled for many trajectories and plotted as critical supercooling versus the ice frost point temperature, as shown in Figure 24. Aqueous sulfuric acid droplets cool 3.0 to 3.5 K below the ice frost point temperature. The relatively flat response of the function arises from the approach of idealized atmospheric trajectories to zero slope in temperature−composition coordinates at dilute compositions. In fact, polar stratospheric clouds, which are dominated by HNO_3/H_2O at T_{frost} of the polar winter, are often treated in models as forming 2.5−3.5 K below T_{frost} due to the homogeneous nucleation of ice.[198−199]

3. Expectation Times and *J* Values. Quite often, a phase transition is stated as occurring at a specific temperature or relative humidity. In fact, more exact statements specify the system volume and the observation time. The expectation time, $\langle\tau\rangle$, for the production of crystalline germ is

$$\langle\tau\rangle = \frac{1}{JV} \tag{5}$$

where J (cm^{-3} s^{-1}) is the volume homogeneous nucleation rate and V (cm^3) is the control volume. When crystal growth is rapid, eq 5 also provides the crystallization time of a particle of volume V. For an ensemble of particles, the distribution in $\langle\tau\rangle$ follows Poisson statistics.[28] Figure 25 provides an example of the stochastic nature of crystallization.[78] The relative humidity around single particles of $(NH_4)_2SO_4/H_2O$ and $NaCl/H_2O$ is cycled several times to observe the reproducibility of the efflorescence RH value in single particles. The dashed lines show the expectation value of the experiments.

Two common types of experiments on phase transitions are (a) those that hold temperature (or relative humidity) constant while the fraction of particles in an observed states changes with time or (b) those that cool (or dry) continuously while the phase of the

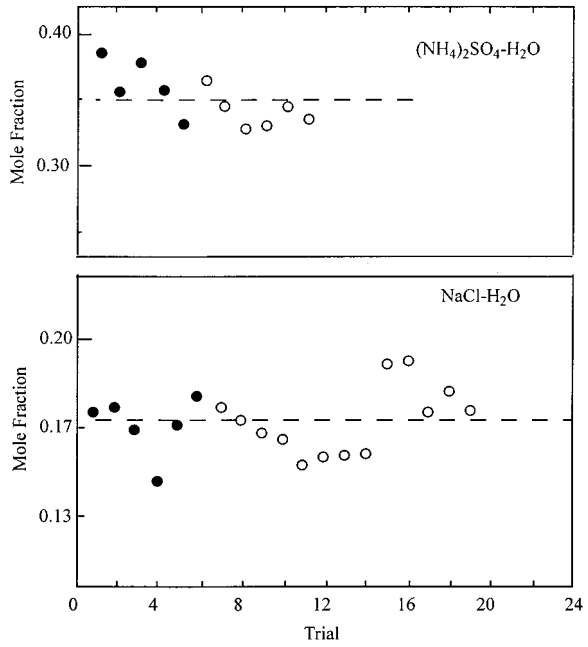

Figure 25. Stochastic nature of crystallization. The mole fraction at which spontaneous crystallization occurs is shown for single particles (20 μm) suspended in an electrodynamic balance. Filled and open symbols are different particles (i.e., a single particle is cycled several times within the same symbol set). (Adapted with permission from ref 78. Copyright 1984 Academic Press.)

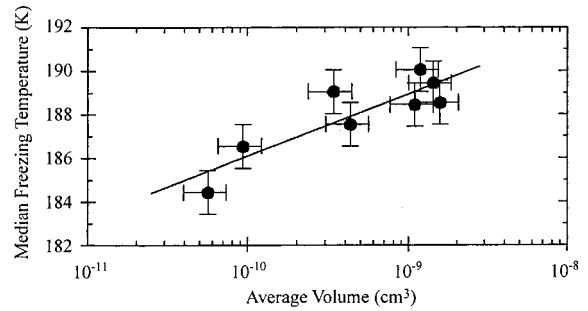

Figure 26. Median freezing temperatures of 7−33 μm of HNO_3/H_2O droplets ($x = 0.33$). (Adapted with permission from ref 192. Copyright 2000 American Geophysical Union.)

particles is observed. J values are calculated from the experimental results for these respective experiments, as follows:[200]

$$J(T) = -\frac{1}{V}\frac{1}{N(t)}\frac{\partial N(t)}{\partial t} \tag{6a}$$

$$J(T) = -\frac{1}{V}\frac{r(T)}{N(T)}\frac{\partial N(T)}{\partial t} \tag{6b}$$

where N is the number of particles still in the initial state (e.g., aqueous) and r is the cooling rate. Monodisperse particles of volume V are assumed; in real applications with polydisperse particles, V is treated as the mean droplet volume.[5]

Equation 5 holds for all system volumes that are much larger than the germ size, approximately 10−25 Å for $NaCl/H_2O$ and $(NH_4)_2SO_4/H_2O$ aqueous solutions at 298 K.[78] Figure 26 shows the dependence of crystallization temperature on system volume for NAD crystals from 0.33 mol fraction of HNO_3/H_2O.[192] The minimum system volume of 5×10^{-11} cm^{-3} corresponds to a sphere of 2.3 μm radius, and the critical germ size is much smaller. In this case, the linear relation anticipated from eq 5 is obeyed. In these experiments, the system is cooling at a constant rate so that the temperature at which 50% of the particles freeze corresponds to observing the particles at a given temperature for specified time period (i.e., the inverse of the cooling rate).

In some cases, the dependence of $<\tau>$ on experimental variables (e.g., temperature) exceeds the experimentalist's control over those variables. Consider an apparatus with a variable observation time, t, containing a large ensemble of particles. A detector in the apparatus responds linearly to the number concentration of particles composed of specific phase. The ideal system will be observed to undergo a phase transition if $<\tau> < t$. In principle, it should then be possible to vary t and some experimental condition such as temperature or composition and thus determine different $<\tau>$ values for the several conditions. In real experiments, however, there are always uncertainties and perhaps gradients in temperature and composition within the apparatus as well as limits to the dynamic range of t. There are important implications on measurements of $<\tau>$. An experiment with a temperature resolution of 1 K provides a convenient example. A freezing temperature is observed, but at 1 K warmer nothing freezes within the longest observation and at 1 K cooler freezing occurs before the shortest observation time. Hence, it is not possible to associate an accurate observation time with the freezing temperature, although it is possible to declare limits on the observation time.

The effects of uncertainties on $<\tau>$ are calculated by obtaining the full derivative of eq 5 as follows:

$$D\langle\tau\rangle = -\frac{1}{J^2V}DJ - \frac{1}{V^2J}DV \tag{7}$$

The volume rate J depends on temperature and chemical composition. As an example, a change in water activity, a, affects J but not V, and we obtain

$$\frac{\partial\langle\tau\rangle}{\partial a} = -\frac{1}{J(a)^2V}\frac{\partial J}{\partial a} - \frac{1}{V^2J(a)}\frac{\partial V}{\partial a} = -\frac{1}{V}\frac{1}{J(a)^2}\frac{\partial J}{\partial a} \tag{8}$$

The capability in the experiment to control a within $\pm\sigma$ is associated with controlling the expectation time, as follows:

$$\langle\tau\rangle_{\min} = \langle\tau(a-\sigma)\rangle \approx \langle\tau(a)\rangle - \sigma\frac{\partial\langle\tau\rangle}{\partial a} = \langle\tau(a)\rangle + \sigma\frac{1}{V}\frac{1}{J(a)^2}\frac{\partial J}{\partial a}$$

$$\langle\tau\rangle_{\max} = \langle\tau(a+\sigma)\rangle \approx \langle\tau(a)\rangle + \sigma\frac{\partial\langle\tau\rangle}{\partial a} = \langle\tau(a)\rangle - \sigma\frac{1}{V}\frac{1}{J(a)^2}\frac{\partial J}{\partial a} \tag{9}$$

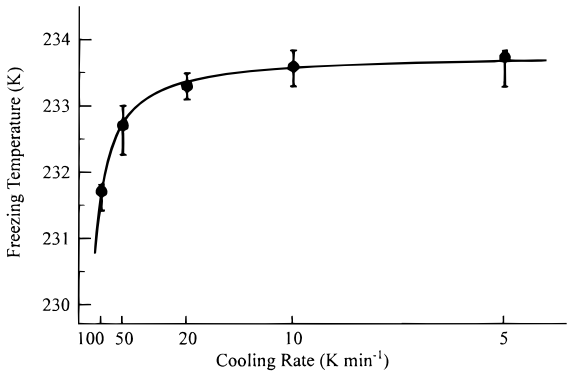

Figure 27. Median freezing temperatures as a function of cooling rate for 3−12 μm of H_2SO_4/H_2O droplets (x = 3.9−4.5 × 10^{-3}). For the rapid cooling rates (>10 K min^{-1}), at least part of the apparent drop in freezing temperatures arises from an experimental artifact of a lag time for temperature propagation from the location of measurement by a thermocouple and the particles' support. The other part of the drop in freezing temperature is accounted for by the reduced observation time due to rapid cooling (cf. eqs 5−9 in text). (Adapted with permission from ref 19. Copyright 1998 American Chemical Society.)

where a Taylor expansion is shown. The expansion is not accurate for typical $\pm\sigma$ values, but it serves to show the essential dependence on the slope of J with a. When the dynamic range of the experiment is less than $<\tau>_{min}$ and $<\tau>_{max}$, then a phase transition activity is stated without an accurate observation time. When the dynamic range of t corresponds to typical range of other applications, this fact is not a problem. Usually laboratory dynamic ranges are seconds to hours, and laboratory intercomparisons are often possible. In contrast, atmospheric processes can sometimes be of weeks, so appropriate awareness of these facts is warranted.

Figure 27 indicates the dependence of reported freezing temperatures on observation time, which is inversely related to cooling rate, for ice formation in 0.004 mol fraction of H_2SO_4/H_2O.[19] In principle, there is no simple relationship (e.g., linear or exponential) between the reported freezing temperature and the observation time because of the dependence of J on both temperature and composition. It is possible to form glasses (i.e., obviate freezing entirely) by rapid quenching of aqueous solution in liquid nitrogen[37,183] or to form crystals at the thermodynamic melting temperature provided an infinite observation time.

Figure 28 shows the dependence of J on temperature for ice formation in water. The slope is directly $\partial J/\partial T$, akin to $\partial J/\partial a$ in eq 9. There is roughly a 10-fold increase in nucleation rate per degree Kelvin. An experiment with ±1 K temperature control and only an order of magnitude capability to vary t would not be able to see any differences in freezing temperature, and thus the experimenter would report a single freezing temperature for ice (at constant system volume). Ice nucleation from water and other aqueous solutions has very strong dependencies of J on T. Figure 29 shows that NAD formation in a stoichiometric aqueous solution has a weaker temperature dependence of roughly a 10-fold increase per 3 degees K. The study of NAD nucleation kinetics in the lab is then less exacting than ice formation. SAT

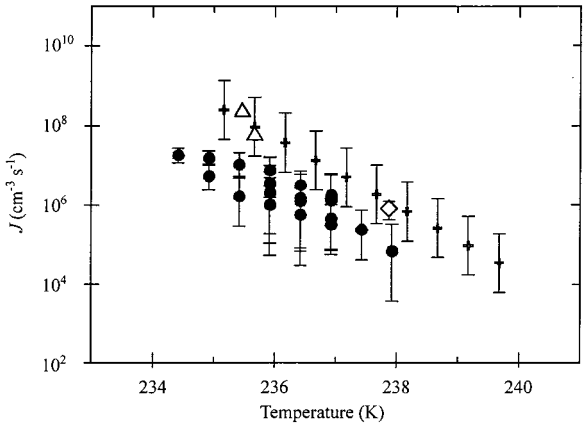

Figure 28. Measured volume nucleation rate in pure water as function of temperature (cf. Figure 31). Solid circles: ref 192. Crosses: ref 201. Open triangles: ref 202. Open diamonds: ref 203. (Adapted with permission from ref 192. Copyright 2000 American Geophysical Union.)

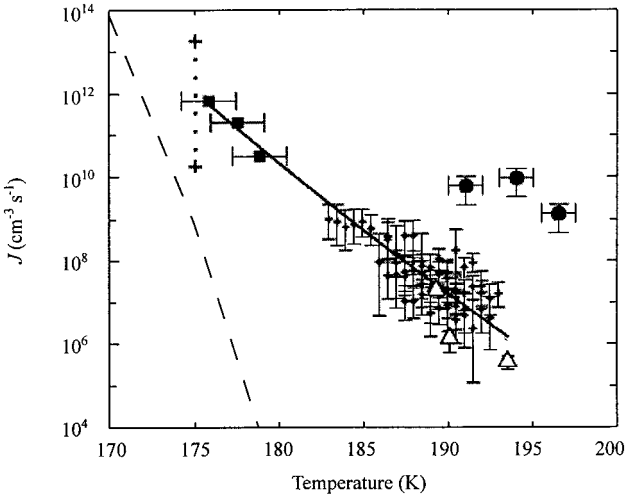

Figure 29. Volume nucleation rates, J, of $HNO_3{\cdot}2H_2O$ in 7−33 μm of HNO_3/H_2O (x = 0.33) droplets. Small crosses: experiments at constant cooling, ref 192. Open triangles: experiments at constant temperature, ref 192. Long dashed line, ref 204. Squares, ref 24. Circles, ref 23. Large crosses/dotted line: limits calculated from ref 64. Solid line: fit to the data. (Adapted with permission from ref 192. Copyright 2000 American Geophysical Union.)

nucleation from stoichiometric solutions is again an order of magnitude in J per degree Kelvin.[205] However, its overall volume nucleation rate is slow and hinders convenient laboratory measurement.[28] At least, however, upper limits to the J values can be calculated. A maximum J value of 5 × 10^{-8} cm^{-3} s^{-1} is obtained, as compared to the much larger values of NAD shown in Figure 29.

Although a composition containing NAT is thermodynamically favored for a 0.33 mol fraction solution (Figure 14A), NAD nucleation often occurs more rapidly. Quite often when an aqueous solution is saturated with respect to one or more solids, the first solid to nucleate is metastable. This phenomenon is termed Ostwald's rule of stages.[178,206] The volume nucleation rate to form a metastable solid tends to be higher than the most thermodynamically stable solid. Metastable solids are less thermodynamically favorable and have higher solubilities. In this case, the surface tension between a crystalline germ of this

material and the aqueous solution tends to be small.[207] Critical germs thus form rapidly because only a small surface energy barrier must be overcome. Later, germs of the thermodynamically stable phase form and the system gradually changes from the metastable to the stable composition through Ostwald's ripening. On the basis of laboratory results, Fox et al. suggested that NAD nucleation is preferable to NAT from supersaturated H_2O and HNO_3 gaseous mixtures and that other metastable phases possibly exist and participate in polar stratospheric cloud formation.[44]

Submicron aqueous particles in the atmosphere may nucleate unexpected crystalline phases as compared to measurements in the laboratory on larger system volumes for several reasons. Because of the small volume of a submicron particle, a single nucleation event requires more time (eq 5) as compared to a larger volume system. As a result, low water activities are reached and, in this case, whereas J_α for an α-modification may be fast at higher water activities, J_β for a β-modification may dominant at the lower water activities. In this case, the β-form would nucleate first in the submicron particles. Another way to obtain a different phase is tied to Ostwald's rule of stages. In this case, both large and small volume systems are assumed to nucleate the β-phase first. In the large volume system, an α-germ forms sparsely but grows through Ostwald's ripening so that the whole system converts from β to α. In a small volume system, the probability to form an α-germ is negligible, so the system persists in the β-form. In atmospheric chemical systems studied to date, there is generally a good correspondence between phases nucleated in large and small volume systems. However, at least one exception is noted for NH_4HSO_4, which appears to form a new crystalline form only known for small particles.[208] Figure 30 shows the Raman spectrum of α- and β-NH_4HSO_4, with respective deliquescence RH values of 40 and 37%.[208] There is some controversy surrounding this solid, and it may form by heterogeneous nucleation on impurities. Other research groups report the persistence of NH_4HSO_4(aq) even to low RH values (Table 3).

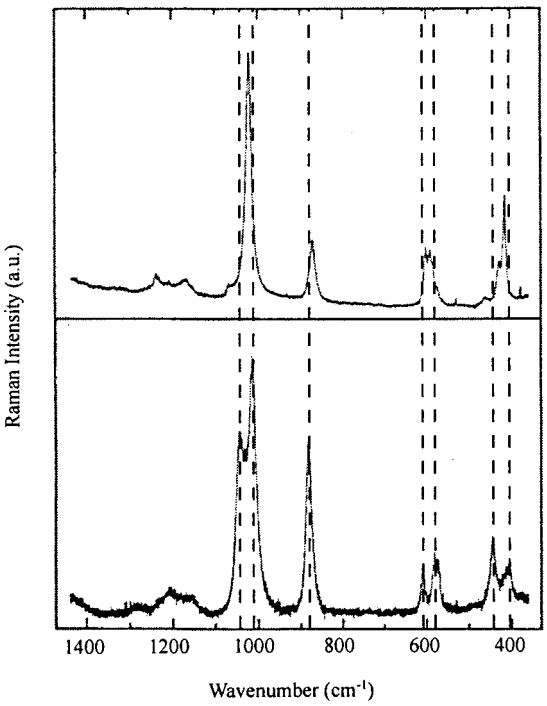

Figure 30. Raman spectra obtained for (top) α-NH_4HSO_4(s) and (bottom) β-NH_4HSO_4(s). The α-form is well-known, but the β-form is hitherto unknown and appears to nucleate only in small (<50 μm) droplets. The small droplets reach high supersaturations without nucleating the α-form, thus making possible β-nucleation. The aqueous droplet probably contains a heterogeneous nucleus because impurity-free NH_4HSO_4(aq) does not readily crystallize, even to 0% RH (see Table 3). (Adapted with permission from ref 208. Copyright 1995 Taylor & Francis.)

E. Heterogeneous Nucleation

i. Nuclei Contained Inside Atmospheric Particles

Aqueous atmospheric particles often contain insoluble inclusions such as soot or mineral dusts.[209−211] Mineral dust components include silicates, aluminosilicates, and iron oxides[212,213] and are known by several names, including metal oxides, crustal components, aeolian dusts, and Harmmatan dusts.[214,215] These materials provide well-ordered atomic arrays that one would suspect of imparting local order into nearby aqueous solutions and thus increasing the frequency of critical cluster formation.[216−218] Common global sources of the crustal components are Saharan and Gobi Desert dusts.[219−228] Satellites provide excellent global images showing wide seasonal and geographical dependencies of Saharan and Gobi Desert dusts.[229] The dusts advect long distances over the Atlantic and Pacific Oceans and become coated with various sea salts, sulfates, nitrates, and other electrolytes when passing through marine or polluted continental regions.[230−235]

Andreae et al.[236] report that a large fraction of the silicate mineral aerosol from the remote marine area is internally mixed with sea salt. Parungo et al.[237] find that dust particles from China are coated by secondary aerosol components emitted from industrial regions. Levin et al. report that mineral dust particles from air masses in the eastern Mediterranean passing into Israel are coated with sulfate and other soluble materials.[238] Piketh et al. report that aeolian dust outflows from South Africa over the Indian Ocean are coated with sulfate.[233] Cloud processing is likely one important coating mechanism.[239] In addition, gas-phase constituents such as NO_2 can deposit on metal oxide surfaces to form surface-adsorbed nitrate,[240,241] and infrared spectroscopy of collected aerosol shows chemisorbed nitrate features on mineral dust components.[242] Dentener et al.,[243] Zhang and Carmichael,[244] and Song and Carmichael[245] employ a combination of field measurements and three-dimensional regional and global model calculations to conclude that mineral particles are frequently coated by nitrates and sulfates in the atmosphere.

There is a common belief that mineral dusts appear in a supermicron mode while electrolytes appear in a submicron mode. While often true on a mass basis, the proper question for heterogeneous nucleation is: How often are submicron mineral dusts constituents

found in association with electrolytes? Niimura et al. report that 30−60% and sometimes up to 100% of Gobi dust particles are coated by sea salt by the time these particles reach Nagasaki.[246] Transmission electron micrographs of particles collected over the open ocean show many examples of submicron oxides coated by sulfates, nitrates, and sea salt.[230,232] In fact, the mode size of African dusts off shore is below 1 μm.[247] In a recent inventory of emissions in the Los Angeles area, 167 kg day^{-1} of PM2.5 is prescribed, of which 67 kg day^{-1} is crustal components.[248] Ichoku et al.[249] also report crustal components in the fine aerosol mode in Israel. In the stratosphere, less is known but Murphy et al. reported that iron is present in about half of the mass spectra of individual particles.[250] Whether the iron is dissolved or incorporated in an crystalline oxide matrix is unknown. In conclusion, although most laboratory work on tropospheric aerosols has focused on homogeneous nucleation of crystalline phases from aqueous electrolytes, the frequent occurrence of heterogeneous nuclei suggests this area is important for future laboratory work.

ii. Observations and Concepts

Initial work on heterogeneous nucleation by metal oxides and soot incorporated inside aqueous electrolytes has been done by several groups.[13,21,196,251−255] A larger literature[6] exists on heterogeneous nucleation of ice in water droplets (i.e., no or very dilute dissolved salts), often related to cloud seeding experiments. Ice formation in mid-troposphere clouds begins at temperatures much warmer than those associated with homogeneous ice nucleation in pure water. For example, mixed-phase clouds as warm at −5 °C are common. Research in this area[6,8] attempts to quantify and understand the temperatures at which naturally occurring heterogeneous nuclei, including those from biogenic sources,[256,257] or anthropogenically produced AgI cloud-seeding[80,258−260] particles induce ice formation in dilute (i.e., water activity approaching unity) aqueous droplets.[200,261−266] Early work also investigated the role of dissolved salts in reducing freezing temperatures, principally for heterogeneous nucleation (typically, −5 to −30 °C).[159,267−270] The contrast should be pointed out that this early work was mainly on dilute solutions (under 1 *m*) whereas today's laboratory investigations on cirrus and PSC formation are on more concentrated electrolytes (1−10 *m*) at temperatures from −40 to −90 °C in connection with the effect of the electrolytes on inhibiting homogeneous ice nucleation.

Gold provides a striking example of effective heterogeneous nucleation; supercooling of 5-μm aqueous sulfuric acid droplets is reduced from 40 to 20 K.[26] The contact angle, Θ, between gold and water is 65.5° (Table 5.2 of ref 2). Koop et al. were able to eliminate heterogeneous nucleation and observe homogeneous nucleation by coating silica (Θ = 43−52°) with a monomolecular hydrophobic silanizing agent (Prosil 28, Θ > 100°).[19] In contrast to the relative ease with which ice nucleates heterogeneously, acid hydrates in concentrated aqueous solutions of H_2SO_4 and HNO_3 do not appear to nucleate readily at low temperatures (<200 K) even when in contact with several metal oxides representative of meteoritic material.[255] At 298 K, however, seven metal oxides increase the efflorescence relative humidity of $(NH_4)_2SO_4/H_2O$ particles from 35% for homogeneous nucleation up to 65%, as shown in Table 4.[13]

Table 4. Relative Humidities (±2%) at Which Efflorescence Occurs for $(NH_4)_2SO_4/H_2O$ Droplets at 298 K[a]

heterogeneous nucleus	RH efflorescence	surface area of inclusion (μm^2)	obsn time (min)	ref
none	33−37	na	na	see Table 3
am-SiO_2	35	3	1	271
$Al_6Si_2O_{13}$	42	3	1	271
$BaSO_4$	46	0.1	1	253
α-Fe_2O_3	47	3	1	271
α-Al_2O_3	48	3	1	271
$CaCO_3$	49	0.6	1	253
δ-Al_2O_3	57	40	1	13
ZrO_2	59	40	1	13
TiO_2	65	40	1	13

[a] Variations in the specific surface areas of the inclusions and in the observation times may affect the observed RH values for efflorescence. The deliquescence relative humidity is 79.5% at 298 K.

For these seven metal oxides as well as other heterogeneous nuclei, crystallization occurs as determined by the heterogeneous nucleation area rate, $j_{k,l}$ (cm^{-2} s^{-1}), specific to each crystal face k of each mineral component l. In addition, the nucleation efficiency of each face depends on its processing, i.e., presence of defects and other nucleation centers. At a specific relative humidity (i.e., a_{H_2O}), each face of area $A_{k,l}$ (cm^2) has a probability of inducing nucleation after a time t as follows: $P_{k,l}(t) = 1 - \exp(-j_{k,l}A_{k,l}t)$. The overall probability of a transition is then as follows:

$$P(t) = 1 - \prod_{k,l}(1 - P_{k,l}) \qquad (10)$$

Even for a particle containing a single component (i.e., $l = 1$), a closed-formed crystal will have at least six faces (i.e., a cube, $k = 6$) and likely many more for real crystals. In addition, each face has numerous defect sites not included in the description for eq 10. In contrast, as shown in Table 4, typical data collected in a heterogeneous nucleation experiment are insufficient to constrain eq 10. However, with the hypothesis that one specific mineral face (viz., k^*,l^*) exceeds the efficiency of all others (i.e., $P_{k^*,l^*} \gg \{P_{k,l}\}_{k\neq k^*,l\neq l^*}$), then eq 10 simplifies: $P(t) \approx P_{k^*,l^*}$. If the hypothesis is accurate, determining the efflorescence RH associated with an assemblage of minerals in a single particle requires knowledge of only the most active component (i.e., maximum RH value shown in Table 4). Furthermore, the effect of differences in size and shape of the same mineral component in one particle versus another (or laboratory versus atmospheric particles) centers upon whether the particles share the critical nucleation site k^*,l^*.

The physical complexity inherent in eq 10 for a single particle is simplified by two common hypotheses regarding either singular or stochastic hetero-

geneous nucleation in a population of particles.[5,262] The stochastic hypothesis views each aqueous particle as containing enough (i.e., very many) heterogeneous nuclei such that each particle is equivalent. In this case, the probability of a single particle undergoing a phase change is stochastic. Phenomenologically, the particles behave just as though they are undergoing homogeneous nucleation except for undergoing a phase change at lower supersaturations. In contrast, the singular hypothesis envisions that heterogeneous nuclei of different efficiencies are distributed among the aqueous particles, and that the total number of heterogeneous nuclei is insufficient for statistical homogeneity among the aqueous particles. Each nuclei is assigned a specific activity (similar to k^*,l^* hypothesis above). Those particles that phase change first are presumed to contain more active heterogeneous nuclei. When the system is cycled, these same particles should again activate first. In addition, the critical temperature (or relative humidity) to induce the phase change is independent of the cooling rate. These last two points phenomenologically distinguish the singular and stochastic hypotheses.

In addition to mineral dusts, soot is a common constituent in tropospheric aerosol, with as much as 10−45% of tropospheric sulfate particles appearing to contain soot even in remote marine aerosol.[272] Recent laboratory work on soot has shown it is not an effective nucleus for ice formation in H_2SO_4/H_2O particles,[252] not for SAT nucleation in $x = 0.20$ particles of H_2SO_4/H_2O,[273] not for crystallization of NaCl droplets at 298 K,[274] and not for crystallization of $(NH_4)_2SO_4/NH_4NO_3/H_2O$ at 298 K.[21] In agreement with these laboratory results, measurements of ice nuclei concentrations in aircraft plumes containing soot particles show no changes from background levels in the upper troposphere.[275] Soot probably is not an effective heterogeneous nucleus because it does not contain a regular array of atoms that induce local order in the nearby aqueous medium. [The structure of soot is usually planar graphite as a hydrophobic core with onion layers of increasing hydrophilic material. The surface exposed to the aqueous medium is often oxygenated, diverse, and amorphous.[276−278]]

It has been suggested that the high frequency with which soot occurs as an evaporation residual of contrail ice particles indicates aircraft soot is a heterogeneous nucleus for ice.[279,280] In light of the laboratory and field evidence to the contrary, however, two alternative explanations appear more tenable. First, the high particle number density of soot particles in a contrail suggests that they may agglomerate with the larger ice particles via coagulation. Second, because relative humidities above 100% with respect to liquid water are obtained due to fast cooling of the jet exhaust, aqueous particles dilute and rapidly freeze via homogeneous nucleation. The unusually high ice particle number densities typical of contrails, as compared to cirrus clouds, are consistent with homogeneous nucleation as the dominant mechanism during rapid cooling. Prior to freezing, the aqueous particles may contain soot particles with high frequency, so the resulting ice particles also contain soot. Both proposed alternatives explain the high frequency of soot in association with contrail ice without invoking soot as a heterogeneous nucleus.

Another possibility for heterogeneous nucleation occurs in atmospheric particles after an initial precipitate forms. For example, in aqueous H_2SO_4/H_2O droplet, if ice homogeneously nucleates, then ice could possibly heterogeneously nucleate acid hydrates from the H_2SO_4-enriched residual liquid. In this type of experiment, ice was found to be a good heterogeneous nucleus for SAT.[26] In related experiments, crystal seeds (e.g., ice, NAT, or SAT) were added to test tubes containing supercooled liquids and workers observed if further crystallization in the liquid was induced.[54] As expected, acid hydrates readily promote further crystallization in solutions already supersaturated with respect to the added hydrates. Most acid hydrates are also good nuclei for ice. However, it is usually found that acid hydrates do not act as good heterogeneous nuclei for other acid hydrates (e.g., NAT is a poor nucleus for SAT and vice versa[45]) and that ice is not a good heterogeneous nucleus for acid hydrates.[28] This relationship is perhaps understood by noting that the acid hydrates, being composed of mixed chemical compositions, require both spatial and chemical matches on underlying heterogeneous substrates for rapid nucleation to occur. Ice, in contrast, requires only a good spatial match because it is composed of a single chemical component. This explanation is consistent with the observation that SAT, once associated with NAT, appears to undergo surface changes to accommodate the NAT crystal. These changes are persistent upon SAT evaporation such that SAT is a good heterogeneous nucleus for NAT condensation when again introduced into a supersaturated NAT conditions.[38] See Koop et al.[109] for a further account of PSC formation pathways or Peter[281] for a history of the development of PSC theories.

V. Implementation in Microphysical Models

The previous section on kinetics discussed nucleation mostly in empirical terms. The next step is to consider data reduction of laboratory data, possibly as simple parametrizations, but preferably in an intellectual framework. Classical nucleation theory achieves limited success in understanding laboratory data, and nonclassical theories have been applied more recently. A successful theory could be employed to obtain accurate values beyond the domain of temperatures, aqueous compositions, and observation times studied in the laboratory. In atmospheric sciences, a further need is to develop the nucleation theories into larger models of microphysics and atmospheric phase transitions important in processes such as polar stratospheric or cirrus cloud formation. The usual approach is to parametrize the results of nucleation theories so that the computationally intensive nucleation calculations can be avoided in a larger model considering microphysics, mass transport, energy transport, and other large-scale processes. These complex models are employed to try to understand issues such as global warming, tropo-

spheric ozone, the ozone hole, or visibility reduction. Baker provides an example of the path from nucleation theory to large-scale calculations of radiative forcing and cloud formation.[3]

This review is not inclusive of the large amount of work done on nucleation theory in the atmospheric sciences. Rather, an introduction with selected references to contemporary approaches is provided. These approaches are conveniently divided into four categories: semiempirical correlations;[126,159,282,283] classical nucleation theory;[35,37,185,198,199,204,205,284,285] nonclassical theories;[286−290] and parametrizations incorporated into microphysical models.[291−295] The first semiempirical correlation is that the lines in a kinetic phase diagram parallel those in an equilibrium phase diagram.[296] This suggestion is perhaps startling because there need be no necessary connection between free energies and nucleation kinetics. Even so, Figure 21 shows that the freezing lines in $(NH_4)_2SO_4/H_2O$, NH_4HSO_4/H_2O, and H_2SO_4/H_2O appear related to the melting lines. Similar correlation between the temperature-dependent deliquescence and efflorescence lines is observed for $(NH_4)_2SO_4/H_2O$.[11,12]

A. Semiempirical Correlations

Quite commonly, the temperature at which nucleation is rapid (ΔT_f) is proportional (λ) to the melting point temperature (ΔT_m), as follows:

$$\Delta T_f(x) = 233 - \lambda \Delta T_m(x) \tag{11}$$

where x is the mole fraction composition of the aqueous solution. Equation 11 holds for a 50% freezing probability for micron-sized droplets; DeMott discusses the generalization of eq 11 in terms of an effective freezing temperature, which allows application to other freezing probabilities and particle sizes.[297] Equation 11 is true for many common salts (e.g., $CaCl_2$, $MgCl_2$, NaCl, KCl, LiCl, and NH_4Cl) for ΔT_m up to 15 K, after which deviations become apparent, over the typical range $1.5 < \lambda < 2.0$. DeMott discusses the accuracy of eq 11 for other atmospheric systems, and the implementation of eq 11 for atmospheric systems is shown in refs 282, 283, and 295. Rasmussen rationalizes eq 11 by stating that the thermodynamic properties (i.e., ΔT_m) relate to the kinetic processes (i.e., ΔT_f) because spinodal decomposition occurs in ice formation in aqueous electrolytes.[126,158,159] In this case, a system reaching the extremal of the thermodynamic function becomes unstable and rapidly nucleates stable phases. Unfortunately, free energy calculations based upon eq B10 (Appendix B) do not support an explanation of spinodal decomposition (unpublished results, Martin). A tenable rationalization of the broad applicability of eq 11 remains an open question.

B. Classical Nucleation Theory

Classical nucleation theory provides another framework to quantify nucleation rates. The basic precepts are covered in original references[298−300] and specifically in the context of atmospheric systems in Chapter 7 of ref 2 and in Chapter XIII of ref 120. The probability of a chemical system forming a critical nucleus after time t is

$$P(t) = 1 - \exp(-JVt) \tag{12}$$

where V is the system volume and J is the volume nucleation rate. The expectation value of the Poisson distribution (eq 12) is provided in eq 5. The volume nucleation rate is

$$J = a \exp\left(\frac{-\Delta G_{germ} - \Delta G_{diff}}{kT}\right) \tag{13}$$

where a is a preexponential factor, k is the Boltzmann constant, T is temperature, ΔG_{germ} is the free energy of germ formation, and ΔG_{diff} is the diffusion activation energy. The preexponential factor is loosely analogous to a kinetic attempt frequency and its full-form is as follows:

$$a = n\frac{kT}{h}\left(\frac{b N_{germ}^{2/3} \Omega_{germ} A^{1/2}}{3\pi^{1/2}}\right) \tag{14}$$

where n is the molecular concentration in the liquid phase, h is Planck's constant, b is the number of molecules per unit area of a liquid in contact with the germ, N_{germ} is the number of molecules in a germ, Ω_{germ} is the surface area of the germ, and A is a constant for the mother liquor. In the case of a spherical germ, eq 14 can be written as follows:

$$a = n\frac{kT}{h}\left(\frac{2\nu b\sqrt{\sigma_{germ}}}{\sqrt{kT}}\right) \tag{15}$$

where ν is the molecular volume and σ_{germ} is the surface tension of the germ in the medium. The term in parentheses of eq 15 often evaluates to near unity, and the approximation below is employed:

$$a \approx n\frac{kT}{h} \tag{16}$$

Equation 16 often also holds for nonspherical germs.

The free energy of germ formation, ΔG_{germ}, is as follows:

$$\Delta G_{germ} = \frac{16\pi\nu^2\sigma_{germ}^3}{3(kT \ln S)^2} \tag{17}$$

where S is the saturation ratio of a metastable phase with respect to a stable phase. The third-order dependence on σ_{germ} means this term is a critical factor in calculations. Luo et al.[205] estimated σ_{germ} based upon the number of bonds broken and formed at the interface and the associated energies of each of those bonds. Pruppaccher[185] tried a similar approach by noting the anomalous behavior of hydrogen bonding in supercooled water. MacKenzie et al.[204] employed the Turnbull correlation to establish a relationship between σ_{germ} and the enthalpy of fusion from the liquid to the crystal. Tabazadeh et al.[199] employed Antonoff's rule to obtain σ_{germ} (i.e., between the crystal and the liquid) as the absolute value of the difference between $\sigma_{crystal/air}$ and $\sigma_{liquid/air}$. Tisdale

et al.[35] and Disselkamp et al.[37] approached the problem from the reverse direction by measuring J values in laboratory experiments and interpreting the data in the structure of eq 13 to obtain σ_{germ}.

The saturation ratio S in eq 17 is calculated by several methods. The models of Clegg et al.,[134,162] which are available on the web, are particularly useful for direct calculations. In systems for which the thermodynamic data are unknown, approximation methods are employed. For example, the free energies and hence the saturation ratios of supercooled chemical systems having approximately temperature-independent heat capacities can be estimated by extrapolation from warmer temperatures by employing a combination of the Gibbs−Helmholtz equation and Kirchhoff's law.[140] MacKenzie et al.[204] provide an example. With a few additional assumptions (see eqs 1−12 of ref 178), the saturation ratio, S_{melt}, of a melt with respect to its solid (i.e., pure water to ice) is further approximated from the extent of supercooling, ΔT, the melting temperature, T_m (i.e., 273.16 K for ice), and the latent heat of melting per molecule, L_m, as follows:

$$kT \ln S_{melt} = \frac{L_m}{T_m}\Delta T \tag{18}$$

We can express S_{melt} as $\Delta\mu_{melt\rightarrow solid} = \mu_{solid} - \mu_{melt} = -RT \ln S_{melt}$ (eq B9). For an aqueous solution supersaturated with respect to ice, we have

$$\begin{aligned} -RT \ln S &= \Delta\mu_{H_2O(aq)\rightarrow H_2O(ice)} \\ &= \mu_{H_2O(ice)} - \mu_{H_2O(aq)} \\ &= \mu_{H_2O(ice)} - \mu^0_{H_2O(melt)} - RT \ln a_{H_2O(aq)} \\ &= -RT \ln S_{melt} - RT \ln a_{H_2O(aq)} \end{aligned} \tag{19}$$

Combining eqs 18 and 19 yields

$$kT \ln S = \frac{L_m}{T_m}\Delta T + kT \ln a_{H_2O} \tag{20}$$

For sufficiently small $\Delta T/T_m$, $\ln(T_m/T) \approx (T_m - T)/T_m$, and eq 20 is then written:

$$kT \ln S \approx L_m \ln\left(\frac{T_m}{T}\right) + kT \ln a_{H_2O} \tag{21}$$

Jensen et al.[284,293] and Tabazadeh et al.[199] employ forms similar to eq 21.

Of the key parameters in eq 13, the most intractable is probably ΔG_{diff} because its microscopic value precludes direct measurement. Fortunately, J values from eq 13 go through a maximum, and if crystallization occurs at all, it usually occurs during the approach to the maximum in most atmospheric systems. During the approach to the maximum, J is not very sensitive to ΔG_{diff}, which is a more important parameter (and actually responsible for) decreasing J after its maximum. By far, the most sensitive parameter in eq 13 is σ_{germ}, a quantity measurable in principle. Most values for ΔG_{diff} are based upon the Arrhenius activation parameter observed in the temperature dependence of viscosities, as follows:

$$\Delta G_{diff} = k\frac{\partial \ln (\eta/T)}{\partial(1/T)} \tag{22}$$

Tabazadeh et al.[199] employed this method based upon the data of Williams and Long.[301] However, the estimation via eq 22 of ΔG_{diff}, for use in the calculation of microscopic nucleation rates, from macroscopic viscous flow measurements is a source of continued uncertainty.[185,199]

The application of eqs 13−22 can often be confusing because, although eq 13 is straightforward, the mire of details in terms of σ, a, S, and other values is often difficult. One specific example including all equations in an appendix table is provided in a pair of papers by Tabazadeh et al.[199,302] The major advantage of classical nucleation theory is that obtained data are conveniently reduced to the functional form of eq 13. However, major conceptual shortcomings appear to exist in assuming macroscopic measurements of η and σ are relevant concepts at the cluster level. In fact, all applications of classical nucleation theory in the atmospheric sciences calibrate at least one term in eqs 13−22 against measurement, and many workers then consider classical nucleation theory as a semiempirical correlation. As such, any extrapolations beyond the domain of calibration should be viewed with caution. Shortcomings of classical nucleation theory are further described in ref 303. Even so, the theory is the most widely applied framework for phase transitions in atmospheric chemistry, and it provides the tools to integrate laboratory data and produce straightforward and comprehensive diagrams of volume nucleation rates as $J = f(T, x)$. An example of calculation results for $J = f(T, 0)$ is shown in Figure 31.[291]

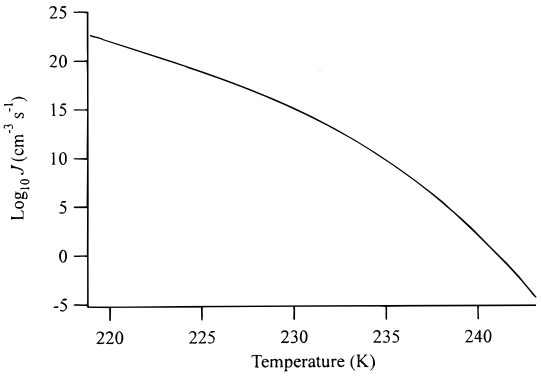

Figure 31. Volume nucleation rate, J, calculated from classical homogeneous nucleation theory as a function of temperature for ice from supercooled water (cf. Figure 28). (Adapted with permission from ref 291. Copyright 1998 American Geophysical Union.)

C. Nonclassical Nucleation Theories

Nonclassical nucleation theories are based on either kinetic or cluster approaches. In the kinetic formulation, the growth of oligomers is treated as a chemical reaction, and n-mer dependent rate constants are applied for a cluster taking up or losing an individual molecule. Classical ideas of surface tension and other energetic considerations are not

necessary in this approach. In the cluster approach, the cornerstone returns to equilibrium among clusters, as in classical theory, but each cluster is modeled microscopically with computer simulations of geometry, energy, and density. A detailed review of these theories appears in ref 289. To date, these theories appear to hold promise but have not yet been incorporated into models practical enough for use in the atmospheric sciences, with pure water as the sole exception.[2,286]

D. Microphysical Models

The details of classical and nonclassical theory are subsumed within eq 12, which is then a starting point for understanding phase transitions in integrated atmospheric systems. For example, a model of cirrus cloud formation must include eq 12 and, if it is a detailed model, a nucleation theory (usually classical) to describe the formulation of J. In addition, the model must include microphysical, radiative, and dynamical components. This point is understood well with the rubric of taking an individual particle as the frame of reference. This particle cools as the air parcel containing it rises, for example, and it also can condense water and dilute as the relative humidity increases with dropping temperatures. If the particle then forms ice, it can grow to be several hundred microns, thus depleting the water vapor. If, however, a nearby particle were to nucleate ice first and deplete the water vapor, then the original particle would remain a concentrated aqueous droplet. The large particle may also act to absorb infrared radiation if it is located at the base of the cloud and thus induce local warming. Alternatively, at the top of the cloud, it may radiate in the infrared and lead to local cooling. Changes in air parcel buoyancy may then induce convection of the air parcel containing the particle, with changes again occurring in temperature and relative humidity. The large particle may also sediment rapidly and separate from the air parcel. Thus, accurate simulations should be based on mass and energy continuity equations, including nucleation, condensation, deposition, evaporation, sublimation, coagulation, sedimentation, advection, diffusion, and radiation.[304]

These elements were integrated in early work on modeling cirrus cloud formation by Starr and Cox.[305,306] An excellent example of recent work is provided by Jensen et al.[292−294] Figure 32 depicts the results of a simulation of cirrus cloud formation for air rising over Wyoming and headed toward Wisconsin. After 90 min, a horizontal cirrus cloud forms. After another 90 min, full-blown sedimentation and evaporation is apparent, reminiscent of the wisps seen for authentic cirrus. As a test of the model's accuracy, direct comparison of the optical depths calculated for the clouds in Figure 32 can be made with satellite measurements. The tradeoff paid for a comprehensive microphysical, radiative, and dynamical model is the computational time. It may not be practical to include this model in larger models where cirrus cloud formation is just one component, e.g., general circulation models (GCMs). In this case, sensitivity studies on the detailed model are carried out in an effort to remove computationally intensive detailed physics that do not affect the overall results and thus present a simplified but still accurate model as a component in still larger GCMs.

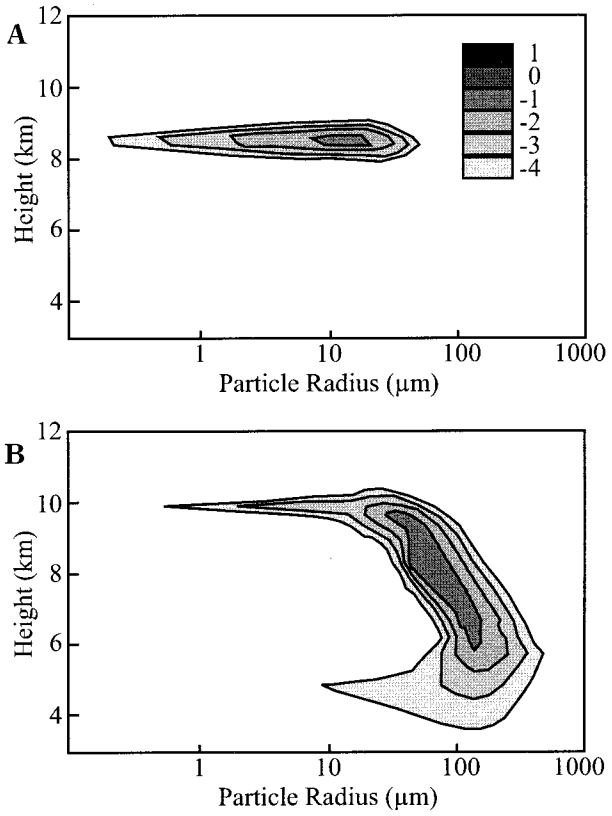

Figure 32. One-dimensional microphysical, radiative, and dynamical model of cirrus cloud formation: (A) 90 and (B) 180 min. Gray scale legend shows ice particle concentration in $\log_{10}$ units (cm^{-3}). (Adapted with permission from ref 293. Copyright 1994 American Geophysical Union.)

Several limitations exist in the parametrizations employed in contemporary microphysical models. For the most part, for example, they do not consider the chemical heterogeneity of atmospheric aerosol. A composition of entirely H_2SO_4/H_2O or $(NH_4)_2SO_4/H_2O$ is usually assumed in upper tropospheric work related to ice nucleation during cirrus cloud formation.[199,282,285,293,307] Furthermore, considerations of heterogeneous nucleation are few.[138,148,150,293] In the lower troposphere, the hygroscopic response of aerosols is often based on the assumption of entirely H_2SO_4/H_2O or $(NH_4)_2SO_4/H_2O$.[308,309] Most work on direct radiative forcing treats global aerosol as entirely H_2SO_4/H_2O.[310,311] Advanced contemporary treatments include minerals dusts[312] and carbonaceous aerosols,[313] but they partition the aerosol into separate compartments of electrolytes, dusts, and soot[314] and do not consider phase transitions and possible interactions (e.g., heterogeneous nucleation) among chemical constituents. Some workers concerned with air visibility have partitioned light extinction data into contributions by specific chemical species,[315−319] but organic molecules are not considered[95] and the crystallization of salts with reduced relative humidity is omitted. These models are applied in haze visibility reduction[320] and tropospheric multiphase aerosol chemistry.[321]

VI. Comparison between Models and Field Measurements

Field measurements of the physical phase of atmospheric particles are complementary to laboratory and modeling work. Can models incorporating microphysical models based upon laboratory work predict particle phases as observed in the atmosphere? If so, the model receives a validation indicating that the important physical and chemical processes are included in the model description. Confidence in the model is crucial because simulations of atmospheric processes are done rapidly and cheaply as compared to field measurements. If model and field work agree poorly, field observations of phase, chemical species, and meteorological variables often suggest areas for continued inquiry in the laboratory. In this section of the review, the main approaches to and interpretations of field measurements of particle phase are considered. Instructive examples are chosen from literature; a complete account of all literature in this area is beyond the scope of this review.

The first goal of field measurements concerning the phase of atmospheric particles is quite simply to identify the phases of ambient particles. The second and more difficult goal is to observe transitions from aqueous to crystalline particles or from one crystalline phase to another. Finally, the third and most valuable goal is to measure processes variables frequently enough over a sufficient duration that, in conjunction with advanced models, constraints on the kinetics of phase transitions can be deduced from field measurements. In this approach, the atmosphere is roughly conceptualized as a large laboratory batch reactor. Typical process variables include rates of change in temperature or relative humidity. Initialization of advanced models also requires quantitative information on the number size distribution and chemical content of atmospheric aerosol, and important analytical advances are a current area of active research through the development of apparatus for single-particle mass spectrometry. The most advanced and successful field programs to date have been accomplished for polar stratospheric clouds and have included detailed models to interpret field observations. Investigations of cirrus cloud formation have achieved the second goal identified above, while observations of boundary layer aerosols have only achieved the first goal sporadically.

The body of literature on field work divides into four broad categories: boundary layer aerosols, mixed phase clouds (including lightning), upper tropospheric cirrus clouds, and polar stratospheric clouds (PSCs). By far, the most advanced measurements and interpretation exists for PSCs, for several reasons. PSCs are integral to annual polar ozone depletion, so field observations have been intense and international for over 10 years. In addition, the chemical composition and transport dynamics of the stratosphere are much simpler as compared to the troposphere. Even so, despite the favorable circumstances of an easier system at the focus of much effort, significant questions remain, and lab work is not fully reconcilable with field observations.

The second body of literature concerning mixed-phase clouds and including extensive accounts of atmospheric electricity and lightning[2] is not covered in detail in this review. As discussed elsewhere in this review, the freezing mechanisms of supercooled dilute aqueous droplets are an area of active research. Often, a cloud between 0 and −40 °C partially glaciates, and the interactions between the ice particles and the supercooled droplets lead to the buildup of an electric field and eventually to lightning. In brief, under fair weather conditions, the electric field at the Earth's surface varies from 70 to 400 V m^{-1}, with an average value of 130 V m^{-1}. The main charging mechanism on a global basis is thunderstorm activity. Within lightning clouds, field strengths as high as 10^5 V m^{-1} have been measured. Field strengths of 10^7 V m^{-1} are required for dielectric breakdown between parallel plates, i.e., the simplest model of lightning formation. These two observations lead to two very important open questions within cloud physics: (1) What are the charging mechanisms to obtain 10^5 V m^{-1} in a cloud? (2) An upper limit of 10^5 V m^{-1} in empirical observations of lightning clouds contrasts sharply with laboratory values for dielectric breakdown of 10^7 V m^{-1}: how does lightning occur? The available evidence strongly supports the view that ice formation and the subsequent collisions and breakup of ice particles are necessary for cloud charging.[322−324] A possible important feedback is the alteration in ice nucleation kinetics by the presence of strong electric fields[325−329] or by electric charges induced on ice forming nuclei inclusions.[328,330−334] The mechanisms for the subsequent triggering of lightning are less clear. Possibly, the curvature of droplets leads to local field enhancement strong enough to initiate ionization. Alternatively, corona discharge may be initiated by droplets during collisions in strong electric fields.

The third body of literature relates to ice formation in the upper troposphere (e.g., cirrus clouds). Earnest work began in 1946 for military applications of cloud seeding and continues to this day for weather modification for agricultural purposes.[335] Ice is relatively easy to study because 10 μm and larger particles form and are thus easily separated from interstitial aerosol. Collected ice particles are examined for chemical content and insoluble inclusions believed to be heterogeneous nuclei.

The fourth body of literature covers submicron particles, which are often subvisible or sometimes observed as haze, in the lower boundary layer. These particles, especially the subvisible component, are important on a global basis because they dominate the number concentrations and surface area distributions of atmospheric particles. At the same time, their study is extremely difficult technically due to their small size, diverse chemical content, complex boundary layer dynamics, and myriad morphologies. No integrated field program to date (e.g., ACE, ACE-2, TARFOX, or INDOEX) has specifically included a component to address the phase (i.e., crystalline or aqueous) of this class of atmospheric aerosols and the phase changes occurring with cycles of relative humidity and temperature. The report below is based

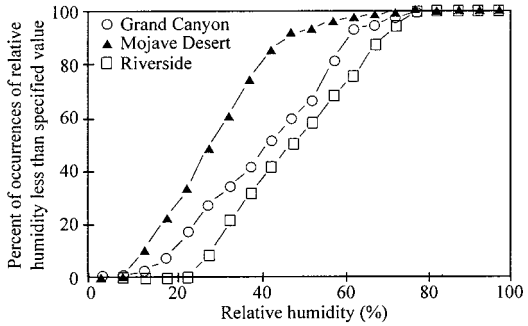

Figure 33. Examples of cumulative distribution of ambient relative humidity conditions during intensive field campaigns at three locations. (Adapted with permission from *Nature* (ref 341). Copyright 1989 Macmillan Magazines Ltd.)

upon the pioneering efforts of several early investigators.

A. Boundary Layer Particles

i. Contravening Hypotheses: All Aqueous versus All Crystalline

Because there is only limited field work on the phase of boundary layer aerosol, two contradicting hypotheses are often advanced. In the first hypothesis, lower tropospheric particles are believed to be aqueous because the complex chemical composition (e.g., dissolved salts and organics) provides enough entropy to inhibit crystallization, even at low relative humidities. ΔG_{germ} increases because the fabrication of a pure germ requires the exclusion of other dissolved electrolytes. The disorder of a multielectrolyte solution is greater than a binary solution so that the free energy required to make an ordered germ increases. The contravening hypothesis is that most tropospheric particles crystallize near the deliquescence point because the complex composition includes many insoluble constituents (e.g., crustal components) that are heterogeneous nuclei for the formation of crystals from supersaturated aqueous droplets. Contrary to these widely quoted hypotheses, there is in fact a sufficient body of literature on field measurements to demonstrate that atmospheric particles show an array of behavior between these two extremes and generally crystallize at sufficiently low relative humidities. The field measurements of the physical state of boundary layer aerosol show evidence of deliquescence, efflorescence, and hysteresis.[21,336−344]

ii. Temporal Variations in Relative Humidity

Most field work in the boundary layer has focused on continental aerosol with comparatively little work done on marine aerosol. In addition, the phase transitions of interest have been cycling between crystalline salts and aqueous solutions with changes in relative humidity. An example of the frequency and range of relative humidities found over the Grand Canyon, Mojave Desert, and Riverside is shown in Figure 33.[341] Over the ocean ($a_{H_2O}^{\text{ocean}} = 0.98$), the relative humidity is about 75% 1 m above the surface due to turbulent mixing with dry air and

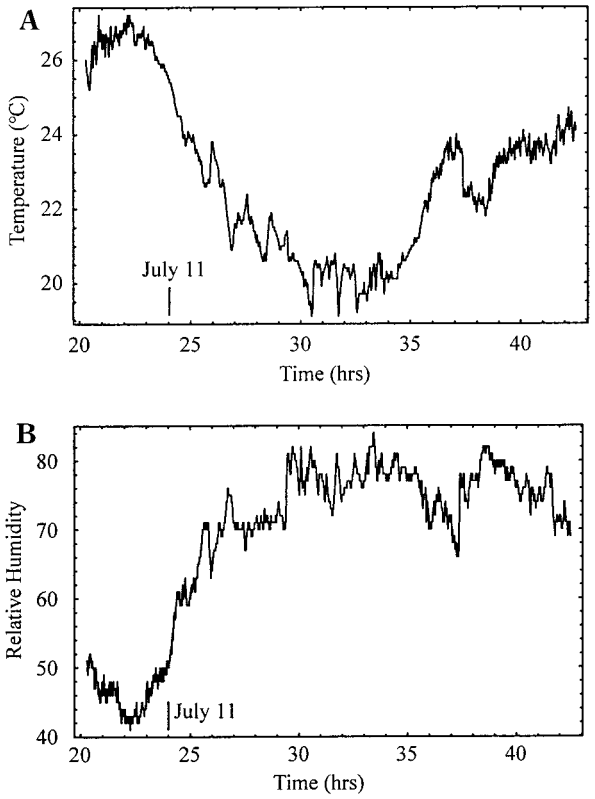

Figure 34. Temperature and relative humidity data collected July 10−11, 1996, during the TARFOX experiment at Wallops Island, VA, about 20 m above the ground. Aerosol travels with the prevailing winds from the eastern United States over the western Atlantic Ocean. These data were obtained from the NASA Langley Research Center Atmospheric Sciences Data Center.[350]

increases with altitude due to cooling.[345−348] In the free troposphere, relative humidity varies widely from under 10% to liquid water saturation.[347,349] In the continental boundary layer, high summer temperatures often yield low relative humidities (6% K^{-1}) (e.g., 35% in August in Atlanta) and so there is a strong diurnal variation. A comparison of the range of atmospheric relative humidities (e.g., Figure 33) with the laboratory results for the deliquescence and efflorescence humidities of chemically pure particles (Table 2) or those containing heterogeneous nuclei (Table 4) shows a strong overlap and thus a high likelihood of the occurrence of phase transitions in the atmosphere.

An example of the temporal variation of temperature and relative humidity in the atmospheric boundary is shown in Figure 34. These data were collected from a building top 20 m above the ground on July 10−11 during the TARFOX experiment at Wallops Island, VA.[350] To a first approximation, relative humidity tracks temperature due to the dependency of water vapor pressure on temperature. The remaining variance in relative humidity is largely accounted for by local eddies mixing dry and moist air. In situ sources and sinks of H_2O are usually small in comparison. To the extent that particles equilibrate with surrounding relative humidity, the variation in relative humidity is accompanied by a change in water activity in the particles. Laboratory work (Tables 2−4) suggest that these changes in water

activity lead to phase changes of atmospheric aerosols. In this way, the phase of atmospheric aerosol in the outflow from eastern United States is probably modulated with the changes in relative humidity as the aerosol passes over the western Atlantic Ocean.

iii. Campaigns and Observations of Ambient Aerosol Phase Changes

A seminal study on the hygroscopic properties of ambient aerosols was carried out in the St. Louis region in 1974,[337,338,351−354] which followed earlier work by Junge and Winkler near Mainz.[86,87] In the 1974 work, Charlson et al.[337] dry the particles by adjusting the relative humidity of flowing ambient aerosol to 20−30% through 10−20 K of heating. The light scattering of the dried aerosol is observed by nephelometry[355] as the relative humidity is increased stepwise. Optionally, NH_3(g) is introduced. The nephelometer integrates the light scattering of the ambient aerosol, across all size and chemical classes including differential hygroscopic responses. In comparison, typical laboratory experiments (Table 2) study a single chemical composition with a uniform hygroscopic response and a monomodal size distribution. Even so, on days when the ambient aerosol is dominated by a single chemical class, insights gained from laboratory experiments appear applicable to the interpretation of the nephelometry measurements of ambient aerosol.

As shown in Figure 35, four classes of humidograms are observed in the work by Charlson et al.,[337] and deliquescence is clearly observable in three cases. Figure 35A is consistent with H_2SO_4(aq) particles with a smooth hygroscopic response but a deliquescence point of 80% RH when NH_3(g) is added. $(NH_4)_2SO_4$ deliquesces at 80%. Figure 35B shows partial deliquescence in the absence of NH_3(g) and a sharper transition with NH_3(g) added, which suggests a partially neutralized H_2SO_4(aq) aerosol. Figure 35C shows sharp deliquescence without the addition of NH_3(g) and no further effect by adding the ammonia. Hence, $(NH_4)_2SO_4$ particles are probably present in the ambient aerosol. Figure 35D does not conform to the $(NH_4)_2SO_4/H_2SO_4/H_2O$ chemical system and is probably composed of other chemical constituents. Similar measurements demonstrating the crystallization of sea salt aerosol are shown in Figure 36, where deliquescence for NaCl is expected at 75% RH.[264] Deliquescence of marine aerosol is also seen by Sinclair et al.[356] Figures 35 and 36 thus demonstrate that atmospheric particles often crystallize when sufficiently low relative humidity is reached, and the field measurements provide a lower limit of 20−30% RH for crystallization for many particles. Figure 33 shows a high frequency of RH values below the lower limit for the crystallization threshold. The rather gentle deliquescence apparent in Figures 35 and 36 arises from a relative humidity "overshoot" problem addressed in refs 77 and 357. This problem is corrected in contemporary nephelometers, and the abrupt transitions expected for deliquescence are apparent.[77,357,358]

A modification[359] of the nephelometer technique allows the crystallization relative humidity and

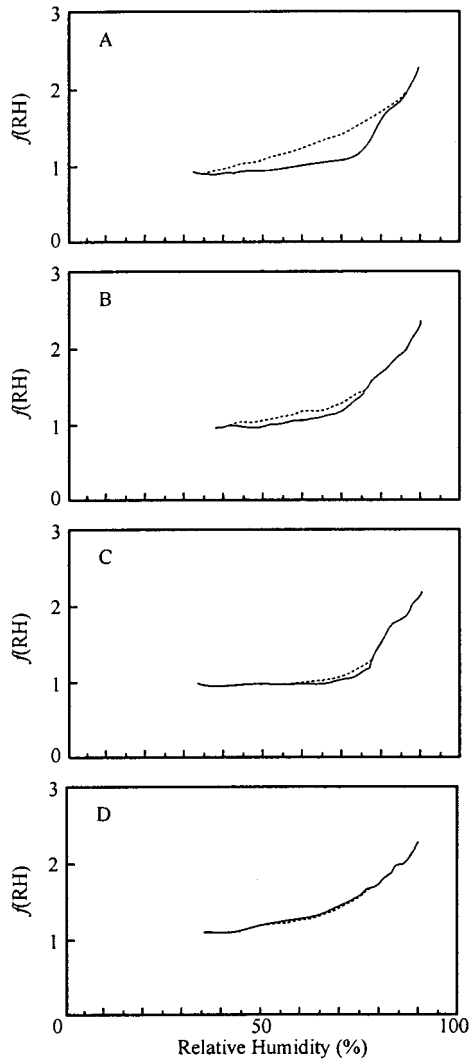

Figure 35. Four classes of humidograms recorded for an ambient aerosol stream (dashed line) and for the same stream with the addition of ammonia gas (solid line). (A) Monotonic (hygroscopic) curve; NH_3 caused inflection point at 80% (deliquescence); September 23, 1973, 12:08−12:19 CDT, Tyson. (B) Inflection point at 80% enhanced by NH_3; September, 24, 1973, 20:30−20:47 CDT, Tyson. (C) Inflection point and no or little enhancement by NH_3; September 24, 1973, 22:45−23:03 CDT, Tyson. (D) Monotonic curve unaffected by NH_3; September 28, 1973, 05:00−05:18, CDT, St. Louis University. (Adapted with permission from ref 337. Copyright 1974 Elsevier Science.)

extent of metastable particles in the atmosphere to be measured.[340−342] Particles at ambient relative humidity are first heated to a temperature T_1 and then cooled to ambient again before entering the nephelometer. If there is no change in the scattering, then the particles are either solid or, if they are aqueous, then the evaporated water at T_1 favorably recondensed upon cooling. Either way, the particles are in the lower half of the hysteresis loop (Figure 19). However, if there is a sudden change in scattering at T_1, then the evaporated water does not recondense because there is a shift from the upper to the lower half of the hysteresis loop. The ambient particles are then metastable. The relative humidity corresponding to T_1 is calculable based upon the ambient relative humidity, if the condensed water content of the particles is negligible as compared to

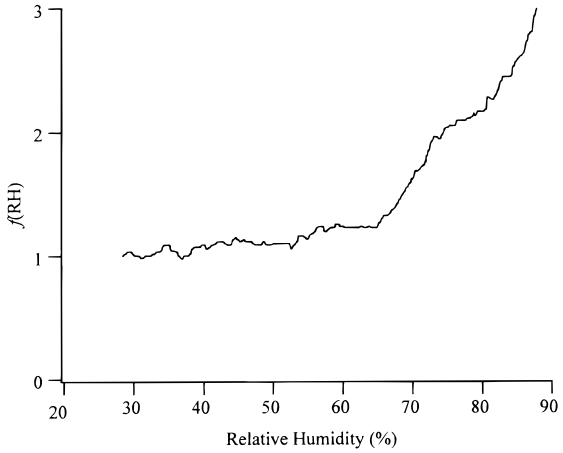

Figure 36. Nephelometer light scattering normalized to that at 30% humidity versus relative humidity at Pt. Reyes, CA, showing the presence of sea salt aerosol. (Adapted with permission from ref 338. Copyright 1974 Tellus.)

the gas. Scanning T_1 upward successively decreases relative humidity, and the metastability and the efflorescence point of ambient aerosol are determined. These methods assume that significant irreversible volatilization of other components does not occur at elevated temperatures T_1.

An uncertainty when this approach is applied to ambient aerosol of unknown chemical composition lies in volatile components besides H_2O that also evaporate at the warmer temperatures (e.g., NH_4NO_3). Upon cooling, these vapors remain supersaturated when the residence time in the nephelometer is insufficient. Alternatively, they condense as new particles or as a layer on the preexisting particles in a way different from the original size distribution. The resulting changes in the particle number size distribution affect the light scattering properties of the aerosol. In this way, some of changes observed in the signal from the integrating nephelometer may not be entirely attributable to the evaporation of metastable water.

Employing these techniques, Rood and coworkers[340−342] report that ambient aerosols are metastable with roughly 50% frequency for 45 < RH < 75% in the Grand Canyon, Mojave Desert, and Riverside, CA.[340] In Riverside, filter sampling is done concurrently, and ion content is determined by chromatography. Particles occur as aqueous droplets with a high percent frequency (86%), and of those droplets, 71% are supersaturated with respect to solids.[341] The frequencies of occurrence for supersaturated droplets are based on in situ light scattering measurements obtained with nephelometry. The ion analysis shows a high nitrate-to-sulfate ratio in the collected particles, which, based on lab measurements, at first would seem to explain why aqueous particles are predominant.[21] However, when the data are sorted for the nitrate-to-sulfate ratio, no trend is apparent.[342] It is possible any trend with chemical composition is obscured by co-variation with particle history, which depends on meteorology and source regions. Because of these factors, particles of one chemical composition could predominantly be sampled when they are on the upper loop of the hysteresis

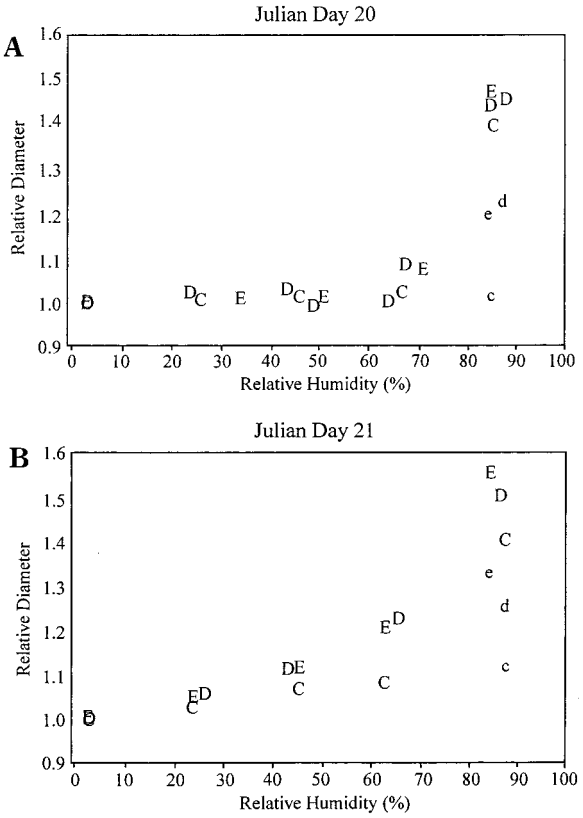

Figure 37. Growth as a function of relative humidity as measured by tandem differential mobility analyzer (TDMA) in winter 1990, Grand Canyon, Arizona. Dry particle diameters: (C) 0.1, (D) 0.2−0.25, and (E) 0.3 μm. The dry particle mode splits into a "more hygroscopic" (capital letters) and "less hygroscopic" (small letters) bimodal distribution at high relative humidities. (Adapted with permission from ref 343. Copyright 1994 Elsevier Science.)

curve, while particles of another are on the lower loop. In such a case, interpretations of metastability based upon chemical content would be confounded. Crystallization relative humidities at all three sites are about the same, and 91% of the samples (as indicated by scattering) effloresce within a parabolic probability distribution from 10 to 45% RH.[342] The authors suggest the distribution could relate to an external mixture of aerosol, but a distribution of heterogeneous nuclei also seems a likely explanation (cf. Table 4).

In addition to nephelometry, a second technique employed widely in contemporary field measurements is the tandem differential mobility analyzer (TDMA).[360,361] Pitchford and McMurry apply the TDMA to study the hygroscopic properties of atmospheric aerosol in the Grand Canyon.[343] The aerosol is first dried to 14 ± 5% RH, and the first DMA selects a monodisperse size. The selected aerosol is then humidified at stepwise RH values, and the particle growth is monitored by a second DMA and a condensation particle counter. In this way, the aerosol growth in several size bins is measured. The results (Figure 37) clearly show deliquescence for a fraction of the aerosol above 80% RH. A chemical composition of $(NH_4)_2SO_4$ appears appropriate. Similar to the results in the St. Louis studies, these TDMA measurements set a lower limit on crystallization RH values of 14 ± 5%. A second fraction of

particles is also seen to show only a weak hygroscopic response. It is believed these particles are composed of hydrophobic organic molecules.[94,361,362] In principle, TDMA techniques should be easily adapted to beginning with a high RH value with the first DMA and then scanning the RH downward to observe the crystallization RH values with the second DMA, but only limited work for ambient aerosol occurs in the literature.[363] An additional point to be emphasized is that the TDMA technique measures the growth of a single size bin of particles, possibly of mixed chemical composition, in contrast to the integrating nephelometer approach (vida supra), which integrates the hygroscopic response over all sizes.

The passage of the Clean Air Act and its amendments[364] has reduced the mass concentration of atmospheric H_2SO_4.[365] The logical speculation is that the occurrence of aerosol of the types shown in Figure 35C has increased relative to Figure 35A so that phase transitions between crystalline and aqueous particles in the continental boundary layer occurs more frequently in recent times than in 1974. However, marine aerosol containing high levels of nonseasalt sulfate from dimethyl sulfide oxidation is probably not neutralized and may thus be difficult to effloresce over the ocean before neutralization by abundant NH_3 in continental regions.[363]

For continental aerosol impacted by the Clean Air Act, the relative importance of NH_4NO_3 increases as an aerosol constituent when the sulfate loading decreases. In laboratory experiments, NH_4NO_3 is generally regarded as inhibiting crystallization.[21] The effect of nitrates has been studied in 1993 by ten Brink and co-workers by applying the humidity controlled nephelometer technique, adapted from Rood and co-workers, to the study of aerosol in The Netherlands.[21,344] The results (Figure 38A) show two water uptake regions of a dried aerosol at 60% and 80% RH, which is consistent with a mixed ammonium nitrate/ammonium sulfate composition. The role of nitrates may be more apparent in 1993 than the St. Louis study in 1974 because of reduced sulfate loadings. The purely hygroscopic aerosol in Figure 38B is similar to Figure 35A, but the chemical composition is believed to be principally nitrate as compared to sulfate. Interestingly, laboratory aerosol of chemical composition similar to Figure 38A does not effloresce even at low RH values. The implication is that insoluble material incorporated in ambient particles but not in laboratory aerosol heterogeneously nucleates the crystalline salts. Finally, an example of the measured hysteresis loop of ambient boundary layer aerosol is shown in Figure 39.[344]

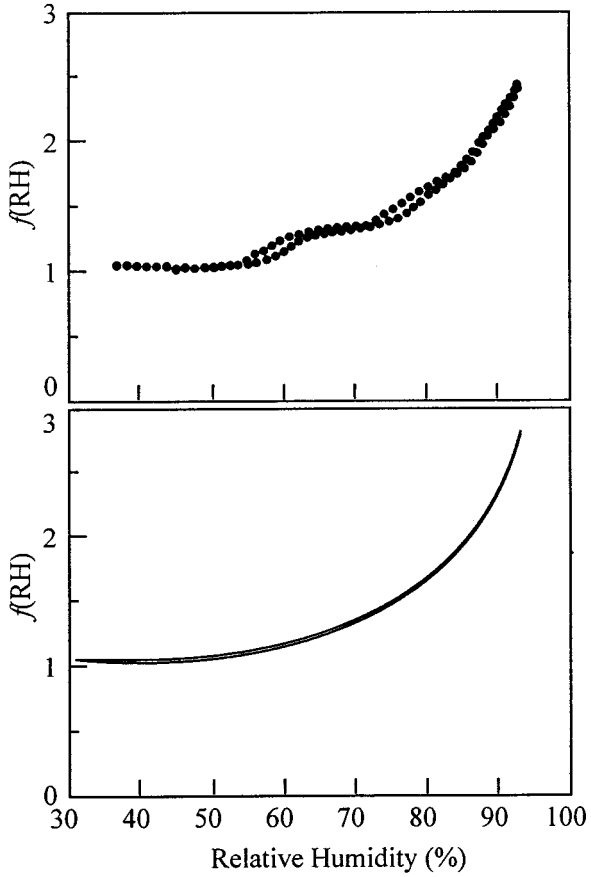

Figure 38. Representative examples of the enhancement in the light scattering by ambient aerosols in The Netherlands as a function of relative humidity, after drying to 30−35% RH, as experessed in the enhancement factor *f*(RH). (A) Afternoon of November 1−2, 1993. (B) Average of afternoon measurements on November 22−25, 1993. (Adapted with permission from ref 21. Copyright 1998 Elsevier Science.)

B. Cirrus Clouds

Upper tropospheric ice clouds are of interest to the global climate because they provide local radiative warming and reflect incoming solar radiation.[3,117,366,367] Although recent intensive field campaigns have improved the understanding of their radiative properties,[368−371] their formation mechanisms remain unclear.[138,148,372] Ice particles, which grow to be several hundred microns, could form via homogeneous nucleation in concentrated (typically $0.01 < x < 0.1$) submicron $NH_4^+/H^+/NO_3^-/SO_4^{2-}$/organics/$H_2O$ droplets or via heterogeneous nucleation on insoluble, probably crustal, constituents. Other mechanisms such as contact freezing or reverse sublimation are not believed to be important.[293] Gas-phase HNO_3 is probably scavenged in significant enough quantities to alter the freezing characteristics of aqueous particles at the lowest temperatures common in the upper troposphere. Scavenging mechanisms include Henry's law partitioning at low temperatures and chemical reaction with basic mineral dusts.[373] Employing field measurements of cirrus clouds occurrence, temperature, and relative humidity, Heymsfield and co-workers[149,374] developed an empirical determination of the lower and upper limits of conditions for ice nucleation in the initial stages of cirrus formation.

A point to be emphasized in cirrus formation is that relative humidity (i.e., gas phase water) and water activity (i.e., condensed phase water) are often different. Cooling updrafts increase the vapor-phase water saturation ratio faster than the gas-phase molecules can transfer to the condensed phase. Important microscopic factors in the water uptake rate include the coefficients for mass condensation and thermal accommodation as well as the Kelvin effect classed by size and chemical composition. An

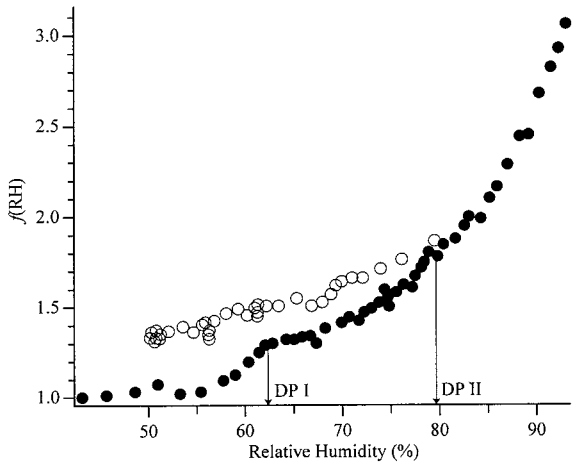

Figure 39. Enhancement of the aerosol light scattering, shown as an enhancement factor *f*(RH), as a function of relative humidity for continental European aerosol November 17, 1993. Closed circles are for aerosol first dried and then subjected to increasing relative humidity, while open circles are for aerosol first humidified and then subjected to decreasing relative humidity. The combination of these two branches records the aerosol hysteresis loop. (Adapted with permission from ref 344. Copyright 1996 Elsevier Science.)

important macroscopic factor is the total cloud surface area. Accurate temporal descriptions of cloud growth and particle trajectories require the numerical solution of the diffusional growth equations, including a feedback for the depletion of the reservoir of vapor phase water, for each size and chemical class. In addition, each class may partially or completely undergo a phase transition to form ice particles, which are the final sink for water vapor. Unfrozen particles increase their aqueous compositions by evaporation until equilibrium with the ice vapor pressure obtains due to cryogenic pumping of the vapor to the ice particles. The picture that emerges is that freezing is selective with regard to particle number and size and that the prediction of overall cloud properties depends strongly on the microscopic physical modeling, which is in turn highly dependent on the existence and the accuracy of laboratory results.

In addition to homogeneous nucleation, heterogeneous nucleation in cirrus formation appears important at times because crustal constituents (identified as containing Si, Al, and Fe) are found at the center of collected ice particles.[375−382] Detailed microphysical models, however, will not be possible until laboratory investigations of heterogeneous nucleation of ice in haze droplets are completed. Following early work by Hoffer on clays,[267] several laboratory groups are currently active in this area. Through a combination of field and modeling results, DeMott et al. determined that the cloud droplet number density and particle size distributions characteristic of cirrus clouds formed by orographic waves are more consistent with heterogeneous than homogeneous nucleation.[156] Field measurements by Strom et al. of young cirrus clouds forming in lee waves also suggest background particles under 0.5 μm are the initiation sites for ice nucleation.[383]

C. Polar Stratospheric Clouds

Surface reactions on PSCs activate chlorine (e.g., $ClONO_2$ hydrolysis) and thus prepare the polar atmospheres for catalytic cycles in ozone depletion when sunlight arrives in the spring.[384] Furthermore, PSCs containing HNO_3 sometimes grow large enough to sediment and thus remove nitrogen species that deactivate chlorine, thus extending both spatially and temporally the annual polar ozone depletion. To quantify the problem, field campaigns, modeling studies, and laboratory investigations began in 1985. This work has led to a general understanding, as follows: background H_2SO_4/H_2O aerosol, called the Junge layer, swell by absorbing H_2O (ca. 4−8 ppm) and HNO_3 (ca. 5−15 ppb) below 195 K. The resulting supercooled liquid ternary aerosol (alternatively labeled STA or SSA) dilutes to a nearly binary HNO_3/H_2O aerosol containing trace H_2SO_4. These particles scatter light relatively weakly and without depolarization because they are small, spherical liquid droplets. Observed by LIDAR, they are called type Ib PSCs. At temperatures 2−4 K below the ice frost point (T_{frost} = 188−190 K), homogeneous nucleation of ice occurs. These particles grow to be large enough to scatter light more strongly and, because they are solid, to depolarize backscattered light. Observed by LIDAR, they are classified as type II PSCs. [In contrast to particle phase transitions in the boundary layer and upper troposphere, heterogeneous nucleation of sulfuric and nitric acid hydrates does not appear important in the temperature and particle chemical compositions occurring along stratospheric trajectories.[255]]

There are discrepancies, however, in other aspects of field measurements, modeling studies, and laboratory results. LIDAR measurements show a weakly scattering, depolarizing aerosol classified as a type Ia PSC. At stratospheric water and nitric acid partial pressures in the temperature range of 190−200 K, the crystal $HNO_3 \cdot 3H_2O$ (NAT) is supersaturated (Figure 40). Small NAT crystals are then believed to be the physical species corresponding to type Ia LIDAR observations. However, laboratory measurements have great difficulty accounting for the formation of NAT crystals because they are not observed to nucleate readily from ternary aerosols. NAT and NAD crystals do crystallize from concentrated HNO_3/H_2O, but the necessary compositions are not readily obtained in equilibrium with the ambient water and nitric acid vapor pressures. Modeling studies have suggested reconciliation based upon rapid cooling associated with air passing over mountains.[32,385] In this case, a kinetic model of gas condensation shows the smallest liquid aerosols transiently become highly concentrated HNO_3/H_2O, which could homogeneously nucleate nitric acid hydrates. The largest of these hydrates would then grow by Ostwald ripening at the expense of all remaining SSA in the following days after passage through the orographic event.

There also remain LIDAR observations that do not fit the type Ia, Ib, and II classifications.[386] There are particles that scatter light more strongly than Ia but less than characteristic of type II, while still depolarizing. To explain these observations, Tsias et al.[387]

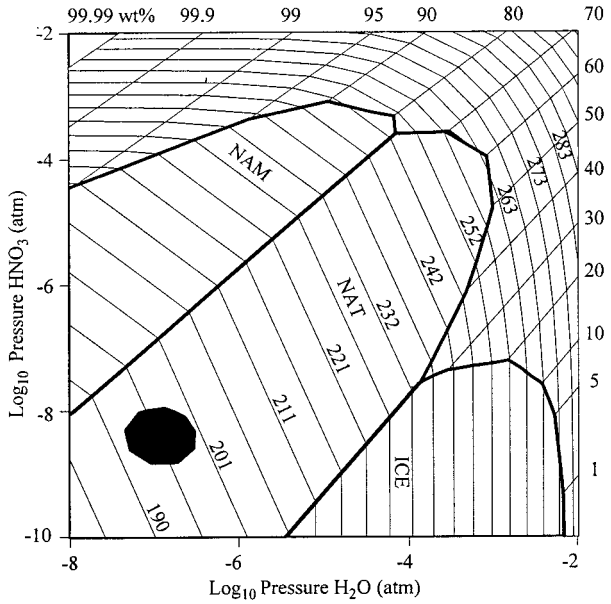

Figure 40. HNO_3 and H_2O vapor pressures over ice, NAT, and NAM crystals and aqueous HNO_3/H_2O solutions indexed by weight percent composition. A temperature axis comes out of the page, and isothermal contours are shown (Kelvin). The dark ellipse shows the domain of partial pressures occuring in the stratosphere. It is seen that NAT crystals are most thermodynamically favorable, i.e., the first phase to have equilibrium vapor pressures equal to partial pressures as temperature cools below 200 K. Under isothermal conditions, the log of the vapor pressures of crystals of fixed stoichiometric composition co-vary linearly with a slope equal to the stoichiometry, i.e., the Gibbs−Duhem relation. These slopes are apparent in the isothermal contours shown for NAM, NAT, and ice (i.e., 1, 3, and inifinity, respectively).

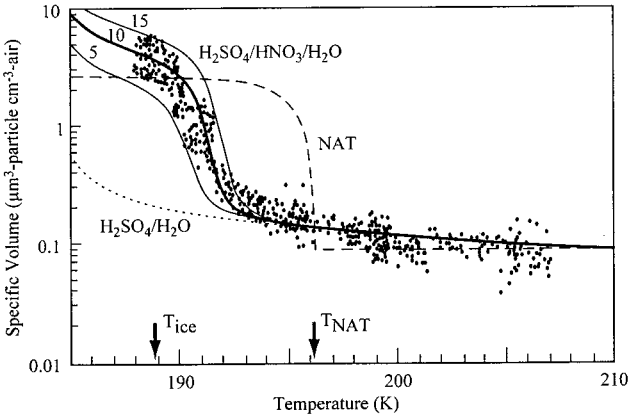

Figure 41. Particle volumes from ref 395 (January 24, 1989) compared with model calculations for the growth of liquid $H_2SO_4/HNO_3/H_2O$ particles (solid lines), for the growth of crystalline NAT particles (dashed line), and for the growth of aqueous H_2SO_4/H_2O particles (dotted line). Results are for 55 mbar pressure, 5 ppmv H_2O, and 5, 10, or 15 ppbv HNO_3. (Adapted with permission from ref 397. Copyright 1994 American Geophysical Union.)

evolve an initialized particle size distribution according to the temperature histories derived from back-trajectories and constrained by the nucleation scenarios derived from laboratory work. An optical simulation is applied to the phase and size distribution of particles at the time point in the model coincident with the LIDAR measurements. A good match is obtained. The corresponding model particles are large NAT crystals, which the authors then ascribe as type Ia-enh for "enhanced." Sophisticated approaches are found in several other studies of PSCs;[388−392] however, similar applications to particle phase transitions in the troposphere are not possible because the initialized chemical and size distribution of particles is not well-known and the nucleation rules are not completed in laboratory work. [A state-of-the-art approach to integrating phase transitions of tropospheric aerosols is provided in ref 393.] Carslaw et al. have also shown it is possible to draw inferences about particle microphysics and phase transitions from constraints placed on these processes by synoptic and mesoscale LIDAR observations.[391,392]

The most common comparison endpoints between field studies and modeling work of PSCs are volume[394−397] and optical properties.[392,398−400] Volume is usually inferred from a particle size distribution obtained by in situ light scattering methods. Aerosol is drawn into an instrument mounted on an airplane and the scattering properties of the aerosol are measured by the forward scattering spectrometer probe (FSSP) in early work and by the multiangle aerosol spectrometer probe (MASP) in later work. Concomitant measurements are obtained for the ambient partial pressures of H_2O (Lyman-α) and HNO_3 (derived from correlation with P_{N_2O}), the condensed phase mass of HNO_3 (via anisokinetic NO_y sampling), the temperature, and the background H_2SO_4 (viz., nonvolatile) aerosol loading. These data are combined into model scenarios of "if" there is a hypothesized type of PSC in equilibrium with HNO_3 and H_2O, then the ambient aerosol would have a certain specific volume (i.e., (μm of aerosol)^3 (cm of air)$^{-3}$). A comparison with in situ specific volumes provides an acceptance test for a proposed PSC type. This technique is applied widely,[394−397,401,402] and an example is shown in Figure 41.

A second common comparison endpoint is based on light scattering, either by a backscatter sonde[400,403,404] or a LIDAR.[390,392,398,399] Optical measurements for a backscatter sonde consist of a backscatter ratio of two compared wavelengths from which information about particle size can be inferred. [Advanced LIDAR systems operate with lasers at three or more wavelengths.[405]] For LIDAR in its simplest form, the backscatter ratio between aerosol-laden and clear air and the depolarization of incident polarized light are measured. Both particle size and physical state (viz. spherical/plate geometry or not) can be inferred. Most measurements with LIDAR are at ground-based stations, but airborne measurements have also been made.[387,390,392] An example of a type II PSC measurement is shown in Figure 42.[386] As described above for Tsias et al., a modeling studying makes comparisons to LIDAR end points by evolving a chemical and particle size distribution through atmospheric processes and then applying an optical simulation to the evolved aerosol.

Volume and optical field measurements can only be translated into chemical composition by modeling work that incorporates laboratory results. In contrast, direct measurements of PSC composition would be preferable. Attempts to collect PSCs on filters or

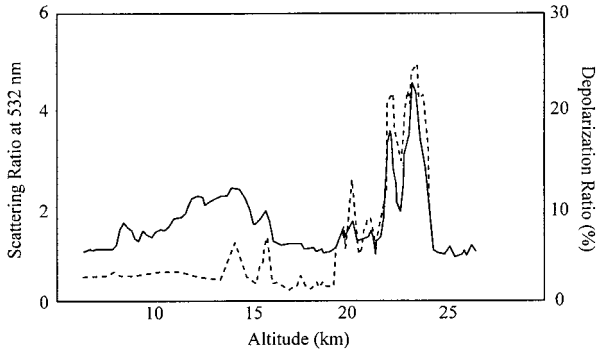

Figure 42. LIDAR investigations of aerosol phase over Dumont d'Urville, July 8, 1990. Scattering ratio (continuous line) and depolarization ratio (dotted line) are shown. The figure shows the Pinatubo volcanic cloud from 8 to 17 km, two depolarizing layers inside the volcanic aerosol (at about 15 km, with a correspondingly low increase in backscattering), and a PSC from 19 up to 26 km. (Adapted with permission from ref 386. Copyright 1995 American Geophysical Union.)

wires are problematic because the particles change with small alterations in environmental conditions (e.g., temperature and H_2O and HNO_3 partial pressures). Recent work with mass spectrometry is more definitive.[406] HNO_3 and H_2O content of PSCs were measured directly and found in the ratio expected for supercooled ternary aerosol. In situ observations with infrared spectroscopy have also been completed, which are consistent with supercooled ternary solutions.[407]

VII. Outlook

Considerable progress has been in the study of the phase transitions of aqueous atmospheric particles, but many important questions remain unanswered. The bulk of recent efforts and progress for laboratory investigations has been the nucleation mechanisms of chemical systems that have been chosen as surrogates for polar stratospheric clouds (viz. H_2SO_4/HNO_3/H_2O). The laboratory results have been incorporated with some success in mesoscale and synoptic models of PSC formation. Although questions and problems remain with regard to PSCs, the uncertainties are larger for every equivalent question in the troposphere, primarily due to the chemical heterogeneity of tropospheric aerosol and the complicated dynamical processes associated with weather. The best quantitative models in the troposphere exist for orographic cirrus clouds formed in mountain lee waves. Laboratory work on ice formation mechanisms in the upper troposphere as well as warmer mixed-phase clouds is also the subject of renewed interest in the past few years. At the time of this writing, the largest uncertainties and a topic of increasing interest relate to phase transitions of atmospheric particles in the boundary layer. In conjunction with these issues, the following areas can be identified as likely to receive increasing attention among atmospheric chemists:

1. The atmospheric chemistry community would benefit by standardizing its reports of phase transitions by adopting mole fraction (x) for composition, free energies (G) and chemical potentials (μ, kJ mol^{-1}) for equilibration, and volume nucleation rates (J, cm^{-3} s^{-1}) to report kinetic results of phase transitions. Comparisons among results for different chemical systems and between laboratories and the incorporation of laboratory results in microphysical models would be easier and more accurate. A particularly important point is that experiments in the laboratory (a) often cool or reduce relative humidity much faster than corresponding atmospheric processes and (b) often employ particles or liquid volumes much larger than characteristic of atmospheric particles. Reporting an intensive property like J values, instead of an extensive property like freezing temperatures, offers an improved pathway for normalizing laboratory results to a form appropriate for incorporation in microphysical models of phase transitions of atmospheric particles.

2. Water-soluble organic molecules are contained in boundary layer particles. Common molecules include oxygenated organics such as acetate, oxalate, or formate and various carbonyls, aldehydes, and phenols. Photochemical processing yields organic materials of sizes and properties similar to fulvic acids common to aquatic chemistry. The study of the effects of these organics on inhibiting or promoting the efflorescence and deliquescence of the salt components, or possibly forming their own crystalline phases, is just beginning.[408−413] Initial results suggest a considerable effect. In addition, even in the absence of organics, synergistic effects on nucleation in multicomponent electrolyte solutions should receive more attention.

3. Other classes of organic molecules include surfactant type materials. Their net effect on CCN activation and thus cloud formation is controversial and likely dependent on their molecular composition.[96,97] The molecules may form a barrier at the water−gas interface that inhibits mass transfer and thus slows phase transitions, possibly both deliquescence and efflorescence. Alternatively, they may reduce surface tension thus modifying the Köhler curve and enhancing CCN activation.[414−416] To the extent that surfactants lead to the salting out of lower molecular weight constituents, surfactants may also inhibit CCN activation.[430]

4. Tropospheric aerosol contains many water-insoluble components such as mineral dusts that are commonly identified as good templates for inducing crystallization. Laboratory work on these systems is just beginning.[13] The variety of mineral dusts and the variable activities of a specific mineral dependent on its history provide several challenges. First, the surfaces present in atmospheric particles must be characterized. Second, the chemistry of these surfaces must be suitably mimicked in laboratory work. Third, conceptual methods must be worked out to apply the necessarily limited laboratory work to the panoply of the ensemble of atmospheric heterogeneous nuclei. Finally, the ensemble of surfaces in the natural atmosphere must be represented in larger-scale models, perhaps by average surface or moment[417] descriptions.

5. Laboratory work on phase transitions is presently limited by uncertainty in the chemical composition of individual atmospheric particles, i.e., what chemical systems should be studied in the lab? Only limited work has been done on compositions of mixed aqueous electrolytes, for example, whereas most hygroscopic atmospheric particles probably are composed of several salts. Synergistic interactions with insoluble components are also noted in point 4 above. At present, the chemical complexity of tropospheric aerosol is being better understood by single-particle mass spectrometry. A significant goal is to improve this technique to the point of providing quantitative results. Understanding the phase transitions of atmospheric particles would be advanced if a single particle hygroscopic growth front-end could be employed prior to mass spectrometric analysis. In this way, the deliquescence or efflorescence of individual atmospheric particles could be related to chemical composition.

6. Ice nucleation in the atmosphere is not quantitatively understood. Ice nucleation in laboratory studies of supercooled aqueous droplets believed representative of polar stratospheric clouds indicates homogeneous nucleation does not occur until several degrees below the ice frost point, yet ice particles are observed in field campaigns in air parcels that do not appear to have a cold enough temperature history to be explained by the laboratory measurements. In cirrus clouds, the conditions favoring homogeneous versus heterogeneous nucleation are not quantified. In mixed-phase clouds, much uncertainty remains about the efficiencies of ice nuclei leading to heterogeneous nucleation. All of these aspects are being addressed by enhanced analytical prowess in field campaigns to identify chemical constituents of particles. In addition, laboratory work must address three points: (a) Particles of complex chemical composition must be studied. For example, in the upper troposphere, sulfate-bearing particles also contain ammonium, nitrate, and oxygenated organics all codissolved at times. (b) Heterogeneous mechanisms on ice nuclei are evidently dominant in mixed-phase clouds and believed important at times in cirrus clouds. Anecdotal laboratory evidence indicates anthropogenic AgI and CuS are effective, yet understanding the variations in activity from one preparation of AgI particles as compared to another remains elusive. Natural ice nuclei are more diverse. Understanding and quantifying the varying efficiencies of ice nuclei requires a molecular level approach, and novel approaches are needed for integrating the minutiae-based knowledge gained through those efforts into larger-scale cloud microphysical models. (c) The laboratory techniques employed in phase transition studies (see Table 2) yield varying results. Efforts must be made for each technique to extract J values from the experiments, incorporating factors such as cooling rates, mass transfer, thermal transfer, sensitivity, particle poly- and chemical dispersity, and other relevant factors for each technique.

7. Microphysical models often treat the hygroscopic response of ambient aerosol as simply sulfuric acid. Instead, methods must be established to include the chemical diversity and different hysteretic hygroscopic responses.

8. The success of integrated field, modeling, and laboratory work completed for PSCs suggests an extension to boundary layer aerosols. The increased difficulty due to weather, chemical complexity, and uncertain mechanisms for phase transitions suggest the most initial success would probably be obtained at a subregional scale.

9. Despite their prevalence, sea salt aerosols have received relatively minor attention in laboratory work. Some laboratory work on synthetic sea salt particles suggests complete crystallization may not occur even at low relative humidities.[25,427] A bulk aqueous liquid persists. Whether this aqueous phase coats the particles so that no crystal surface is exposed to the gas-phase or, instead, morphologically separates is unknown. Additionally, it is uncertain whether the crystallization behavior of synthetic sea salt aerosol studied in the laboratory represents the behavior of atmospheric sea salt aerosol containing organic molecules, including surfactants, and mineral dust components. If a crystalline interface does form with the gas phase (due to complete crystallization of the particle or morphological separation with the residual bulk liquid), it should be covered by several monolayers of water. Existing work points out the need to consider this interfacial region as a separate surface phase, described by its own free energy function.[175] The surface phase appears to be liquidlike in the chemical reactions it promotes, while the bulk crystal remains dry. Although laboratory studies have succeeded to some extent in characterizing surface phases, surface phase transitions in atmospheric systems remain to be explored.

10. Although the field and laboratory work is still incomplete, sufficient evidence exists to outline some rules governing aqueous particle phase transitions in the atmospheric boundary layer near 298 K. Aqueous particles are favored (i.e., persistent supersaturation approaching 0% RH) when the particles are highly acidic or contain high nitrate content. Particles enriched in ammonium sulfate and especially those particles containing mineral dust inclusions crystallize more readily at higher RH values (i.e., 30−65%). Soot inclusions appear not to affect the crystallization behavior.

An improved understanding of atmospheric phase transitions should lead to increased accuracy in modeling heterogeneous chemistry, cloud microphysics and chemistry, lightning, air visibility, polar ozone depletion, and global radiative forcing. Several recent global models of radiative forcing and atmospheric chemistry considering the effects of relative humidity[313,418] on purely hygroscopic aerosol or dry deposition of electrolytes onto mineral dusts.[243−245] These models appear poised to consider more advanced treatments of aerosol hygroscopic response including homogeneous and heterogeneous nucleation of phase transitions.

VIII. Acknowledgments

Paul DeMott, Harry ten Brink, Jonathan Abbatt, Kenneth Carslaw, Gregory Dash, Thomas Koop, and

Hui-Ming Hung graciously criticized specific sections and corrected errors in the manuscript. Mario Molina, Douglas Worsnop, Anthony Prenni, Allan Bertram, Azadeh Tabazadeh, Lyatt Jaegle, Simon Clegg, Mark Rood, Marc Pitchford, and Anthony Wexler provided useful suggestions. Anonymous reviewers of the paper's outline provided valuable suggestions on emphasis and content, while reviewers of the manuscript itself provided many important suggestions and clarifications. Jeong-Ho Han and Holly Chelf kindly aided in the preparation of many figures. S.T.M. is grateful for support received from the NSF Atmospheric Chemistry Program and a Presidential Early Career Award in Science and Engineering.

IX. Appendix A: Free Energy Calculations

The details of the free energy calculations (Figure 1) are formidable, so an example is provided here. The first step is the acquisition of thermodynamic data from literature for the species involved at 298.15 K, as shown in Table 5. The standard chemical potentials at several temperatures are needed and are evaluated by the following equation:

$$\mu_i^0(T) = T\left[\frac{\Delta G_f^{\ 0}}{T_0} + \Delta H_f^0\left(\frac{1}{T} - \frac{1}{T_0}\right) + C_P^0\left(\ln\frac{T_0}{T} - \frac{T_0}{T} + 1\right)\right] \quad \text{(A1)}$$

The results at 220, 275, 298, and 330 K are given in Table 6.

As an example, a 0.1 mol fraction of $(NH_4)_2SO_4/H_2O$ system is considered. The corresponding ion molalities (m_i) are 12.346 for NH_4^+, 6.173 for SO_4^{2-}, and 55.556 (always) for H_2O. From the Clegg and Wexler website [www.uea.ac.uk/~e770/aim.html], the following mole fraction activity coefficients, f, are obtained at 275 K: 0.4697 for NH_4^+, 0.01355 for SO_4^{2-}, and 1.047 for H_2O. The chemical potential of each component is calculated according to

$$\mu_i(T,m_i) = \mu_i^0(T) + RT \ln \gamma_i m_i \quad \text{(A2)}$$

[The effect of increased pressure due to particle curvature can raise the chemical potential inside small particles (i.e., the Kelvin effect). Typically, this effect is negligible for spherical particles larger than 1 μm, is small between 100 nm and 1 μm, and is important under 100 nm. In this way, the deliquescence relative humidity of small particles is size dependent. See refs 85 and 296. However, in cloud activation processes described by Köhler curves, the Kelvin effect is an important factor even for micron-sized aqueous particles.] The conversion factor between the mole fraction activity coefficients and molal activity coefficients, γ, is as follows:

$$\gamma = (1 + 0.018(m_{NH_4^+} + m_{SO_4^{2-}}))^{-1} f \quad \text{(A3)}$$

In the case of the 0.1 mol fraction of $(NH_4)_2SO_4/H_2O$, the conversion factor is 0.75. From eqs A1−A3, the chemical potentials are calculated as follows: −80.15 kJ/mol for NH_4^+, −763.38 kJ/mol for SO_4^{2-}, and −241.53 kJ/mol for H_2O.

The free energy of formation of a system is

$$G_f = \sum_i n_i \mu_i \quad \text{(A4)}$$

where n_i is the moles of species i. For a system containing 0.1 mol of $(NH_4)_2SO_4$ and 0.9 mol of H_2O, the aqueous free energy of formation at 275 K is

$$\begin{aligned} G_f^{\text{aqueous}} &= 0.2\mu_{NH_4^+} + 0.1\mu_{SO_4^{2-}} + 0.9\mu_{H_2O} \\ &= 0.2(-80.15) + 0.1(-763.38) + 0.9(-241.53) \\ &= -309.75 \text{ kJ mol}^{-1} \end{aligned} \quad \text{(A5)}$$

The next question to ask is: Has this one mole organized itself in a way to minimize the free energy? To answer it, one imagines other ways the mole could be organized and calculates the free energy for comparison. One obvious way would be for the $(NH_4)_2SO_4$ to remain as a crystal and the water to remain as liquid water. The free energy is calculated as

$$\begin{aligned} G_f^{\text{crystal/liquid}} &= 0.1\mu_{(NH_4)_2SO_4(s)} + 0.9\mu_{H_2O(l)} \\ &= 0.1(-923.52) + 0.9(-240.98) \\ &= -309.23 \text{ kJmol}^{-1} \end{aligned} \quad \text{(A6)}$$

In this comparison, the mole is better arranged as an aqueous solution because its free energy is lower. A reaction to form the crystal and liquid water is 0.52 kJ mol^{-1} endoergic.

Another consideration is the arrangement as crystalline ammonium sulfate and water vapor. The chemical potential of water gas equals that of water in the aqueous solution. The free energy is then as follows:

Table 5. Free Energy of Formation, Enthalpy of Formation, and Heat Capacity at Constant Pressure for Chemical Species in the Binary System $(NH_4)_2SO_4/H_2O$ at Standard Conditions[419,420]

	$G°_f$ (kJ/mol)	$H°_f$ (kJ/mol)	$C_P°$ (J mol^{-1} K^{-1})
α-$(NH_4)_2SO_4$(s)	−901.67	−1180.85	187.49
$H_2O(l)$	−237.13	−285.83	75.29
NH_4^+(aq), 1 *m*	−79.31	−132.51	79.9
SO_4^{2-}(aq), 1 *m*	−744.53	−909.27	−293
H_2O(s), 273.15 K	−241.29	−293.72	37.66
H_2O(g)	−228.57	−241.82	33.58

Table 6. Chemical Potentials (μ_i) Evaluated at Four Temperatures for Species in the Binary System $(NH_4)_2SO_4/H_2O$

	$\mu_i°$ (T)			
	220 K	275 K	330 K	298.15 K
α-$(NH_4)_2SO_4$(s)	−976.96	−923.52	−872.15	−901.67
$H_2O(l)$	−250.74	−240.98	−232.05	−237.13
NH_4^+(aq), 1 *m*	−94.16	−83.51	−73.76	−79.31
SO_4^{2-}(aq), 1 *m*	−784.41	−757.05	−726.45	−744.53
H_2O(s)	−251.70	−240.94	−230.59	−236.54
H_2O(g)	−232.42	−229.63	−227.21	−228.57

$$G_f^{\text{crystal/vapor}} = 0.1\mu_{(NH_4)_2SO_4(s)} + 0.9\mu_{H_2O(g)}$$
$$= 0.1(-923.52) + 0.9(-241.53)$$
$$= -309.73\,\text{kJ mol}^{-1} \quad \text{(A7)}$$

An aqueous solution is more favorable than a crystal and water vapor, i.e., deliquescence should occur (thermodynamically). The reaction would be 0.02 kJ mol^{-1} exoergic. For comparison, the equilibrium relative humidity maintained over a 0.1 mol fraction solution (275 K) is 78.5%, which is approximately the deliquescence relative humidity. Similar calculations for 0.05 mol fraction at 275 K yield G_f^{aqueous} of −275.54 kJ/mol and $G_f^{\text{crystal/vapor}}$ of −275.32 kJ/mol. The aqueous solution is favored in this case, and the RH is 90.6%.

Below 273 K, another plausible configuration is the arrangement as ice and crystalline ammonium sulfate. For 0.10 mol fraction at 220 K, the calculation of G_f^{aqueous} yields −323.41 kJ/mol. The alternative arrangement is

$$G_f^{\text{crystal/ice}} = 0.1\mu_{(NH_4)_2SO_4(s)} + 0.9\mu_{H_2O(s)}$$
$$= 0.1(-976.96) + 0.9(-251.70)$$
$$= -324.34\,\text{kJ mol}^{-1} \quad \text{(A8)}$$

Ice and the crystalline ammonium sulfate are favorable compared to the aqueous solution.

The case-by-case procedure can be generalized into a minimum free energy formulation at 0.1 mole fraction, as follows:

$$G_f = F(0.2\mu_{NH_4^+} + 0.1\mu_{SO_4^{2-}} + 0.9\mu_{H_2O(aq)}) + (1-F)(0.1\mu_{(NH_4)_2SO_4(s)} + 0.9(a\mu_{H_2O(l)} + b\mu_{H_2O(g)} + (1-a-b)\mu_{H_2O(s)})) \quad \text{(A9)}$$

where F, a, and b vary from 0 to 1. F is the fraction of the chemical system composed of aqueous solution. Of the water not in aqueous solution, a and b are the respective fractions occurring as liquid water and gas. The parameters a, b, and F are varied to minimize G_f. The additive form of the equation and the decoupling of F from a and b shows that, in fact, any minimization of this particular function yields F as 0 or 1 and $\{a,b\}$ as $\{0,0\}$, $\{1,0\}$, or $\{0,1\}$ except at special points such as melting or aqueous saturation when F has no unique solution or sublimation when b has no unique solution. This result is Gibbs Phase Rule. The approach is obviously generalized to other mole fractions. For more complex systems, it is more convenient to write the mass and charge balance conditions as separate equations. An example is given by Ansari and Pandis.[419]

Some commonly employed thermodynamic models cover different chemical domains. For example, Tabazadeh et al. (APCM)[402] and Carslaw et al.[127] cover chemical species (mainly but not limited to HNO_3, H_2SO_4, and H_2O), phases, and temperatures relevant to polar stratospheric cloud formation. Clegg et al. extend the work of Carslaw et al.[127] to include chemical species and temperatures relevant to the upper troposphere (viz. NH_4^+)[134] or to consider species relevant to sea-salt aerosols (viz. NH_4^+, Na^+, and Cl^-), albeit only at 298 K.[162] In boundary layer tropospheric chemistry, a model by Wexler and Seinfeld (AIM-2)[128] is available that covers 283 to 313 K and boundary layer constituents such as Na^+, NO_3^-, SO_4^{2-}, Cl^-, H^+, and NH_4^+. Marion and Farren[421] (FREEZECHEM) offer a model relevant to the freezing of all chemical constituents of seawater (e.g., Na−K−Mg−Ca−Cl−SO_4−H_2O). Most research groups make their models available to any interested user upon enquiry. Clegg and Wexler offer the unique interaction with their model through a web-based server (including batch calculations), which makes accessing their model for the casual user very easy. Otherwise, a FORTRAN compiler is typically needed for implementing other workers' models. A comparative review of several models is provided by Zhang et al.[422]

X. Appendix B: Saturation Ratio

There are no universal definitions for the saturation ratio and the supersaturation of one phase with respect to another, and a careful reader must always clarify an author's intentions. Even so, there are some definitions more common than others.

Water. When only water is involved, the vapor saturation ratios with respect to liquid water, $S_{\text{liq}}^{\text{vap}}$, and ice, $S_{\text{ice}}^{\text{vap}}$, are defined as

$$S_{\text{liq}}^{\text{vap}} = \frac{P_{\text{gas}}}{P_{\text{liq}}^{\text{eq}}}, \quad S_{\text{ice}}^{\text{vap}} = \frac{P_{\text{gas}}}{P_{\text{ice}}^{\text{eq}}} \quad \text{(B1)}$$

Note that these values are the respective relative humidities divided by 100. The supersaturation, often also denoted S, is the saturation ratio minus one. Supersaturation is sometimes expressed as a percent (%) or tenth of percent (‰).

The saturation ratio of liquid water to ice, $S_{\text{ice}}^{\text{liq}}$, is conveniently expressed by taking advantage of the commonality of P_{gas}, as follows:

$$S_{\text{ice}}^{\text{liq}} = \frac{S_{\text{ice}}^{\text{vap}}}{S_{\text{liq}}^{\text{vap}}} = \frac{P_{\text{liq}}^{\text{eq}}}{P_{\text{ice}}^{\text{eq}}} \quad \text{(B2)}$$

Salts. When aqueous species are present in equilibrium with their crystalline salt, the chemical potential of a solid phase is the sum of the chemical potentials of its constituents. In addition, the chemical potential of each constituent in the solid is separately equal to the chemical potential in the aqueous solution. An example for NaCl(s) is helpful:

$$\mu(\text{NaCl})(s) = \mu(Na^+)(s) + \mu(Cl^-)(s) \quad \text{(B3)}$$

$$\mu(Na^+)(s) = \mu(Na^+)(aq),\ \mu(Cl^-)(s) = \mu(Cl^-)(aq) \quad \text{(B4)}$$

Combining eqs B3 and B4 at aqueous saturation, we obtain

$$\mu(\mathrm{NaCl})(\mathrm{s;sat}) = \mu(\mathrm{Na^+})(\mathrm{aq;sat}) + \mu(\mathrm{Cl^-})(\mathrm{aq;sat}) \quad \text{(B5)}$$

This value is the reference chemical potential for the solid, $\mu^0(\mathrm{NaCl})(\mathrm{s})$. At other aqueous concentrations, we write

$$\mu(\mathrm{NaCl})(\mathrm{s}) = \mu(\mathrm{Na^+})(\mathrm{aq}) + \mu(\mathrm{Cl^-})(\mathrm{aq}) \quad \text{(B6)}$$

The term $\mu(\mathrm{NaCl})(\mathrm{s})$ is the virtual chemical potential, which means that if NaCl(s) were to exist in equilibrium with the indicated concentrations of Na^+ and Cl^-, then it would have a potential $\mu(\mathrm{NaCl})$. However, in point of fact, the NaCl crystal is only in equilibrium at $\mu^0(\mathrm{NaCl})(\mathrm{s})$ and the solution is subsaturated or supersaturated otherwise.

The free energy for dissolution, $\Delta\mu$, is the difference between the virtual chemical potential and the saturation chemical potential, as follows:

$$\begin{aligned}\Delta\mu &= \mu(\mathrm{NaCl})(\mathrm{s}) - \mu^0(\mathrm{NaCl})(\mathrm{s}) \\ &= \mu(\mathrm{Na^+})(\mathrm{aq}) + \mu(\mathrm{Cl^-})(\mathrm{aq}) - \mu(\mathrm{Na^+})(\mathrm{aq;sat}) - \\ &\qquad \mu(\mathrm{Cl^-})(\mathrm{aq;sat}) \quad \text{(B7)}\end{aligned}$$

Expansion of the definition of chemical potential in terms of activity yields (eq A2):

$$\begin{aligned}\Delta\mu &= \mu^0(\mathrm{Na^+})(\mathrm{aq}) + RT \ln a(\mathrm{Na^+})(\mathrm{aq}) + \\ &\qquad \mu^0(\mathrm{Cl^-})(\mathrm{aq}) + RT \ln a(\mathrm{Cl^-})(\mathrm{aq}) \\ &\quad - \mu^0(\mathrm{Na^+})(\mathrm{aq}) - RT \ln a(\mathrm{Na^+})(\mathrm{aq;sat}) - \\ &\qquad \mu^0(\mathrm{Cl^-})(\mathrm{aq}) - RT \ln a(\mathrm{Cl^-})(\mathrm{aq;sat}) \\ &= RT \ln \frac{a^{\mathrm{aq}}_{\mathrm{Na^+}} a^{\mathrm{aq}}_{\mathrm{Cl^-}}}{a^{\mathrm{aq,sat}}_{\mathrm{Na^+}} a^{\mathrm{aq,sat}}_{\mathrm{Cl^-}}} \quad \text{(B8)}\end{aligned}$$

The quotient in eq B8 is the salt saturation ratio, S. With the familiar substitutions of $\Delta G = \Delta\mu$, $K_{sp} = a^{\mathrm{aq,sat}}_{\mathrm{Na^+}} a^{\mathrm{aq,sat}}_{\mathrm{Cl^-}}$, and $S = a^{\mathrm{aq}}_{\mathrm{Na^+}} a^{\mathrm{aq}}_{\mathrm{Cl^-}}/K_{sp}$, we then obtain from eq B8 the following:

$$\Delta G = RT \ln S \quad \text{(B9)}$$

where the familiar substitutions for ΔG and K_{sp} are made. According to eq B9, for $S > 1$ (i.e., supersaturated), $\Delta G > 0$. Equation B7 shows the formulation is the solid going to aqueous products. Thus, in a supersaturated environment, the solid does not dissolve.

It should be noted that $\mu^0(\mathrm{NaCl})$ is defined strictly for a NaCl crystal in equilibrium with is own solution. When another salt is added (e.g., KCl), then the stoichiometry of NaCl(s) will change slightly and $\mu(\mathrm{NaCl})(\mathrm{s;sat})$ will be theoretically different from $\mu^0(\mathrm{NaCl})$. However, in most cases, this numerical difference is so small as to be negligible, and solid crystals are assumed to have constant $\mu(\mathrm{NaCl})(\mathrm{s;sat})$.

Attention should be drawn to the relationship between S and thus ΔG and the quantities μ discussed in Appendix A. From the Clegg website, we can obtain $S = 1.455$ and thus $\Delta G = 0.857$ kJ mol^{-1} for 0.1 mol fraction of $(NH_4)_2SO_4$ at 275 K. The calculation based solely on supersaturation is incomplete per se because it considers only the crystal (viz. $\mu((NH_4)_2SO_4)(s) - \mu^0((NH_4)_2SO_4)(s)$) and does not consider the free energy of the entire system. However, eqs A5 and A7 show that $\mu(H_2O)$ remains constant as a gas-phase or aqueous-phase species. Then, 0.1 mol of $(NH_4)_2SO_4(s)$ combining with 0.9 mol of $H_2O(g)$ to form an aqueous solution is endoergic by 0.857 kJ mol^{-1} at 275 K (see comment below). This value is $\Delta G_{\mathrm{deliquescence}}$. In Appendix A, the free energy of a mole of atoms arranged as a crystal and a gas is calculated as 0.02 kJ mol^{-1} less favorable than an aqueous solution. The corresponding saturation ratio is 0.99. There is thus some inconsistency between the model of Clegg et al.[134] and the data of Wagman et al.[420] Ansari and Pandis[419] addressed this discrepancy by suggesting a standard free energy of formation for $(NH_4)_2SO_4$ of -903.15 rather than -901.67 kJ mol^{-1}. In this case, $\Delta G = +0.13$ kJ mol^{-1} instead of -0.02 kJ mol^{-1}. In fact, the Clegg et al. model is more accurate than the free energy calculations employed in Appendices A and B because eq A1 is a simplification of the temperature-dependent behavior.

The Clegg and Wexler website provides outputs of saturation ratio and relative humidity. The free energy of formation of a solution (eq A5) is then calculated as follows:

$$\begin{aligned}G(\mathrm{kJ\ mol^{-1}}) &= 2x\mu_{\mathrm{NH_4^+,aq}} + x\mu_{\mathrm{SO_4^{2-},aq}} + (1-x)\mu_{\mathrm{H_2O}} \\ &= x\Delta\mu + 2x\mu_{\mathrm{NH_4^+,aq,sat}} + x\mu_{\mathrm{SO_4^{2-},aq,sat}} + \\ &\qquad (1-x)(-237.13 + 2.478 \ln \mathrm{RH}) \\ &= 2.478x \ln S - 901.67x + (-237.13 + \\ &\qquad 2.478 \ln \mathrm{RH})(1-x) \quad \text{(B10)}\end{aligned}$$

where eqs A2, A4, and B7 are employed at 298 K with data from Table 5. For the scenario accompanying eq A5, eq B10 yields

$$G = 2.286(0.1) \ln 0.99 - 923.52(0.1) + (-240.98 + 2.286 \ln 0.785)(0.9) = -309.73 \quad \text{(B11)}$$

The slight discrepancy between -309.73 (eq B11) and -309.75 (eq A5) arises because eq B11 is based upon the temperature dependency of $(NH_4)_2SO_4$ (Table 2) whereas the results associated with eq A5 arise from the temperature dependencies of NH_4^+ and SO_4^{2-}. Temperature dependencies in each case are only calculated approximately, according to eq A1.

As a final comment, at 275 K and 78.5% RH in the example considered, 0.1 mol of $(NH_4)_2SO_4(s)$ is constrained to combine with 0.9 mol of $H_2O(g)$ to form an aqueous solution. If other molar ratios were employed, then $\mu(H_2O)$ would not correspond to 78.5% RH and water would either evaporate or condense until a 0.1 mole fraction aqueous solution were obtained. No other aqueous composition is stable at 78.5% RH.

XI. References

(1) Seinfeld, J. H.; Pandis, S. N. *Atmospheric Chemistry and Physics*; Wiley: New York, 1998.
(2) Pruppacher, H. R.; Klett, J. D. *Microphysics of Clouds and Precipitation*; Kluwer: Dordrecht, 1997.
(3) Baker, M. B. *Science* **1997**, *276*, 1072−1078.

(4) Baker, M. B. In *Ice Physics and the Natural Environment*; Wettlaufer, J. S., Dash, J. G., Untersteiner, N., Eds.; Springer-Verlag: Berlin, 1999.
(5) Franks, F. In *Water, A Comprehensive Treatise*; Franks, F., Ed.; Plenum: New York, 1982; Vol. 7.
(6) Gotz, G.; Meszaros, E.; Vali, G. *Atmospheric Particles and Nuclei*; Akademiai Kiado: Budapest, 1991.
(7) Angell, C. A. In *Water, A Comprehensive Treatise*; Franks, F., Ed.; Plenum: New York, 1982; Vol. 7.
(8) Hobbs, P. V. *Ice Physics*; Clarendon: Oxford, 1974.
(9) Weis, D. D.; Ewing, G. E. *J. Geophys. Res.* **1999**, *104*, 21275−21285.
(10) Koop, T.; Bertram, A. K.; Molina, L. T.; Molina, M. J. *J. Phys. Chem. A* **1999**, *103*, 9042−9048.
(11) Onasch, T. B.; Siefert, R. L.; Brooks, S. D.; Prenni, A. J.; Murray, B.; Wilson, M. A.; Tolbert, M. A. *J. Geophys. Res.* **1999**, *104*, 21317−21326.
(12) Cziczo, D. J.; Abbatt, J. P. D. *J. Geophys. Res.* **1999**, *104*, 13781−13790.
(13) Han, J.; Martin, S. T. *J. Geophys. Res.* **1999**, *104*, 3543−3553.
(14) Chelf, J. H.; Martin, S. T. *Geophys. Res. Lett.* **1999**, *26*, 2391−2394.
(15) Chang, H. Y. A.; Koop, T.; Molina, L. T.; Molina, M. J. *J. Phys. Chem. A* **1999**, *103*, 2673.
(16) Yao, Y.; Massucci, M.; Clegg, S. L.; Brimblecombe, P. *J. Phys. Chem. A* **1999**, *103*, 3678−3686.
(17) Iraci, L. T.; Fortin, T. J.; Tolbert, M. A. *J. Geophys. Res.* **1998**, *103*, 8491−8498.
(18) Martin, S. T.; Salcedo, D.; Molina, M. J. *Geophys. Res. Lett.* **1998**, *25*, 31−34.
(19) Koop, T.; Ng, H. P.; Molina, L. T.; Molina, M. J. *J. Phys. Chem. A* **1998**, *102*, 8924−8931.
(20) Bertram, A. K.; Sloan, J. J. *J. Geophys. Res.* **1998**, *103*, 13261−13265.
(21) Dougle, P. G.; Veefkind, J. P.; ten Brink, H. M. *J. Aerosol Sci.* **1998**, *29*, 375−386.
(22) Xu, J.; Imre, D.; McGraw, R.; Tang, I. *J. Phys. Chem. B* **1998**, *102*, 7462−7469.
(23) Prenni, A. J.; Onasch, T. B.; Tisdale, R. T.; Siefert, R. L.; Tolbert, M. A. *J. Geophys. Res.* **1998**, *103*, 28439−28450.
(24) Bertram, A. K.; Sloan, J. J. *J. Geophys. Res.* **1998**, *103*, 3553−3561.
(25) Cziczo, D. J.; Nowak, J. B.; Hu, J. H.; Abbatt, J. P. D. *J. Geophys. Res.* **1997**, *102*, 18843−18850.
(26) Martin, S. T.; Salcedo, D.; Molina, L. T.; Molina, M. J. *J. Phys. Chem. B* **1997**, *101*, 5307−5313.
(27) Anthony, S. E.; Onasch, T. B.; Tisdale, R. T.; Disselkamp, R. S.; Tolbert, M. A.; Wilson, J. C. *J. Geophys. Res.* **1997**, *102*, 10777−10784.
(28) Koop, T.; Luo, B. P.; Biermann, U. M.; Crutzen, P. J.; Peter, T. *J. Phys. Chem. A* **1997**, *101*, 1117−1133.
(29) Carleton, K. L.; Sonnenfroh, D. M.; Rawlins, W. T.; Wyslouzil, B. E.; Arnold, S. *J. Geophys. Res.* **1997**, *102*, 6025−6033.
(30) Imre, D. G.; Xu, J.; Tridico, A. C. *Geophys. Res. Lett.* **1997**, *24*, 69−72.
(31) Imre, D. G.; Xu, J.; McGraw, R. *J. Phys. Chem.* **1997**, *101*, 4191.
(32) Tsias, A.; Prenni, A. J.; Carslaw, K. S.; Onasch, T. P.; Luo, B. P.; Tolbert, M. A.; Peter, T. *Geophys. Res. Lett.* **1997**, *24*, 2303−2306.
(33) Tang, I. N.; Fung, K. H. *J. Chem. Phys.* **1997**, *106*, 1653−1660.
(34) Clapp, M. L.; Niedziela, R. F.; Richwine, L. J.; Dransfield, T.; Miller, R.; Worsnop, D. R. *J. Geophys. Res.* **1997**, *102*, 8899−8907.
(35) Tisdale, R. T.; Middlebrook, A. M.; Prenni, A. J.; Tolbert, M. A. *J. Phys. Chem. A* **1997**, *101*, 2112−2119.
(36) Middlebrook, A. M.; Tolbert, M. A.; Drdla, K. *Geophys. Res. Lett.* **1996**, *23*, 2145−2148.
(37) Disselkamp, R. S.; Anthony, S. E.; Prenni, A. J.; Onasch, T. B.; Tolbert, M. A. *J. Phys. Chem.* **1996**, *100*, 9127−9137.
(38) Zhang, R. Y.; Leu, M. T.; Molina, M. J. *Geophys. Res. Lett.* **1996**, *23*, 1669−1672.
(39) Bertram, A. K.; Patterson, D. D.; Sloan, J. J. *J. Phys. Chem.* **1996**, *100*, 2376−2383.
(40) Lamb, D.; Moyle, A. M.; Brune, W. H. *Aerosol Sci. Technol.* **1996**, *24*, 263−278.
(41) Weis, D. D.; Ewing, G. *J. Geophys. Res.* **1996**, *101*, 18709−18720.
(42) Ji, K.; Petit, J. C.; Negrier, P.; Haget, Y. *Geophys. Res. Lett.* **1996**, *23*, 981−984.
(43) Anthony, S. E.; Tisdale, R. T.; Disselkamp, R. S.; Tolbert, M. A.; Wilson, J. C. *Geophys. Res. Lett.* **1995**, *22*, 1105−1108.
(44) Fox, L. E.; Worsnop, D. R.; Zahniser, M. S.; Wofsy, S. C. *Science* **1995**, *267*, 351−355.
(45) Iraci, L. T.; Middlebrook, A. M.; Tolbert, M. A. *J. Geophys. Res.* **1995**, *100*, 20969−20977.
(46) Zhang, R.; Leu, M. T.; Keyser, L. F. *J. Geophys. Res.* **1995**, *100*, 18845−18854.
(47) Koop, T.; Biermann, U. M.; Raber, W.; Luo, B. P.; Crutzen, P. J.; Peter, T. *Geophys. Res. Lett.* **1995**, *22*, 917−920.
(48) Izmailov, A. F.; Myerson, A. S.; Na, H. S. *Phys. Rev. E* **1995**, *52*, 3923−3935.
(49) Myerson, A. S.; Izmailov, A. F.; Na, H. S. *J. Crystal Growth* **1996**, *166*, 981−988.
(50) Richardson, C. B.; Snyder, T. D. *Langmuir* **1994**, *10*, 2462−2465.
(51) Tang, I. N.; Munkelwitz, H. R. *J. Geophys. Res.* **1994**, *99*, 18,801−18,808.
(52) Tang, I. N.; Munkelwitz, H. R. *J. Appl. Meteorol.* **1994**, *33*, 791−796.
(53) Iraci, L. T.; Middlebrook, A. M.; Wilson, M. A.; Tolbert, M. A. *Geophys. Res. Lett.* **1994**, *21*, 867−870.
(54) Beyer, K. D.; Seago, S. W.; Chang, H. Y.; Molina, M. J. *Geophys. Res. Lett.* **1994**, *21*, 871−874.
(55) Marti, J. J.; Mauersberger, K. *J. Phys. Chem.* **1994**, *98*, 6897−6899.
(56) Snyder, T. D.; Richardson, C. B. *Langmuir* **1993**, *9*, 347−351.
(57) Tang, I. N.; Munkelwitz, H. R. *Atmos. Environ.* **1993**, *27A*, 467−473.
(58) Koehler, B. G.; Mcneill, L. S.; Middlebrook, A. M.; Tolbert, M. A. *J. Geophys. Res.* **1993**, *98*, 10563−10571.
(59) Middlebrook, A. M.; Iraci, L. T.; Mcneill, L. S.; Koehler, B. G.; Wilson, M. A.; Saastad, O. W.; Tolbert, M. A.; Hanson, D. R. *J. Geophys. Res.* **1993**, *98*, 20473−20481.
(60) Zhang, R.; Wooldridge, P. J.; Abbatt, J. P. D.; Molina, M. J. *J. Phys. Chem.* **1993**, *97*, 7351−7358.
(61) Molina, M. J.; Zhang, R.; Wooldridge, P. J.; McMahon, J. R.; Kim, J. E.; Chang, H. Y.; Beyer, K. D. *Science* **1993**, *261*, 1418−1423.
(62) Ohtake, T. *Tellus* **1993**, *45B*, 138−144.
(63) Worsnop, D. R.; Fox, L. E.; Zahniser, M. S.; Wofsy, S. C. *Science* **1993**, *259*, 71−74.
(64) Barton, N.; Rowland, B.; Devlin, J. P. *J. Phys. Chem.* **1993**, *97*, 5848−5851.
(65) Marti, J.; Mauersberger, K. *Geophys. Res. Lett.* **1993**, *20*, 359−362.
(66) Ji, K.; Petitt, J. C. *C.R. Acad. Sci. Paris* **1993**, *316*, 1743−1748.
(67) Koehler, B. G.; Middlebrook, A. M.; Tolbert, M. A. *J. Geophys. Res.* **1992**, *97*, 8065−8074.
(68) Tolbert, M. A.; Koehler, B. G.; Middlebrook, A. M. *Spectrosc. Acta A Mol. Spectrosc.* **1992**, *48*, 1303−1313.
(69) Middlebrook, A. M.; Koehler, B. G.; McNeill, L. S.; Tolbert, M. A. *Geophsy. Res. Lett.* **1992**, *19*, 2417−2420.
(70) Tolbert, M. A.; Middlebrook, A. M. *J. Geophys. Res.* **1990**, *95*, 2423−2431.
(71) Cohen, M. D.; Flagan, R. C.; Seinfeld, J. H. *J. Phys. Chem.* **1987**, *91*, 4563−4574.
(72) Richardson, C. B.; Hightower, R. L. *Atmos. Environ.* **1987**, *21*, 971−975.
(73) Cohen, M. D.; Flagan, R. C.; Seinfeld, J. H. *J. Phys. Chem.* **1987**, *91*, 4575−4582.
(74) Cohen, M. D.; Flagan, R. C.; Seinfeld, J. H. *J. Phys. Chem.* **1987**, *91*, 4583−4590.
(75) Tang, I. N.; Munkelwitz, H. R. The Growth and Nucleation of Hygroscopic Aerosols. In *Aerosols: Formation and Reactivity*, Proceedings of the 2nd International Aerosol Conference, Berlin, September 22−26; Pergamon: Oxford, 1986.
(76) Spann, J. F.; Richardson, C. B. *Atmos. Environ.* **1985**, *19*, 819−825.
(77) Rood, M. J.; Larson, T. V.; Covert, D. S.; Ahlquist, N. C. *Atmos. Environ.* **1985**, *19*, 1181−1190.
(78) Tang, I. N.; Munkelwitz, H. R. *J. Colloid Interface Sci.* **1984**, *98*, 430−438.
(79) Richardson, C. B.; Spann, J. F. *J. Aerosol Sci.* **1984**, *15*, 563−571.
(80) Aguerd, M.; Broto, F.; Babin, L.; Clausse, D. *Colloids Surf.* **1984**, *12*, 333−340.
(81) Tang, I. N. In *Generation of Aerosols and Facilities for Exposure Experiments*; Willeke, K., Ed.; Ann Arbor Science Publishers: Ann Arbor, MI, 1980.
(82) Charlson, R. J.; Covert, D. S.; Larson, T. V.; Waggoner, A. P. *Atmos. Environ.* **1978**, *12*, 39−53.
(83) Tang, I. N.; Munkelwitz, H. R.; Davis, J. G. *J. Aerosol Sci.* **1978**, *9*, 505−511.
(84) Tang, I. N.; Munkelwitz, H. R. *J. Aerosol Sci.* **1977**, *8*, 321−330.
(85) Orr, C.; Hurd, F. K.; Corbett, W. J. *J. Colloid Sci.* **1958**, *13*, 472−482.
(86) Winkler, P.; Junge, C. *J. Rech. Atmos.* **1972**, *6*, 617−638.
(87) Winkler, P. *Aerosol Sci.* **1973**, *4*, 373−387.
(88) Hänel, G. *Adv. Geophys.* **1976**, *19*, 73−188.
(89) Gupta, A.; Tang, D.; McMurry, P. H. *J. Atmos. Chem.* **1995**, *20*, 117−139.
(90) Viisanen, Y.; Kulmala, M.; Laaksonen, A. *J. Chem. Phys.* **1997**, *107*, 920−926.
(91) Ball, S. M.; Hanson, D. R.; Eisele, F. L.; McMurry, P. H. *J. Geophys. Res.* **1999**, *104*, 23,709−23,718.
(92) Kulmala, M.; Pirjola, L.; Makela, J. M. *Nature* **2000**, *404*, 66.
(93) Houze, R. A. *Cloud Dynamics*; Academic Press: New York, 1993.
(94) McMurry, P. H.; Litchy, M.; Huang, P. F.; Cai, X.; Turpin, B. J.; Dick, W. D.; Hanson, A. *Atmos. Environ.* **1996**, *30*, 101−108.

(95) Saxena, P.; Hildemann, L. M.; McMurry, P. H.; Seinfeld, J. H. *J. Geophys. Res.* **1995**, *100*, 18755−18770.
(96) Gill, P. S.; Graedel, T. E.; Weschler, C. J. *Rev. Geophys. Space Phys.* **1983**, *21*, 903−920.
(97) Ellison, G. B.; Tuck, A. F.; Vaida, V. *J. Geophys. Res.* **1999**, *104*, 11633−11641.
(98) Lupis, C. H. P. *Chemical Thermodynamics of Materials*; North-Holland: Amsterdam, 1983.
(99) Walas, S. M. *Phase Equilibria in Chemical Engineering*; Butterworth: Boston, 1985.
(100) Hillert, M. *Phase Equilibria, Phase Diagrams, and Phase Transformations: Their Thermodynamic Basis*; Cambridge University Press: Cambridge, 1998.
(101) West, A. R. *Solid State Chemistry and Its Applications*; Wiley: New York, 1984.
(102) Bergeron, C. G.; Risbud, S. H. *Introduction to Phase Equilibria in Ceramics*; American Ceramic Society: Columbus, OH, 1984.
(103) Klein, C.; Hurlbut, C. S. *Manual of Mineralogy*; Wiley: New York, 1993.
(104) Balbuena, P. B. *Science* **1999**, *286*, 430−432.
(105) Phase. ftp://isua.iastate.edu, Tian, K. S., Iowa State University, 1997.
(106) Hallett, J.; Lewis, R. E. J. *Weather* **1967**, *22*, 56−65.
(107) Tolbert, M. A. *Science* **1994**, *264*, 527−528.
(108) Tolbert, M. A. *Science* **1996**, *272*, 1597.
(109) Koop, T.; Carslaw, K. S.; Peter, T. *Geophys. Res. Lett.* **1997**, *17*, 2199−2202.
(110) Tabazadeh, A.; Turco, R. P.; Drdla, K.; Jacobson, M. Z.; Toon, O. B. *Geophys. Res. Lett.* **1994**, *21*, 1619−1622.
(111) Carslaw, K. S.; Peter, T.; Clegg, S. L. *Rev. Geophys.* **1997**, *35*, 125−154.
(112) Kolb, C. E.; Worsnop, D. R.; Zahniser, M. S.; Davidovits, P.; Keyser, L. F.; Leu, M. T.; Molina, M. J.; Hanson, D. R.; Ravishankara, A. R. In *Progress and Problems in Atmospheric Chemistry*; Barker, J. R., Ed.; World Scientific: Singapore, 1995.
(113) Peter, T. *Annu. Rev. Phys. Chem.* **1997**, *48*, 785−822.
(114) Wexler, A. S.; Potukuchi, S. In *Atmospheric Particles*; Harrison, R. M., Grieken, R. V., Eds.; Wiley: New York, 1998.
(115) Peter, T. In *Ice Physics and the Natural Environment*; Wettlaufer, J. S., Ed.; Springer-Verlag: Berlin, 1999.
(116) Turco, R. P. In *Atmospheric Chemistry and Global Change*; Brasseur, G. P., Orlando, J. J., Tyndall, G. S., Eds.; Oxford University Press: New York, 1999.
(117) Vali, G. In *Proceedings of the Fourteenth International Conference on Nucleation and Atmospheric Aerosols*; Kulmala, M., Wagner, P. E., Eds.; Pergamon: Oxford, 1996.
(118) Köhler, H. *Trans. Faraday Soc.* **1936**, *32*, 1152−1161.
(119) Junge, C. *Ann. Meteorol.* **1952**, *5*, 1−55.
(120) Dufour, L.; Defay, R. *Thermodynamics of Clouds*; Academic Press: New York, 1963.
(121) Finlayson-Pitts, B. J.; Pitts, J. N. *Chemistry of the Upper and Lower Atmosphere: Theory, Experiments and Applications*; Academic Press: New York, 1999.
(122) Warneck, P. *Chemistry of the Natural Atmosphere*; Academic Press: San Diego, 1999.
(123) Hinds, W. C. *Aerosol Technology: Properties, Behavior, and Measurement of Airborne Particles*; Wiley: New York, 1982.
(124) Reist, P. C. *Introduction to Aerosol Science*; MacMillan: New York, 1984.
(125) Willeke, K.; Baron, P. A. *Aerosol Measurement: Principles, Techniques, and Applications*; Wiley: New York, 1993.
(126) Rasmussen, D. H. *J. Microsc.* **1982**, *128*, 167−174.
(127) Carslaw, K. S.; Clegg, S. L.; Brimblecombe, P. *J. Phys. Chem.* **1995**, *99*, 11557−11574.
(128) Wexler, A. S.; Seinfeld, J. H., *Atmos. Environ.* **1991**, *25A*, 2731−2748.
(129) Wooldridge, P. J.; Zhang, R.; Molina, M. J. *J. Geophys. Res.* **1995**, *100*, 1389−1396.
(130) Stumm, W.; Morgan, J. J. *Aquatic Chemistry*; Wiley: New York, 1996.
(131) *Gmelins Handbuch der anorganischen chemie*; Verlag Chemie: Berlin, 1988; Vol. 4, p 969.
(132) Gable, C. M.; Betz, H. F.; Maron, S. H. *J. Am. Chem. Soc.* **1950**, *72*, 1445−1448.
(133) *Gmelins Handbuch der anorganischen chemie*; Verlag Chemie: Berlin, 1988; Vol. 6, p 215.
(134) Clegg, S. L.; Brimblecombe, P.; Wexler, A. S. *J. Phys. Chem. A* **1998**, *102*, 2137−2154.
(135) Hossain, M. A.; Srivastava, J. P.; Sattar, A.; Khulbe, P. K.; Bist, H. D. *Phys. Status Solidi A* **1994**, *141*, 335−344.
(136) *Gmelins Handbuch der anorganischen chemie*; Verlag Chemie: Berlin, 1988; Vol. 21, p 332.
(137) *Gmelins Handbuch der anorganischen chemie*; Verlag Chemie: Berlin, 1988; Vol. 23, p 122.
(138) Martin, S. T. *Geophys. Res. Lett.* **1998**, *25*, 1657−1660.
(139) Bajpai, P. K.; Jain, Y. S.; Bist, H. D. *J. Raman Spectrosc.* **1990**, *21*, 327−32.
(140) Atkins, P. W. *Physical Chemistry*; Oxford University Press: Oxford, 1988.
(141) *Gmelins Handbuch der anorganischen chemie*; Verlag Chemie: Berlin, 1988.
(142) Seidell, A. *Solubilities of Inorganic and Metal Organic Compounds*; Nostrand: New York, 1940.
(143) Silcock, H. L. *Solubilities of Inorganic and Organic Compounds*; Pergamon: Oxford, 1979.
(144) Hanson, D.; Mauersberger, K. *Geophys. Res. Lett.* **1988**, *15*, 855−858.
(145) Hanson, D.; Mauersberger, K. *J. Phys. Chem.* **1988**, *92*, 6167−6170.
(146) Zhang, R. Y.; Wooldridge, P. J.; Molina, M. J. *J. Phys. Chem.* **1993**, *97*, 8541−8548.
(147) Hulsmann, O.; Biltz, W. *Z. Anorg. Allg. Chem.* **1934**, *218*, 369−378.
(148) DeMott, P. J.; Rogers, D. C.; Kreidenweis, S. M. *J. Geophys. Res.* **1997**, *102*, 19575−19584.
(149) Heymsfield, A. J.; Miloshevich, L. M.; Twohy, C.; Sachse, G.; Oltmans, S. *Geophys. Res. Lett.* **1998**, *25*, 1343−1346.
(150) Jensen, E. J.; Toon, O. B. *Geophys. Res. Lett.* **1997**, *24*, 249−252.
(151) Ohara, M.; Reid, R. C. *Modeling Crystal Growth Rates from Solution*; Prentice Hall: Englewood Cliffs, NJ, 1973.
(152) Molina, M. J. In *The Chemistry of the Atmosphere: Its Impact on Global Change*; Calvert, J. G., Ed.; Blackwell: Oxford, 1994.
(153) Thibert, E.; Domine, F. *J. Phys. Chem. B* **1997**, *101*, 3554−3565.
(154) Thibert, E.; Domine, F. *J. Phys. Chem. B* **1998**, *102*, 4432−4439.
(155) Iribarne, J. V.; Godson, W. L. *Atmospheric Thermodynamics*; Reidel: Dordrecht, 1981.
(156) DeMott, P. J.; Rogers, D. C.; Kreidenweis, S. M.; Chen, Y.; Twohy, C.; Baumgardner, D.; Heymsfield, A. J.; Chan, K. R. *Geophys. Res. Lett.* **1998**, 1387−1390.
(157) Jensen, E. J.; Toon, O. B.; Tabazadeh, A.; Sachse, G. W.; Anderson, B. E.; Chan, K. R.; Twohy, C. W.; Gandrud, B.; Aulenbach, S. M.; Heymsfield, A.; Hallet, J.; Gary, B. *Geophys. Res. Lett* **1998**, *25*, 1363−1366.
(158) Rasmussen, D. H. *J. Cryst. Growth* **1982**, *56*, 45−55.
(159) Rasmussen, D. H. *J. Cryst. Growth* **1982**, *56*, 56−66.
(160) Ferguson, F. D. *The Phase Rule*; Butterworth: London, 1966.
(161) Potukuchi, S.; Wexler, A. S. *Atmos. Environ.* **1995**, *29*, 3357−3364.
(162) Clegg, S. L.; Brimblecombe, P.; Wexler, A. S. *J. Phys. Chem. A* **1998**, *102*, 2155−2171.
(163) Tang, I. N. *J. Aerosol Sci.* **1976**, *7*, 361−371.
(164) Hemminger, J. C. *Int. Rev. Phys. Chem.* **1999**, *18*, 387−417.
(165) van der Veen, J. F. In *Phase Transitions in Surface Films*; Traub, H., Ed.; Plenum: New York, 1991.
(166) Thiel, P. A.; Madey, T. E. *Surf. Sci. Rep.* **1987**, *7*, 211.
(167) Barraclough, P. B.; Hall, P. B. *Surf. Sci.* **1974**, *46*, 393.
(168) Beaglehole, D.; Nason, D. *Surf. Sci.* **1980**, *96*, 357.
(169) Furukawa, Y.; Yamato, M.; Kuroda, T. *J. Cryst. Growth* **1987**, *82*, 665.
(170) Bluhm, H.; Salmeron, M. *J. Chem. Phys.* **1999**, *111*, 6947.
(171) Dash, J. G.; Fu, H.; Wettlaufer, J. S. *Rep. Prog. Phys.* **1995**, *58*, 115.
(172) Dash, J. G. *Rev. Modern Phys.* **1999**, *71*, 1737−1743.
(173) Wettlaufer, J. S. In *Ice Physics and the Natural Environment*; Wettlaufer, J. S., Dash, J. G., Untersteiner, N., Eds.; Springer-Verlag: Berlin, 1999.
(174) Adamson, A. W.; Gast, A. P. *Physical Chemistry of Surfaces*, 5th ed.; Wiley: New York, 1997.
(175) Allen, H. C.; Laux, J. M.; Vogt, R.; Finlayson-Pitts, B. J.; Hemminger, J. C. *J. Phys. Chem.* **1996**, *100*, 6371−6375.
(176) Ubbelhode, A. R. *Melting and Crystal Structure*; Clarendon: Oxford, 1965.
(177) *Handbook of Crystal Growth*; Hurle, D. T. J., Ed.; Elsevier: Amsterdam, 1993; Vol. 1a.
(178) Markov, I. V. *Crystal Growth for Beginners*; World Scientific: Singapore, 1995.
(179) Pamplin, B. R., Ed. *Crystal Growth*; Pergamon: Oxford, 1980.
(180) Shi, G.; Seinfeld, J. H. *J. Mater. Res.* **1991**, *6*, 2097−2102.
(181) Shi, G.; Seinfeld, J. H. *J. Mater. Res.* **1991**, *6*, 2091−2096.
(182) Kadiyala, R. K.; Angell, C. A. *Colloids Surf.* **1984**, *11*, 341−351.
(183) Vuillard, G. *Soc. Chim. Mem.* **1954**, *5*, 802−807.
(184) McDonald, J. E. *J. Meteorol.* **1953**, *10*, 416−433.
(185) Pruppacher, H. R. *J. Atmos. Sci.* **1995**, *52*, 1924−1933.
(186) Jeffery, C. A.; Austin, P. H. *J. Geophys. Res.* **1997**, *102*, 25269−25279.
(187) Seeley, L. H.; Seidler, G. T.; Dash, J. G. *Rev. Sci. Instrum.* **1999**, *70*, 3664−3667.
(188) Bacon, N. J.; Swanson, B. D.; Baker, M. B.; Davis, J. E. *J. Geophys. Res.* **1998**, *103*, 13763−13775.
(189) Swanson, B. D.; Bacon, N. J.; Davis, J. E.; Baker, M. B. *Q. J. R. Meteorol. Soc.* **1999**, *125*, 1039−1058.
(190) Mason, B. L.; Dash, J. G. *J. Geophys. Res.* **2000**, *105*, 10185.
(191) Bertram, A. K.; Dickens, D. B.; Sloan, J. J. *J. Geophys. Res.* **2000**, *105*, 9283−9290.
(192) Salcedo, D.; Molina, L. T.; Molina, M. J. *Geophys. Res. Lett.* **2000**, *27*, 193−196.

(193) Cziczo, D. J.; Abbatt, J. P. D. *J. Phys. Chem. A* **2000**, *104*, 2038−2047.
(194) Bertram, A. K.; Koop, T.; Molina, L. T.; Molina, M. J. *J. Phys. Chem. A* **2000**, *104*, 584−588.
(195) Chen, Y.; DeMott, P. J.; Kreidenweis, S. M.; Rogers, D. C.; Sherman, D. E. *J. Atmos. Sci.* **2000**, in press.
(196) Han, J. H.; Martin, S. T. *Aerosol Sci. Technol.* **2000,** in press.
(197) Tabazadeh, A.; Toon, O. B.; Clegg, S. L.; Hamill, P. *Geophys. Res. Lett.* **1997**, *24*, 1931−1934.
(198) Tabazadeh, A.; Toon, O. B.; Jensen, E. *Geophys. Res. Lett.* **1997**, *24*, 2007−2010.
(199) Tabazadeh, A.; Jensen, E. J.; Toon, O. B. *J. Geophys. Res.* **1997**, *102*, 23845−23850.
(200) Vali, G. *J. Atmos. Sci.* **1994**, *51*, 1843−1856.
(201) DeMott, P. J.; Rogers, D. C. *J. Atmos. Sci.* **1990**, *47*, 1056−1064.
(202) Krämer, B.; Schwell, M.; Hübner, O.; Vortisch, H.; Leisner, T.; Rühl, E.; Baumgärtel, H.; Wöste, L. *Ber. Bunsen-Ges. Phys. Chem.* **1996**, *100*, 1911−1914.
(203) Shaw, R. A.; Lamb, D. *Geophys. Res. Lett.* **1999**, *26*, 1181−1184.
(204) MacKenzie, A. R.; Laaksonen, A.; Batris, E.; Kulmala, M. *J. Geophys. Res.* **1998**, *103*, 10875−10884.
(205) Luo, B.; Peter, T.; Crutzen, P. *Geophys. Res. Lett.* **1994**, *21*, 1447−1450.
(206) Ostwald, W. *Z. Phys. Chem.* **1897**, *22*, 306.
(207) Nielson, A. E. In *Geochemical Processes at Mineral Surfaces*; Davis, J. A., Hayes, K. F., Eds.; American Chemical Society: Washington, DC, 1986.
(208) Tang, I. N.; Fung, K. H.; Imre, D. G.; Munkelwitz, H. R. *Aerosol Sci. Technol.* **1995**, *23*, 443−453.
(209) Murphy, D. M.; Thomson, D. S. *J. Geophys. Res.* **1997**, *102*, 6353−6368.
(210) Murphy, D. M.; Thomson, D. S. *J. Geophys. Res.* **1997**, *102*, 6341−6352.
(211) Noble, C. A.; Prather, K. A. *Environ. Sci. Technol.* **1996**, *30*, 2667−2680.
(212) Pye, K. *Aeolian Dust and Dust Deposits*; Academic Press: San Diego, 1987.
(213) Sokolik, I. N.; Toon, O. B. *J. Geophys. Res.* **1999**, *104*, 9423−9444.
(214) McTainsh, G.; Walker, P. H. *Z. Geomorph.* **1982**, *26*, 417−435.
(215) Kahn, A. E. In *Saharan Dust: Mobilization, Transport, Deposition*; Morales, C., Ed.; Wiley: New York, 1979.
(216) Vonnegut, B. *J. Appl. Phys.* **1947**, *18*, 593−595.
(217) Hillier, A. C.; Ward, M. D. *Phys. Rev. B* **1996**, *54*, 14037−14051.
(218) Bryant, G. W.; Hallet, J.; Mason, B. J. *J. Phys. Chem. Solids* **1959**, *12*, 189−195.
(219) *Saharan Dust: Mobilization, Transport, Deposition*; Morales, C., Ed.; Wiley: New York, 1979.
(220) Carlson, T. N.; Prospero, J. M. *J. Appl. Meteorol.* **1972**, *11*, 283−297.
(221) Ferguson, W. S.; Friffin, J. J.; Goldberg, E. D. *J. Geophys. Res.* **1970**, *75*, 1137−1139.
(222) Li, X.; Maring, H.; Savoie, D.; Koss, V.; Prospero, J. M. *Nature* **1996**, *380*, 416−419.
(223) Perry, K. D.; Cahill, T. A.; Eldred, R. A.; Dutcher, D. D.; Gill, T. E. *J. Geophys. Res.* **1997**, *102*, 11225−11238.
(224) Prospero, J. M. In *The Impact of Desert Dust Across the Mediterranean*; Guerzoni, S., Chester, R., Eds.; Kluwer: Dordrecht, 1996.
(225) Schulz, M.; Balkanski, Y. J.; Guelle, W.; Dulac, F. *J. Geophys. Res.* **1998**, *103*, 10579−10592.
(226) Talbot, R. W.; Harriss, R. C.; Browell, V.; Gregory, G. L.; Sebacher, D. I.; Beck, S. M. *J. Geophys. Res.* **1986**, *91*, 5173−5182.
(227) Uematsu, M.; Duce, R. A.; Prospero, J. M. *J. Atmos. Chem.* **1985**, *3*, 123−138.
(228) Westphal, D. L.; Toon, O. B.; Carlson, T. N. *J. Atmos. Sci.* **1988**, *45*, 2145−2175.
(229) Husar, R. B.; Prospero, J. M.; Stowe, L. L. *J. Geophys. Res.* **1997**, *102*, 16689−16909.
(230) Buseck, P. R.; Posfai, M. *Proc. Natl. Acad. Sci.* **1999**, *96*, 3372−3379.
(231) Posfai, M.; Anderson, J. R.; Buseck, P. B.; Shattuck, T. W.; Tindale, N. W. *Atmos. Environ.* **1994**, *28*, 1747−1756.
(232) Posfai, M.; Anderson, J. R.; Buseck, P. R.; Sievering, H. *J. Geophys. Res.* **1995**, *100*, 23063−23074.
(233) Piketh, S. J.; Annegarn, H. J.; Tyson, P. D. *J. Geophys. Res.* **1999**, *104*, 1597−1607.
(234) Ganor, E.; Levin, Z.; van Grieken, R. *Atmos. Environ.* **1998**, *32*, 1631−1642.
(235) Cantrell, W.; Shaw, G.; Benner, R.; Veazey, D. *Geophys. Res. Lett.* **1997**, *24*, 3005−3008.
(236) Andreae, M. O.; Charlson, R. J.; Bruynseels, F.; Storms, H.; Van Grieken, R.; Maenhaut, W. *Science* **1986**, *232*, 1620−1623.
(237) Parungo, F.; Kim, Y.; Zhu, C. J.; Harris, J.; Schnell, R.; Li, X. S.; Yang, D. Z.; Fang, X. M.; Zhou, M. Y.; Chen, Z.; Park, K. *Asian dust storms and their effects on radiant and climate, Part I*; Science and Technology Corporation: 1995.
(238) Levin, Z.; Ganor, E.; Gladstein, V. *J. Appl. Meteorol.* **1996**, *35*, 1511−1523.
(239) Wurzler, S.; Reisin, T. G.; Levin, Z. *J. Geophys. Res.* **2000**, *105*, 4501−4512.
(240) Underwood, G. M.; Miller, T. M.; Grassian, V. H. *J. Phys. Chem. A* **1999**, *103*, 6184−6190.
(241) Goodman, A. L.; Underwood, G. M.; Grassian, V. H. *J. Phys. Chem. A* **1999**, *103*, 7217−7223.
(242) Cunningham, P. T.; Johnson, S. A.; Yang, R. T. *Environ. Sci. Technol.* **1974**, *8*, 131−135.
(243) Dentener, F. J.; Carmichael, G. R.; Zhang, Y.; Lelieveld, J.; Crutzen, P. J. *J. Geophys. Res.* **1996**, *101*, 22869−22889.
(244) Zhang, Y.; Carmichael, G. R. *J. Appl. Meteorol.* **1999**, *38*, 353−366.
(245) Song, C. H.; Carmichael, G. R. *Atmos. Environ.* **1999**, *33*, 2203−2218.
(246) Niimura, N.; Okada, K.; Fan, X. B.; Kai, K.; Arao, K.; Shi, G. Y.; Takahashi, S. *J. Meteorol. Soc. Jpn.* **1998**, *76*, 275−288.
(247) Afeti, G. M.; Resch, F. J. European Aerosol Conference, Prague, 1999.
(248) Eldering, A.; Cass, G. R. *J. Geophys. Res.* **1996**, *101*, 19343−19369.
(249) Ichoku, C.; Andreae, M. O.; Andreae, T. W.; Meixner, F. X.; Schebeske, G.; Formenti, P.; Maenhaut, W.; Cafmeyerr, J.; Ptasinski, J.; Karnieli, A.; Orlovksy, L. *J. Geophys. Res.* **1999**, *104*, 24371−24393.
(250) Murphy, D. M.; Thomason, D. S.; Mahoney, M. J. *Science* **1998**, *282*, 1664−1669.
(251) Martin, S. T.; Yu, J.; Han, J. H.; Verdier, M.; Li, J.; Buseck, P. R. *J. Aerosol Sci.* **2000**, in press.
(252) DeMott, P. J.; Chen, Y.; Kreidenweis, S. M.; Rogers, D. C.; Sherman, D. E. *Geophys. Res. Lett.* **1999**, *26*, 2429−2432.
(253) Oatis, S.; Imre, D.; McGraw, R.; Xu, J. *Geophys. Res. Lett.* **1998**, *25*, 4469−4472.
(254) Bogdan, A.; Kulmala, M. *Geophys. Res. Lett.* **1999**, *26*, 1433−1436.
(255) Biermann, U. M.; Presper, T.; Koop, T.; Mössinger, J.; Crutzen, P. J.; Peter, T. *Geophys. Res. Lett.* **1996**, *23*, 1693−1696.
(256) Schnell, R. C.; Vali, G. *J. Atmos Sci.* **1976**, *33*, 1554−1564.
(257) Ashworth, E. N.; Davis, G. A.; Anderson, J. A. *Plant Physiol.* **1985**, *79*, 1033−1037.
(258) Finnegan, W. G. *J. Colloid Interface Sci.* **1998**, *202*, 518−526.
(259) Vonnegut, B.; Baldwin, M. *J. Climate Appl. Meteorol.* **1984**, *23*, 486-490.
(260) Braham, R. R., Ed. *Meteor. Monogr.* **1986**, *No. 21*, 171 pp.
(261) Weissbuch, I.; Popovitz-Biro, R.; Lahav, M.; Leiserowitz, L. *Acta Crystallogr.* **1995**, *B51*, 115−148.
(262) Vali, G.; Stansbury, E. J. *Can. J. Phys.* **1966**, *44*, 477−502.
(263) Fletcher, N. H. *J. Atmos. Sci.* **1969**, *26*, 1266−1271.
(264) Vali, G. *J. Atmos. Sci.* **1971**, *28*, 402−409.
(265) Deshler, T.; Vali, G. *J. Atmos. Sci.* **1992**, *49*, 773−784.
(266) Kreidenweis, S. M.; Chen, Y.; Rogers, D. C.; DeMott, P. J. *Atmos. Res.* **1998**, *46*, 263−278.
(267) Hoffer, T. E. *J. Meteorol.* **1961**, *18*, 766−778.
(268) Reischel, M. T.; Vali, G. *Tellus* **1975**, *27*, 414−427.
(269) Pruppacher, H. R.; Neiburger, M. *J. Atmos. Sci.* **1963**, *20*, 376−385.
(270) Ganguly, S.; Adiseshaiah, K. S. *Colloids Surf.* **1992**, *66*, 105−111.
(271) Martin, S. T. Unpublished results.
(272) Posfai, M.; Anderson, J. R.; Buseck, P. R.; Sievering, H. *J. Geophys. Res.* **1999**, *104*, 21685−21693.
(273) Kärcher, B.; Peter, T.; Biermann, U. M.; Schumann, U. *J. Atmos. Sci.* **1996**, *53*, 3066−3083.
(274) Even, A.; Khlystov, A.; ten Brink, H. M. European Aerosol Conference, Prague, 1999.
(275) Rogers, D. C.; DeMott, P. J.; Kreidenweis, S. M.; Chen, Y. *Geophys. Res. Lett.* **1998**, *25*, 1383−1386.
(276) Goldberg, E. D. *Black Carbon in the Environment*; Wiley: New York, 1985.
(277) Wolff, G. T., Klimisch, R. L., Eds. *Particulate Carbon: Atmospheric Life Cycle*; Plenum: New York, 1982.
(278) Strommen, M. R.; Kamens, R. M. *Environ. Sci. Technol.* **1997**, *31*, 2983−2990.
(279) Petzold, A.; Strom, J.; Ohlsson, S.; Schroder, F. P. *Atmos. Res.* **1998**, *49*, 21−34.
(280) Strom, J.; Ohlsson, S. *J. Geophys. Res.* **1998**, *103*, 11355−11361.
(281) Peter, T. In *Nucleation and Atmospheric Aerosols*; Kulmala, M., Wagner, P. E., Eds.; Pergamon: Oxford, 1996.
(282) Sassen, K.; Dodd, G. C. *J. Atmos. Sci.* **1988**, *45*, 1357−1369.
(283) Sassen, K.; Dodd, G. C. *J. Atmos. Sci.* **1989**, *46*, 3005−3014.
(284) Jensen, E. J.; Toon, O. B. *Geophys. Res. Lett.* **1991**, *18*, 1857−1860.
(285) Heymsfield, A. J.; Sabin, R. M. *J. Atmos. Sci.* **1989**, *46*, 2252−2264.
(286) Eadie, W. J. Ph.D. Thesis, University of Chicago, 1971.
(287) Schenter, G. K.; Kathmann, S. M.; Garrett, B. C. *Phys. Rev. Lett.* **1999**, *82*, 3484−3487.

(288) Schenter, G. K.; Kathmann, S. M.; Garrett, B. C. *J. Chem. Phys.* **1999**, *110*, 7951−7959.
(289) Laaksonen, A.; Talanquer, V.; Oxtoby, D. W. *Annu. Rev. Phys. Chem.* **1995**, *46*, 489−524.
(290) Anisimov, M. P.; Hopke, P. K.; Rasmussen, D. H.; Shandakov, S. D.; Pinaev, V. A. *J. Chem. Phys.* **1998**, *109*, 1435−1444.
(291) Khvorostyanov, V.; Sassen, K. *Geophys. Res. Lett.* **1998**, *25*, 3155−3158.
(292) Jensen, E. J.; Toon, O. B. *Geophys. Res. Lett.* **1994**, *21*, 2019−2022.
(293) Jensen, E. J.; Toon, O. B.; Westphal, D. L.; Kinne, S.; Heymsfield, A. J. *J. Geophys. Res.* **1994**, *99*, 10421−10442.
(294) Jensen, E. J.; Toon, O. B.; Westphal, D. L.; Kinne, S.; Heymsfield, A. J. *J. Geophys. Res.* **1994**, *99*, 10443−10454.
(295) DeMott, P. J.; Meyers, M. P.; Cotton, W. R. *J. Atmos. Sci.* **1994**, *51*, 77−90.
(296) Chen, J. P. *J. Atmos. Sci.* **1994**, *51*, 3505−3516.
(297) DeMott, P. J. In *Cirrus*; Lynch, D. K., Ed.; Oxford University Press: London, 2000, in press.
(298) Volmer, H.; Weber, A. *Z. Phys. Chem.* **1925**, *119*, 277.
(299) Becker, R.; Döring, W. *Ann. Phys.* **1935**, *24*, 719.
(300) Turnbull, D.; Vonnegut, B. *Ind. Eng. Chem.* **1952**, *44*, 1292.
(301) Williams, L. R.; Long, F. S. *J. Phys. Chem.* **1995**, *99*, 3748−3751.
(302) Tabazadeh, A.; Martin, S. T.; Lin, J. S. *Geophys. Res. Lett.* **2000**, *27*, 1111−1114.
(303) Oxtoby, D. W. *J. Phys. Condens. Matter* **1992**, *4*, 7627.
(304) Jacobson, M. Z. *Fundamentals of Atmospheric Modeling*; Cambridge University Press: Cambridge, 1999.
(305) Starr, D. O. C.; Cox, S. K. *J. Atmos. Sci.* **1985**, *42*, 2663−2681.
(306) Starr, D. O. C. *J. Atmos. Sci.* **1985**, *42*, 2682−2694.
(307) Lin, H.; Noone, K. J.; Strom, J.; Heymsfield, A. J. *J. Atmos. Sci.* **1998**, *55*, 1928−1939.
(308) U.S. Environmental Protection Agency. *Air Quality Criteria for Particulate Matter*; EPA/600/P-95/001aF; U.S. Government Printing Office: Washington, DC, 1996; Chapter 3.
(309) *Hygroscopic Aerosols*; Ruhnke, L. H., Deepak, A., Eds.; A. Deepak Publishing: Hampton, VA, 1984.
(310) Boucher, O.; Schwartz, S. E.; Ackerman, T. P.; Anderson, T. L.; Bergstrom, B.; Bonnel, B.; Chylek, P.; Dahlback, A.; Fouquart, Y.; Fu, Q.; Halthore, R. N.; Haywood, J. M.; Iversen, T.; Kato, S.; Kinne, S.; Kirkevag, A.; Knapp, K. R.; Lacis, A.; Laszlo, I.; Mishchenko, M. I.; Nemesure, S.; Ramaswamy, V.; Roberts, D. L.; Russell, P.; Schlesinger, M. E.; Stephens, G. L.; Wagener, R.; Wang, M.; J., W.; F., Y. *J. Geophys. Res.* **1998**, *103*, 16979−16998.
(311) Schwartz, S. E. *J. Aerosol Sci.* **1996**, *27*, 359−382.
(312) Tegen, I.; Lacis, A.; Fung, I. *Nature* **1996**, *380*, 419−422.
(313) Penner, J. E.; Chuang, C. C.; Grant, K. *Climate Dyn.* **1998**, *14*, 839−851.
(314) Tegen, I.; Hollrig, P.; Chin, M.; Fung, I.; Jacob, D.; Penner, J. *J. Geophys. Res.* **1997**, *102*, 23895−23915.
(315) White, W. H. *Atmos. Environ.* **1986**, *20*, 1659−1672.
(316) Sloane, C. S. *Atmos. Environ.* **1984**, *18*, 871−878.
(317) Sloane, C. S.; Wolff, G. T. *Atmos. Environ.* **1985**, *19*, 669−680.
(318) Sloane, C. S. *Atmos. Environ.* **1986**, *20*, 1025−1037.
(319) Malm, W. C.; Gebhart, K. A.; Molenar, J.; Cahill, T.; Eldred, R.; Huffman, D. *Atmos. Environ.* **1994**, *28*, 347−360.
(320) Sloane, C. S.; Watson, J. G.; Chow, J. C.; Prichett, L. C.; Richards, L. W. *Atmos. Environ.* **1991**, *25A*, 1013−1024.
(321) Ravishankara, A. R. *Science* **1997**, *276*, 1058−1064.
(322) Baker, M. B.; Dash, J. G. *J. Geophys. Res.* **1994**, *99*, 10621−10626.
(323) Baker, M. B.; Dash, J. G. *J. Cryst. Growth* **1989**, *97*, 770−776.
(324) Wettlaufer, J. S.; Dash, J. G. *Sci. Am.* **2000**, *February*, 50−53.
(325) Pruppacher, H. R. *J. Geophys. Res.* **1963**, *68*, 4463.
(326) Doolittle, J. B.; Vali, G. *J. Atmos. Sci.* **1975**, *32*, 375.
(327) Dawson, G. A.; Cardell, S. R. *J. Geophys. Res.* **1973**, *78*, 8864.
(328) Abbas, M. A.; Latham, J. *J. Meteorol. Soc. Jpn.* **1969**, *47*, 65.
(329) Smith, M. H.; Griffiths, R. R.; Latham, J. *Q. J. R. Meteorol. Soc.* **1971**, *97*, 495.
(330) Pruppacher, H. R. *Z. Angew. Math. Phys.* **1963**, *14*, 590.
(331) Gabarashvili, T. G.; Gliki, N. V. *Izv. Acad. Sci., U.S.S.R., Atmos. Ocean. Phys.* **1967**, *3*, 324.
(332) Gabarashvili, T. G.; Kartsivadze, A. I. *Preprints of the Conference on Cloud Physics*; University of Toronto: Toronto, 1968; p188.
(333) Gabarashvili, T. G.; Kartsivadze, A. I. *Proceedings of the Conference on Condensation and Ice Nuclei*, Prague-Vienna; Czechoslovak Academy of Science: Prague, 1969; p 220.
(334) Morgan G. M.; Langer, G. *Q. J. R. Meteorol. Soc.* **1973**, *99*, 387.
(335) Schaefer, V. J.; Day, J. A. *A Field Guide to the Atmosphere*; Houghton: Boston, 1981.
(336) Koloutsou-Vakakis, S.; Rood, M. J. *Tellus* **1994**, *46B*, 1−15.
(337) Charlson, R. J.; Vanderpol, A. H.; Covert, D. S.; Waggoner, A. P.; Ahlquist, N. C. *Atmos. Environ.* **1974**, *8*, 1257−1267.
(338) Charlson, R. J.; Porch, W. M.; Waggoner, A. P.; Ahlquist, N. C. *Tellus* **1974**, *3*, 345−360.
(339) Hänel, G.; Lehmann, M. *Cont. Atmos. Phys.* **1981**, *54*, 57−71.
(340) Rood, M. J.; Covert, D. S.; Larson, T. V. *Tellus* **1987**, *39B*, 383−397.
(341) Rood, M. J.; Shaw, M. A.; Larson, T. V.; Covert, D. S. *Nature* **1989**, *337*, 537−539.
(342) Shaw, M. A.; Rood, M. J. *Atmos. Environ.* **1990**, *24A*, 1837−1841.
(343) Pitchford, M. L.; McMurry, P. H. *Atmos. Environ.* **1994**, *28*, 827−839.
(344) ten Brink, H. M.; Veefkind, J. P.; Waijers-Ijpelaan, A.; van der Hage, J. C. *Atmos. Environ.* **1996**, *30*, 4251−4261.
(345) Fitzgerald, J. W. *Atmos. Environ.* **1991**, *25A*, 533−545.
(346) Fitzgerald, J. W.; Marti, J. J.; Hoppel, W. A.; Frick, G. M.; Gelbard, F. *J. Geophys. Res.* **1998**, *103*, 16103−16117.
(347) DIAL Water Vapor Distributions. http://asd-www.larc.nasa.gov/lidar/las/lase_ val.html.
(348) Baumgardner, D.; Clarke, A. *J. Geophys. Res.* **1998**, *103*, 16525−16534.
(349) White, A. B.; Fairall, C. W.; Thomason, D. W. *J. Atmos. Oceanic Technol.* **1991**, *8*, 639−658.
(350) NASA Langley Atmospheric Sciences Data Center. http://eoswe-b.larc.nasa.gov.
(351) Cobourn, W. G.; Djukic-Husar, J.; Husar, R. B. *J. Geophys. Res.* **1980**, *85*, 4487−4494.
(352) Charlson, R. J.; Vanderpol, A. H.; Covert, D. S.; Waggoner, A. P.; Ahlquist, N. C. *Science* **1974**, *184*, 156−157.
(353) Weiss, R. E.; Waggoner, A. P.; Charlson, R. J.; Ahlquist, N. C. *Science* **1977**, *195*, 979−981.
(354) Vanderpol, A. H.; Carsey, F. D.; Covert, D. S.; Charlson, R. J.; Waggoner, A. P. *Science* **1975**, *190*, 570.
(355) Heintzenberg, J.; Charlson, R. J. *J. Atmos. Oceanic Technol.* **1996**, *13*, 987−1000.
(356) Sinclair, D.; Countess, R. J.; Hoopes, G. S. *Atmos. Environ.* **1974**, *8*, 1111−1117.
(357) Rood, M. J.; Covert, D. S.; Larson, T. V. *Aersol Sci. Technol.* **1987**, *7*, 57−65.
(358) Ten Brink, H. M. Personal communication.
(359) Larson, T. V.; Ahlquist, N. C.; Weiss, R. E.; Covert, D. C.; Waggoner, A. P. *Atmos. Environ.* **1982**, *16*, 1587−1590.
(360) Liu, B. Y. H.; Pui, D. Y. H.; Whitby, K. T.; Kittelson, D. B.; Kousaka, Y.; McKenzie, R. L. *Atmos. Environ.* **1978**, *12*, 99−104.
(361) McMurry, P. H.; Stolzenburg, M. R. *Atmos. Environ.* **1989**, *23*, 497−507.
(362) Zhang, W. G.; McMurry, P. H.; Hering, S. V.; Casuccio, G. S. *Atmos. Environ.* **1993**, *27A*, 1593−1608.
(363) Berg, O. H.; Swietlicki, E.; Krejci, R. *J. Geophys. Res.* **1998**, *103*, 16535−16545.
(364) Boubel, R. W.; Fox, D. L.; Turner, D. B.; Stern, A. C. *Fundamentals of Air Pollution*; Academic: San Diego, 1994.
(365) Stoddard, J. L.; Jeffries, D. S.; Lukewille, A.; Clair, T. A.; Dillon, P. J.; Driscoll, C. T.; Forsius, M.; Johannessen, M.; Kahl, J. S.; Kellogg, J. H.; Kemp, A.; Mannio, J.; Montelth, D. T.; Murdoch, P. S.; Patrick, S.; Rebsdorf, A.; Skjelkvale, B. L.; Stainton, M. P.; Traaen, T.; van Dam, H.; Webster, K. E.; Wieting, J.; Wilander, A. *Nature* **1999**, *401*, 575−578.
(366) Stephens, G. L.; Tsay, S. C.; Stackhouse, P. W.; Flatau, P. J. *J. Atmos. Sci.* **1990**, *47*, 1742−1753.
(367) Rogers, D. C. *Bull. Am. Meteorol. Soc.* **1994**, *75*, 2312−2314.
(368) Cox, S. K.; McDougal, D. S.; Randall, D. A.; Schiffer, R. A. *Bull. Am. Meteorol. Soc.* **1987**, *68*, 114−118.
(369) asd-www.larc.nasa.gov/fire/fire1.html.
(370) Stephens, G. L. *J. Atmos. Sci.* **1995**, *52*, 4041.
(371) Toon, O. B.; Miake-Lye, R. C. *Geophys. Res. Lett.* **1998**, *25*, 1109−1112.
(372) Tabazadeh, A.; Toon, O. B. *Geophys. Res. Lett.* **1998**, *25*, 1379−1382.
(373) Tabazadeh, A.; Jacobsen, M. Z.; Singh, H. B.; Toon, O. B.; Lin, J. S.; Chatfield, R. B.; Thakur, A. N.; Talbot, R. W.; Dibb, J. E. *Geophys. Res. Lett.* **1998**, *25*, 4185−4188.
(374) Heymsfield, A. J.; Miloshevich, L. M. *J. Atmos. Sci.* **1995**, *52*, 4302−4326.
(375) Isono, K.; Komabayasi, M.; Ono, A. *J. Meteorol. Soc. Jpn.* **1959**, *37*, 211−233.
(376) Bertrand, J. J. Mesure de la concentration en noyaux de congélation en Afrique Occidentale. In Reunions de Travail sur les Caractéristiques Physico-Chimiques et le Transport des Poussières d'Origine Africaine, *Inst. Observatoire Phys. Globe Puy-de-Dôme*, *26*, Clermont-Ferrand, **1974**.
(377) Hagen, D. E.; Podzimek, J.; Heymsfield, A. J.; Trueblood, M. B.; Lutrus, C. K. *Atmos. Res.* **1994**, *31*, 123−135.
(378) Hagen, D. E.; Podzimek, J.; Trueblood, M. B. *J. Atmos. Sci.* **1995**, *52*, 4196−4209.
(379) Heintzenberg, J.; Okada, K.; Ström, J. *Atmos. Res.* **1996**, *41*, 81−88.
(380) Twohy, C. H.; Gandrud, B. W. *Geophys. Res. Lett.* **1998**, *25*, 1359−1362.
(381) Talbot, R. W.; Dibb, J. E.; Loomis, M. B. *Geophys. Res. Lett.* **1998**, *25*, 1367−1370.

(382) Chen, Y.; Kreidenweis, S. M.; McInnes, L. M.; Rogers, D. C.; DeMott, P. J. *Geophys. Res. Lett.* **1998**, *25*, 1391−1394.
(383) Strom, J.; Strauss, B.; Anderson, T.; Schroder, F.; Heintzenberg, J.; Wendling, P. *J. Atmos. Sci.* **1997**, *54*, 2542−2553.
(384) World Meteorological Organization. *Scientific Assessment of Stratospheric Ozone: 1994*; WMO Global Ozone Research and Monitoring Project Report 37; 1994.
(385) Meilinger, S. K.; Koop, T.; Luo, B. P.; Hutwelker, T.; Carslaw, K. S.; Krieger, U.; Crutzen, P. J.; Peter, T. *Geophys. Res. Lett.* **1995**, *22*, 3031−3034.
(386) Stefanutti, L.; Morandi, M.; Del Guasta, M.; Godin, S.; David, C. *Geophys. Res. Lett.* **1995**, *22*, 2377−2380.
(387) Tsias, A.; Wirth, M.; Carslaw, K. S.; Biele, J.; Mehrtens, H.; Reichardt, J.; Wedekind, C.; Weiss, V.; Renger, W.; Neuber, R.; von Zahn, U.; Stein, B.; Santacesaria, V.; Stafanutti, L.; Fierli, F.; Bacmeister, J.; Peter, T. *J. Geophys. Res.* **1999**, *104*, 23961−23969.
(388) Carslaw, K. S.; Peter, T.; Bacmeister, J. T.; Eckermann, S. D. *J. Geophys. Res.* **1999**, *104*, 1827−1836.
(389) Tabazadeh, A.; Toon, O. B.; Gary, B. L.; Bacmeister, J. T.; Schoeberl, M. R. *Geophys. Res. Lett.* **1996**, *23*, 2109−2112.
(390) Wirth, M.; Tsias, A.; Dornbrack, A.; Weiss, V.; Carslaw, K. S.; Leutbecher, M.; Renger, W.; Volkert, H.; Peter, T. *J. Geophys. Res.* **1999**, *104*, 23971−23981.
(391) Carslaw, K. S.; Wirth, M.; Tsias, A.; Luo, B. P.; Dörnbrack, A.; Leutbecher, M.; Volkert, H.; Renger, W.; Bacmeister, J. T.; Reimer, E.; Peter, T. *Nature* **1998**, *391*, 675−678.
(392) Carslaw, K. S.; Wirth, M.; Tsias, A.; Luo, B. P.; Dörnbrack, A.; Leutbecher, M.; Volkert, H.; Renger, W.; Bacmeister, J. T.; Peter, T. *J. Geophys. Res.* **1998**, *103*, 5785−5796.
(393) Koloutsou-Vakakis, S.; Rood, M. J.; Nenes, A.; Pilinis, C. *J. Geophys. Res.* **1998**, *103*, 17009−17032.
(394) Fahey, D. W.; Kelly, K. K.; Ferry, G. V.; Poole, L. R.; Wilson, J. C.; Murphy, D. M.; Loewenstein, M.; Chan, K. R. *J. Geophys. Res.* **1989**, *94*, 11299−11315.
(395) Dye, J. E.; Baumgardner, D.; Gandrud, B. W.; Kawa, S. R.; Kelly, K. K.; Loewenstein, M.; Ferry, G. V.; Chan, K. R.; Gary, B. L. *J. Geophys. Res.* **1992**, *97*, 8015.
(396) Del Negro, L. A.; Fahey, D. W.; Donnelly, S. G.; Gao, R. S.; Keim, E. R.; Wamsley, R. C.; Woodbridge, E. L.; Dye, J. E.; Baumgardner, D.; Gandrud, B. W.; Wilson, J. C.; Jonsson, H. H.; Loewenstein, M.; Podolske, J. R.; Webster, C. R.; May, R. D.; Worsnop, D. R.; Tabazadeh, A.; Tolbert, M. A.; Kelly, K. K.; Chan, K. R. *J. Geophys. Res.* **1997**, *102*, 13255−13282.
(397) Carslaw, K. S.; Luo, B. P.; Clegg, S. L.; Peter, T.; Brimblecombe, P.; Crutzen, P. J. *Geophys. Res. Lett.* **1994**, *21*, 2479−2482.
(398) Browell, E. V.; Butler, C. F.; Ismail, S.; Robinette, P. A.; Carter, A. F.; Higdon, N. S.; Toon, O. B.; Schoeberl, M. R.; Tuck, A. F. *Geophys. Res. Lett.* **1990**, *17*, 385−388.
(399) Toon, O. B.; Browell, E. V.; Kinne, S.; Jordan, J. *Geophys. Res. Lett.* **1990**, *17*, 393−396.
(400) Rosen, J. M.; Kjome, N. *Appl. Opt.* **1991**, *30*, 1552−1561.
(401) Drdla, K.; Tabazadeh, A.; Turco, R. P.; Jacobson, M. Z.; Dye, J. E.; Twohy, C.; Baumgardner, D. *Geophys. Res. Lett.* **1994**, *21*, 2475−2478.
(402) Tabazadeh, A.; Turco, R. P.; Jacobson, M. Z. *J. Geophys. Res.* **1994**, *99*, 12897−12914.
(403) Larsen, N.; Rosen, J. M.; Kjome, N. T.; Knudsen, B. *Geophys. Res. Lett.* **1995**, *22*, 1233−1236.
(404) Larsen, N.; Knudsen, B. M.; Rosen, J. M.; Kjome, N. T.; Kyrö, E. *Geophys. Res. Lett.* **1996**, *23*, 1091−1094.
(405) Stein, B.; Wedekind, C.; Wille, H.; Immler, F.; Muller, M.; Woste, L.; del Guasta, M.; Morandi, M.; Stefanutti, L.; Antonelli, A.; Agostini, P.; Rizi, V.; Readelli, G.; Mitev, V.; Matthey, R.; Kivi, R.; Kyro, E. *J. Geophys. Res.* **1999**, *104*, 23983−23993.
(406) Schreiner, J.; Voigt, C.; Kohlmann, A.; Arnold, F.; Mauersberger, K.; Larsen, N. *Science* **1999**, *283*, 968−970.
(407) Toon, O. B.; Tolbert, M. A. *Nature* **1995**, *375*, 218−221.
(408) Andrews, E.; Larson, S. M. *Environ. Sci. Technol.* **1993**, *27*, 857−865.
(409) Hämeri, K.; Rood, M.; Hansson, H. C. *J. Aerosol Sci.* **1992**, *23*, S437−S440.
(410) Hansson, H. C.; Wiedensohler, A.; Rood, M. J.; Covert, D. S. *J. Aerosol Sci.* **1990**, *21*, S241−S244.
(411) Hansson, H. C.; Orsini, D. A.; Wiedensohler, A.; Rood, M. *J. Aerosol Sci.* **1994**, *25*, S129−S130.
(412) Wagner, J.; Andrews, E.; Larson, S. M. *J. Geophys. Res.* **1996**, *101*, 19533−19540.
(413) Hansson, H. C.; Rood, M. J.; Koloutsou-Vakakis, S.; Hämeri, K.; Orsini, D.; Wiedensohler, A. *J. Atmos. Chem.* **1998**, *31*, 321−346.
(414) Rodhe, H. *Nature* **1999**, *401*, 223.
(415) Shulman, M. L.; Jacobson, M. C.; Carlson, R. J.; Synovec, R. E.; Young, T. E. *Geophys. Res. Lett.* **1996**, *23*, 277−280.
(416) Facchini, M. C.; Mircea, M.; Fuzzi, S.; Charlson, R. J. *Nature* **1999**, *401*, 257−259.
(417) McGraw, R.; Huang, P. I.; Schwartz, S. E. *Geophys. Res. Lett.* **1995**, *22*, 2929−2932.
(418) Grant, K. E.; Chuang, C. C.; Grossman, A. S.; Penner, J. E. *Atmos. Environ.* **1999**, *33*, 2603−2620.
(419) Ansari, A. S.; Pandis, S. N. *Atmos. Environ.* **1999**, *33*, 745−757.
(420) Wagman, D. D.; Evans, W. H.; Parker, V. B.; Harlow, I.; Baily, S.; Schumm, R. H. *Selected values of chemical thermodynamic properties; tables for the first thirty-four elements in the standard order of arrangment*; NBS Technical Note 270-273; National Bureau of Standards: Gaithersburgh, MD, 1968.
(421) Marion, G. M.; Farren, R. E. *Geochim. Cosmochim. Acta* **1999**, *63*, 1305−1318.
(422) Zhang, Y.; Seigneur, C.; Seinfeld, J. H.; Jacobson, M.; Clegg, S. L.; Binkowski, F. S. *Atmos. Environ.* **2000**, *34*, 117−137.
(423) Meilinger, S. K.; Tsias, A.; Dreiling, V.; Kuhn, M.; Feigl, C.; Ziereis, H.; Schlager, H.; Curtius, J.; Sierau, B.; Arnold, F.; Zöger, M.; Schiller, C.; Peter, T. *Geophys. Res. Lett.* **1999**, *26*, 2207−2210.
(424) Jensen, E. J.; Read, W. G.; Mergenthaler, J.; Sandor, B. J.; Pfister, L.; Tabazadeh, A. *Geophys. Res. Lett.* **1999**, *26*, 2347−2350.
(425) Hornung, E. W.; Brackett, T. E.; Giauque, W. F. *J. Am. Chem. Soc.* **1956**, *78*, 5747−5751.
(426) Mootz, D.; Merschenz-Quack, A. *Z. Naturforsch. B* **1987**, *42*, 1231−1236.
(427) Tang, I. N.; Tridico, A. C.; Fung, K. H. *J. Geophys. Res.* **1997**, *102*, 23269−23275.
(428) Smith, R. S.; Kay, B. D. *Nature* **1999**, *398*, 788−791.
(429) Elliott, S.; Turco, R. P.; Toon, O. B.; Hamill, P. *Geophys. Res. Lett.* **1990**, *17*, 425−428.
(430) Li, Z.; Williams, A. L.; Rood, M. J. *J. Atmos. Sci* **1998**, *55*, 1859−1866.

CR990034T